EXPERIMENTAL ANALYSIS OF FULGURITE FORMATION

Ayşe Zeynep Çalışkanoğlu

München 2024

EXPERIMENTAL ANALYSIS OF FULGURITE FORMATION

Ayşe Zeynep Çalışkanoğlu

Dissertation zur Erlangung des Doktorgrades
an der Fakultät für Geowissenschaften
der Ludwig–Maximilians–Universität
München

vorgelegt von
Ayşe Zeynep Çalışkanoğlu
aus Istanbul, Türkei

München, den 1. Februar 2024

Erstgutachter: Prof. Dr. Donald B. Dingwell

Zweitgutachter: PD Dr. Corrado Cimarelli

Tag der mündlichen Prüfung: 21.06.2024

Nothing in life is to be feared; it is only to be understood.
Now is the time to understand more so that we may fear less.

- Marie Curie

Table of contents

List of figures

List of tables

Summary

Lightning discharges are typically associated with destructive forces; however, they also generate remarkable structures known as fulgurites, discovered in various geological substrates, including sand, soil, and rock. Over time, they have captivated the attention of both scientists and enthusiasts due to their unique and enigmatic features. These distinctive forms exhibit notable variation, influenced by the protolith materials' chemistry and the characteristics of lightning discharges. However, their formation process has remained unknown due to uncertainties regarding the timing and location of lightning discharges.

Lightning discharges cause extreme conditions, including high temperature and pressure, when they strike the ground. They might trigger significant chemical reactions in the material they hit. Therefore, lightning discharges have already been suggested as alternative catalysis for chemical reactions that form the building blocks (i.e., nucleotide and amino acids) to initiate pre-biotic life.

Phosphorus is one of the most critical elements present in building blocks in various forms, but it is thermodynamically stable in nature and low reactive. Therefore, it was not readily available on the early Earth's surface. It has been proposed that lightning can create a more active form of phosphorus due to its power to trigger chemical reactions. Some active forms (i.e., schreibersite and phosphite) have also been identified in sand fulgurites, but sand is not a suitable geological substrate for early Earth environments. Therefore, the possibility that fulgurite formed these structures in the early Earth was unclear.

Under extreme conditions, such as high temperature and pressure, fulgurites undergo chemical reactions that form new compounds, including metallic globules and reduced minerals.

Notably, reduced minerals like phosphite are significant components in pre-biotic chemistry. Thus, fulgurites may be considered a potential source of these minerals and could have played an essential role in the proto-life processes on early Earth. Unfortunately, there is no geological record from early Earth, and obtaining a sample of fulgurite from that time is also impossible. Therefore, replicating fulgurites from possible geological sources might help uncover the formation mechanisms and conditions that are challenging to investigate directly.

Nonetheless, a fulgurite is more than just a product of chemical and morphological changes; it is a time capsule. Each fulgurite captures a moment, preserving tangible evidence of lightning discharge events and the specific environmental conditions during its formation. This record might provide a unique opportunity to gain insights into the properties of lightning discharges in detail.

This thesis focuses on three key objectives to understand the formation and significance of the fulgurites. These objectives include (1) investigating the feasibility of creating experimental fulgurites using a new experimental setup that closely simulates the natural lightning discharges, (2) determining whether the fulgurites produced in these experiments exhibit properties comparable to those found in naturally occurring fulgurite formations, and (3) exploring the potential role of fulgurites in the origin of life and examining the extent to which they could contribute to this phenomenon.

Previous efforts to generate experimental fulgurites were hindered by the inability to replicate similar formation conditions in lightning simulations due to technical limitations. In this thesis, I overcame this struggle using a DC source with a trigger-pulse setup in a high-voltage laboratory designed to mimic natural lightning discharges, according to the lightning research

community. To synthesize fulgurite experimentally, I used a well-characterized sample from the literature, Laacher See volcanic ash, as the target material (**Chapter 2**). Six experiments were systematically conducted on the same target sample under similar controlled conditions, each with a different experiment duration: almost 100 microseconds and 100, 200, 300, 400, and 500 milliseconds. Fulgurites were successfully generated from 100 to 500 milliseconds, except for the 100 microseconds experiment. These results suggest that, beyond a specific duration, the length of a lightning discharge does not significantly influence fulgurite formation. These experimental fulgurites closely resembled natural fulgurites in both state and texture. Additionally, each experimental fulgurite exhibits similar morphological and chemical features. The methodology applied in this study showed how fulgurite can be systematically analyzed and what the basic needs for the formation mechanism are.

Following that, creating an experimental fulgurite in the designated setup highlighted the importance of conducting a systematic comparison to assess its similarity to natural formations to advance our understanding of fulgurite formation mechanisms and contribute valuable insights to the fields of lightning science, geology, and materials science.

In **Chapter 3**, I examined a natural fulgurite recently discovered in situ in Eastern Türkiye, its adjacent protolith, and a fulgurite generated using the same experimental setup mentioned in **Chapter 2**, using the original co-sampled protolith. The first systematic and technically oriented comparison between natural and experimental fulgurites has been made. Both fulgurites exhibited similar morphological and chemical features, including melting sequences and post-melting crystallization. This demonstrates that, through the recommended fulgurite synthesis technique, experimentally generated fulgurites can closely resemble those found in nature. Furthermore, using data from the World Wide Lightning Network, I determined the parameters of cloud-to-ground lightning based on the fulgurite's location and the possible

formation date range. These findings provide initial evidence regarding the parameters of lightning discharges that may be responsible for natural fulgurite formation.

Lastly, I conducted an experiment to assess the potential of fulgurites in generating the essential components required for pre-biotic chemistry (**Chapter 4**). To synthesize fulgurite, I used apatite, the most common phosphorus-containing mineral in primary igneous rocks, thought to have been present on early Earth. I chose apatite over heterogeneous rocks to minimize potential contamination from other mineral compositions. I examined both the pre-experiment apatite and the post-experiment fulgurite in terms of their state, texture, and chemistry. The results indicate that the generated fulgurite contains a reactive P phase, suggesting that fulgurite could have been a source of reactive P phases on the early Earth.

Preamble

Chapters 2 and 4 of this dissertation have been successfully published in peer-reviewed journals. Chapter 3 is currently undergoing review at a peer-reviewed journal. The content of these publications remains unchanged within this dissertation. However, the original format has been modified to align with the thesis's overall layout and format. Additionally, my scientific contribution to an individual study is further listed below.

The complete references for the papers are as follows:

Çalışkanoğlu, A.Z., Camara, A.S.B., Cimarelli, C., Dingwell, D.B. and Kai-Uwe, H. (2023). Experimental generation of fulgurite under realistic lightning discharge conditions. Scientific Reports, 13, 11685 (2023b). https://doi.org/10.1038/s41598-023-38781-8. (**Chapter 2**)

Çalışkanoğlu, A.Z., Cimarelli, C., Dingwell, D.B. and Camara, A.S.B. Experimental vs. natural fulgurite: A comparison and implications for the formation process. *Under review at American Mineralogist.* (**Chapter 3**)

Çalışkanoğlu, A.Z., Dingwell, D.B., Cimarelli, C., Camara, A.S.B., Breitzke, H., Buntkowsky, G., Pasek, M.A., Braun, D., Scheu, B. and Molaverdikhani, K. (2023a). Reactive phosphorus via simulated lightning discharge: A role for fulgurites in pre-biotic chemistry. Chemical Geology, 620, 121343. https://doi.org/10.1016/j.chemgeo.2023.121343. (**Chapter 4**)

Matreux, T., Le Vay, K., Schmid, A., Aikkila, P., Belohlavek, L., **Çalışkanoğlu, A.Z.**, Salibi, E., Kühnlein, A., Springsklee, C., Scheu, B., Dingwell, D.B., Braun, D., Mutschler, H. & Mast, C.B. (2021). Heat flows in rock cracks naturally optimize salt compositions for ribozymes. Nature Chemistry, 13(11), 1038-1045. https://doi.org/10.1038/s41557-021-00772-5. (**an additional outcome of this thesis**)

Chapter 1. Introduction

1.1. Motivation

Lightning discharges are mostly known as destructive forces because they pose significant hazards to both people and the environment (cause fires, damage structures, etc.). Additionally, they sometimes have constructive impacts. When lightning discharges hit the ground, it creates a product known as fulgurite. However, the formation mechanism of the fulgurite has not been fully understood.

Notably, the tremendous energy associated with lightning discharges has sparked theories regarding its possible role in the emergence of life because its extreme heat and pressure might trigger chemical reactions and the fusing of minerals within the fulgurites. This process could potentially create significant compounds for pre-biotic chemistry.

Natural lighting discharges regarding fulgurite formation are very difficult to examine directly due to their unknown time, location, and dangerous high energic features for humans. Might fulgurites be experimentally generated by simulated lightning discharges in the laboratory? Is it possible for experimentally generated fulgurites to closely resemble their natural counterparts? Can these produced fulgurites be used to find answers to their role in pre-biotic chemistry? Those questions led this thesis to focus on fulgurites.

1.2. Fulgurites

Fulgurites are fascinating geological products. They are natural glasses of irregular tubes formed in rock, sand, or soil by cloud-to-ground lightning strikes such as thunderstorms or volcanic eruptions (Fig. 1.1). Lightning discharges strike the conductive surfaces (around 20 kA peak current, Uman et al., 1978), instantly melting the ground material up to 30,000 K (Uman 1969) and causing the grains to fuse within a few microseconds. The molten material

rapidly cools down, resulting in the formation of unique fulgurite shapes. They include a void in the center as a trace of lightning discharge, a fully molten (glassy) zone around the central void, and partially- and non-melted particles surrounding the glassy zone.

Initially, the fulgurites were broadly classified as a sand type (Anderson 1925; Petty 1936; Galliot 1980; Mohling 2004) and a rock type (Purdom 1966; Libby 1986). Later, a detailed classification (Type-I, II, III, and IV) was provided by Pasek et al. (2012) based on the composition, morphology, and textural features of the fulgurites. Type I fulgurites are sand fulgurites characterized by thin walls made of glass. Type II fulgurites are clay fulgurites with thick walls rich in melted material. Type III fulgurites, known as caliche fulgurites, feature thick walls with a low glass content. Lastly, type IV fulgurites are rock fulgurites, which exhibit glass walls surrounding unmelted rock. Examples of different fulgurites can be seen in Fig. 1.2. Although the classification offers valuable insights into the naming of fulgurites, it has overlooked the other potential target materials (such as volcanic) and the influence of material state (such as grain size), both of which are significant for developing a more comprehensive understanding of fulgurite formation and sorting.

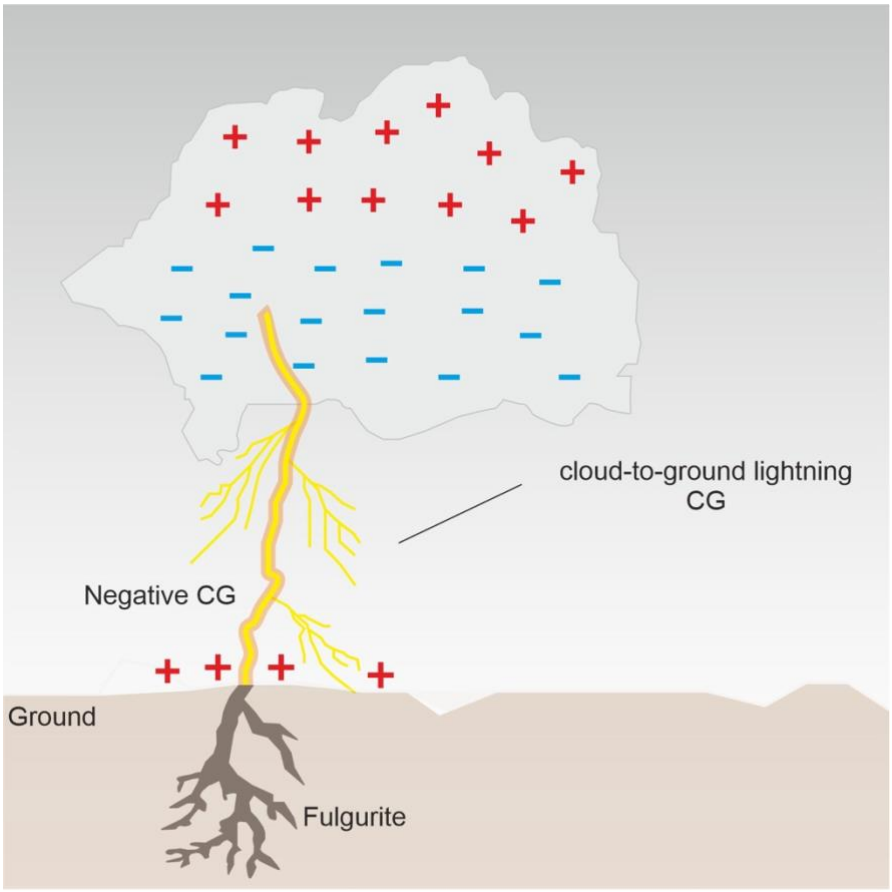

Figure 1.1: Schematic view of fulgurite formation via cloud-to-ground (CG) lightning discharge. Negative CG lightning is more common than positive CG lightning and makes up about 95% of all lightning discharges (Rakov and Uman, 2003).

The fulgurites can have a wide range of compositions, morphology, and colors, as they are influenced by factors such as the protolith material chemistry, potential interactions and reactions, and the diffusion of chemicals between phases upon melting. They are more often found in sand (e.g.., Kenny et al., 2021; Pasek et al., 2012; Ende et al., 2012; Wright, 1999; Sponholz et al., 1993) and less frequently in rocks (basalt - Purdom, 1966; basaltic andesite lava - Castro et al., 2020; gabbro - Grapes and Müller-Sigmund, 2010; granite - Libby, 1988; Elmi et al., 2017; Kuo et al., 2021) (Fig. 1.1). Most of the sand fulgurites present tube-like structures, while rock fulgurites usually display irregular forms in solid material. Despite this variability, fulgurites share common morphological traits. The detailed morphological features of natural fulgurites are described in Chapter 3.

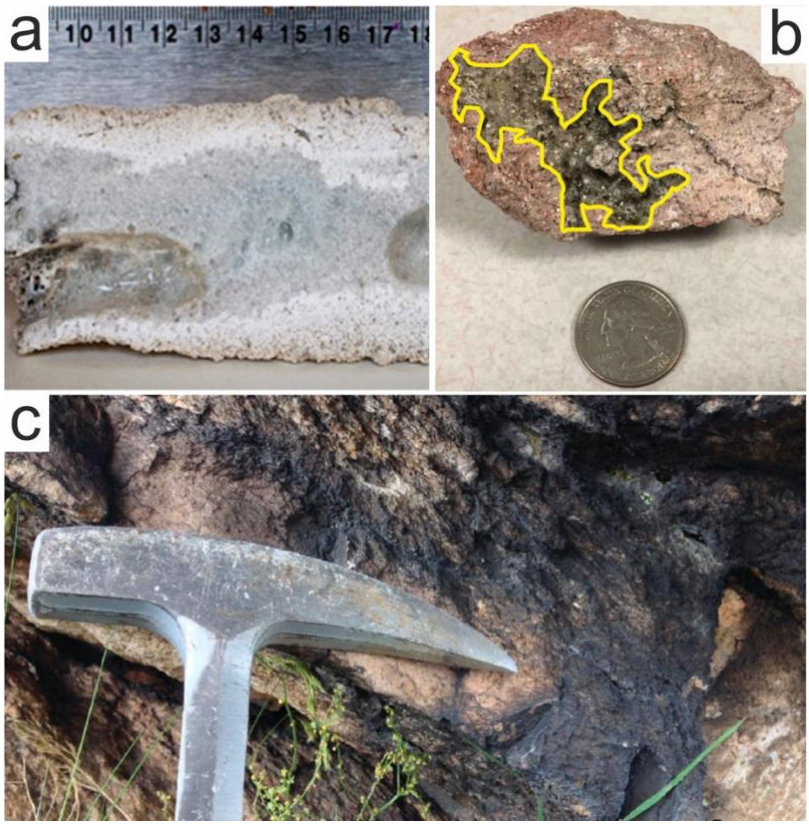

Figure 1.2: Examples of natural fulgurites from previous studies. (**a**) A sand fulgurite was found at Sand Hills, Nebraska (Pasek and Pasek, 2018). (**b**) A natural fulgurite was formed in the basaltic andesite lava at Cascadian volcanic peak, California (Castro et al., 2020). The yellow line outlines the fulgurite. (**c**) The granite surface of Mt. Mottarone, Italy, reveals a dark brown layer, representing a rock fulgurite (Elmi et al., 2017).

Researchers have been conducted on fulgurites to investigate their various morphological and chemical characteristics (e.g., Pasek et al., 2012; Ende et al., 2012). Essene and Fisher (1986) determined an extreme reduction and metal-silica immiscibility in the natural fulgurite, which showed a high-temperature effect on the fulgurite generation. This exploration has encompassed the study of high-temperature mineralization processes, aiming to understand the formation processes and the types of minerals that develop under such extreme conditions (Ballhaus et al., 2017). Daly et al. (1993) made another discovery in the Winans Lake fulgurite, revealing its composition as pure carbon. Later, the elemental form of carbon was found in impact rocks and fire soot.

Furthermore, examining fulgurites has offered valuable insights into reconstructing palaeoecological conditions, as these unique glassy formations can provide evidence of past environmental conditions and their impact on the surrounding landscape (Navarro-González et al., 2007). Moreover, by analyzing the chemical composition and structure of fulgurites, researchers have examined the availability and suitability of these lightning-induced glass formations as sources for the chemical building blocks of life (Pasek and Block, 2009; Hess et al., 2021; Bindi et al., 2023). Through these studies, natural fulgurites have unveiled a wealth of information about Earth's history, geological processes, and the potential role they may have played in the origins of life on our planet.

1.3. The basic mechanism of lightning discharges

Lightning is a sudden electrostatic discharge caused by an imbalance between cloud-to-ground (CG, either thunderstorm or volcanic lightning) or cloud-to-cloud (IC). The CG lightning discharges are subdivided into two main groups: positive and negative, depending on the direction of the current between the ground and the cloud. The IC lightning discharges are categorized based on where they occur: either between two separated clouds or within a single cloud (intra-cloud). Although the frequency of ICs is higher than the CG globally, the CG lightning discharges are the main interest of this thesis due to their significant role in fulgurite formation.

The lighting mechanism has already been explained in literature (e.g., Rakov and Uman (2003); Bazelyan and Raizer (2000); Mazur 2016). Here, the primary mechanism of lightning discharges is explained, with a detailed description of the essential elements required for this phenomenon. The CG lightning discharges start with the breakdown process in the cloud. This process creates a channel of partially ionized air. Next, initial lightning discharge forms and propagates downward. Additionally, the polarity of lightning discharge plays a role in how it

spreads and branches in space and time. When the initial lightning reaches near the ground, opposite polarities from the ground rise. After the initial discharge successfully connects to the ground, a very bright (first) return stroke propagates back to clouds. The current associated with the return strokes mostly lasts for a few hundred microseconds; however, it may sometimes continue to flow at a low current for a few tens to a few hundred milliseconds. Those long-lasting currents are called continuous currents. A slow-rising, long-duration electromagnetic pulse, known as an M component, typically occurs after or during the lightning discharge. It might sometimes be detected as a continuing current. The schematic diagram of the lightning discharges can be seen in Fig. 1.3.

In the end, the initial stroke, first return stroke, and continuing current are the main elements of the natural lightning discharges.

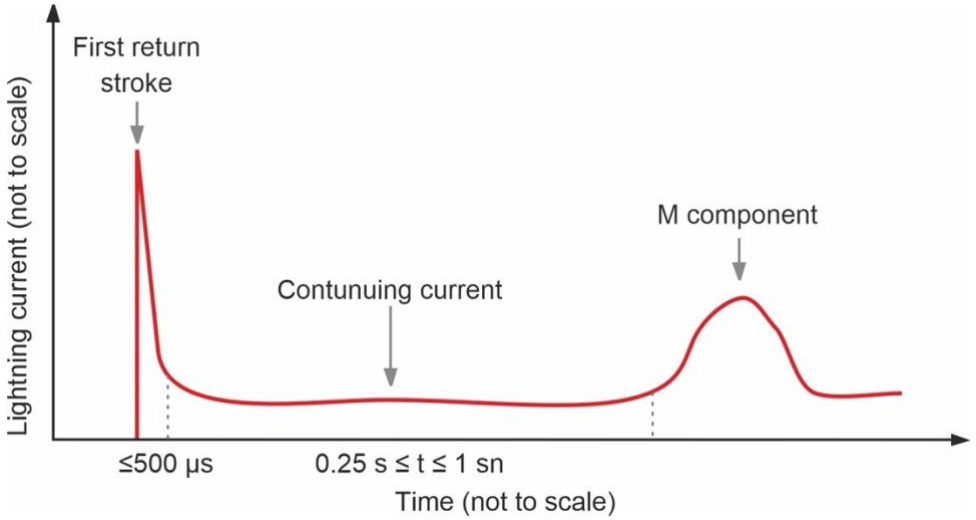

Figure 1.3: Schematic diagram of lightning discharges with important elements. The original diagram was made by Rakov and Uman (2003), and a simplified version is presented here. The M component refers to a slow and continuous current that contributes to the overall duration of a lightning event.

1.4. Background of experimental fulgurite generation

Fulgurites provide valuable insights into various fields, such as geology, physics, and material science. However, the rarity and unpredictable nature of fulgurites limits scientific studies.

Therefore, experimental fulgurite generation provides an excellent opportunity to investigate the formation mechanism and the chemical transformations under extreme conditions. Additionally, it allows the evaluation of the influence of various target compositions and electrical parameters on the final fulgurite properties.

Here, I will provide an overview of the prior experiments (electrical discharge and laser-induced experiments) to generate fulgurites. Later, in **Chapter 2**, the setup used in this thesis will be explained and compared with prior experimental techniques.

1.4.1. Electrical discharge experiments

Lightning was one of the most destructive forces in the 18th century, making it a topic of various discussions in scientific societies. However, natural fulgurites were mentioned only briefly in the earliest publications. The invention of batteries in the late 18th century opened a new door for studying lightning discharges and fulgurites, which resulted in the start of electrical discharge experiments. Beudant et al. (1828) conducted pioneering research on fulgurites, utilizing the Leyden jar battery for their experimental study. They successfully produced a fulgurite (approximately 25 mm) from crushed glass in a brick hole. To enhance the probability of fulgurite formation, they employed a combination of crushed glass and sodium chlorite (low melting degree), producing a nearly 30 mm long fulgurite. In a subsequent study, Butcher (1907) expanded upon the research by employing a set of 12 Leyden jar batteries and using a range of low melting point materials, such as salt, sugar, borax, resin, and sealing wax, as targets. One noteworthy discovery from this investigation was that the generation of fulgurites was not achieved through abrupt and oscillatory discharges. Instead, the probability of fulgurite formation was heightened when employing a less oscillatory current flow aided by a wet string. It is estimated that, at maximum, the Leyden jar batteries could be charged to 20,000 to 60,000 V, which was insufficient to create fulgurites. Arai (1969) presented the first detailed schema of the experiment setup for fulgurite generation (Fig. 1.4). He used a high-voltage DC setup.

However, a crucial element was missing, particularly concerning the component that initiates the entire process: the first-return stroke, an essential component of the lightning discharge responsible for breaking down the dielectric field strength of the original material. Additional circuit elements were required to replicate this high-intensity, rapid, and short-duration component accurately. Incorporating these extra elements, such as capacitors discharged through inductors and resistors, was essential. These components played a vital role in reproducing the realistic characteristics of the first-return stroke. The circuit could mimic this critical lightning component's intense and fleeting nature by discharging capacitors through inductors and resistors. This addition was necessary to ensure a more faithful representation of fulgurite generation and to capture the complex dynamics associated with actual lightning events.

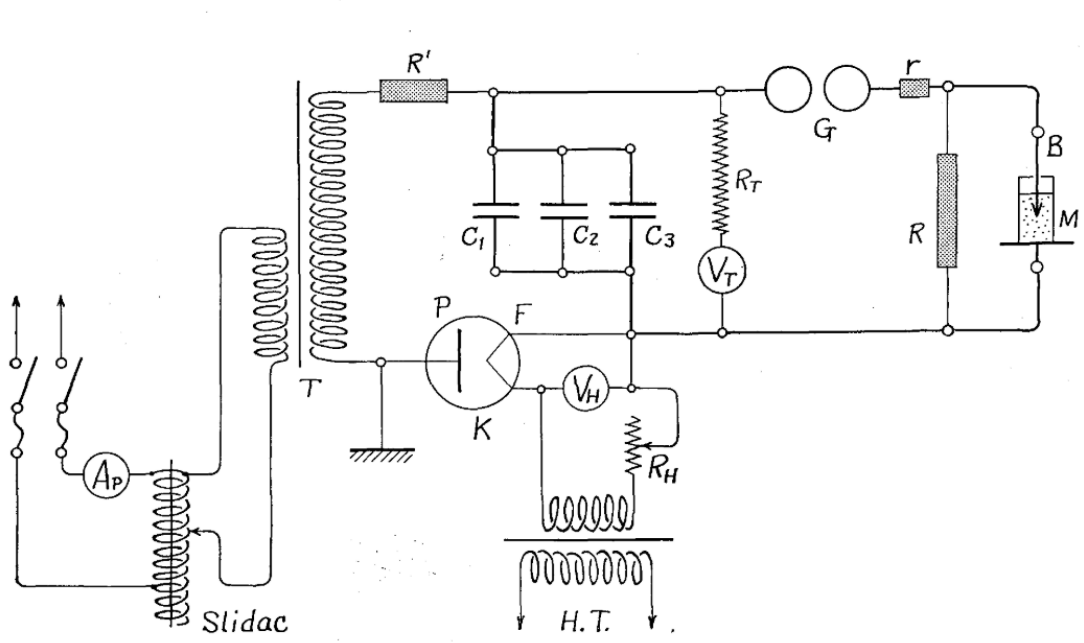

Figure 1.4: The first known detailed experimental setup sketch by Arai (1969), and the details of abbreviations can be seen in his study. It indicates a DC high-tension source and an impulse circuit. Basically, the Slidac–phase voltage transformer, on the left bottom side of the diagram, controls the primary voltage of the high-tension transformer. Then, the charge is carried to the copper plate electrode, on the right side of the diagram for lightning discharge simulation.

Kumazaki et al. (1997) conducted experiments on varying compositions (i.e., natural river sand, fluorite powder, and polyethylene) and grain sizes (coarse, middle, fine). The lightning simulations performed in their experiments were limited to generating solely the first-return stroke. They repeatedly applied the impulse voltage (maximum 3600 kV) several times without any break, which increased the power, of the material and eventually generated a fulgurite. Genareau et al. (2017) conducted a similar experiment using only the first stroke component without repetition. No fulgurites were found; however, lightning-induced volcanic spherules (LIVS) have been generated.

The first known experimental fulgurite generation trial on rock specimens (granite and basalt) was done by Elmi et al. (2018) using a high-voltage Alternating Current (AC) power source (15 kVA). Even though they managed to melt the target material, the AC operated at lower voltages and currents over extended periods than natural lightning discharges. As a result, their setup was less likely to produce the energy required for fulgurite formation because it does not simulate the intense and rapid energy transfer of natural lightning discharges.

Castro et al. (2020) used a modified form of an Electro Melt Simulator (EMS) arc-welder configured by Mueller et al. (2018) to produce the fulgurite. The EMS was used to generate a current maximum of 50 A for 200-300 ms, which was sufficient to melt the material. However, it is important to note that the current produced during their simulations was significantly lower than the immense currents observed in natural lightning phenomena. Natural lightning discharges typically exhibit current magnitudes of approximately 30 kA for negative polarity flashes and around 300 kA for positive polarity flashes, as documented by Uman (2001). This disparity in current characteristics emphasizes researchers' challenge in replicating lightning's accurate scale and power in laboratory conditions.

1.4.2. Laser-induced experiment

Bidin et al. (2018) generated an experimental fulgurite using a high-power laser to extract high-purity silica from synthetic sand from rice husk ash, which is an agricultural waste and causes massive environmental damage. This study provides promising evidence that experimental fulgurite can emerge as a valuable material in the industrial field. However, the laser-induced experiment falls significantly short of mimicking the formation mechanism of lightning in nature, such as energy distribution and time scale. Natural lightning discharge occurs over a relatively large area in a very short duration. In contrast, high-intensity laser beams focus on a small spot and often have a more prolonged interaction duration. Thus, it does not fully capture the natural lightning strikes' complete range of phenomena and mechanisms.

In conclusion, despite the extensive efforts made in previous studies, they have yet to successfully simulate natural lightning discharges with a high degree of accuracy in laboratory settings. The complex and dynamic nature of lightning, with its rapidly changing voltage, current, and electrical path, poses significant technical challenges for replication.

1.5. Significance of fulgurite in pre-biotic chemistry

Early life is an intriguing enigma, captivating the attention of scientists and enthusiasts alike. The mysteries surrounding the emergence of life on Earth, including the questions of when and where it began, remain some of the most fascinating subjects in scientific exploration. To answer these fundamental questions, researchers explore the building blocks of life, such as organic molecules, amino acids, and nucleotides, and investigate plausible environments conducive to the organic process.

Carbon, Hydrogen, Oxygen, Nitrogen, Phosphorus, and Sulfur are the most significant elements for organic life. These elements form necessary compounds in prebiotic chemistry, and studies on their role are ongoing.

One of the complex problems is phosphorus, which is a critical component of essential biomolecules, such as nucleotides and phospholipids. Additionally, a reduced/reactive form of phosphorus is discovered to be used by organics. However, phosphorus is thermodynamically stable in geological settings, which makes it hard to reach for the pre-biotic process. Where the reactive phosphorus forms come from is still unclear. Previously proposed scenarios are: (1) as a result of core formation in early Earth (Schwartz 1972), (2) meteoric delivery of phosphide minerals (Pasek and Lauretta, 2005; Bryant and Kee, 2006), (3) reduction of phosphate to phosphite by under low-temperature condition (Herschy et al., 2018), and (4) reduction of phosphate to phosphite by lightning (Glindemann et al., 1999; De Graaf and Schwartz, 2000; Pasek and Block, 2019; Hess et al., 2021).

The discoveries of reactive phosphorus forms in a sand fulgurite (22% of iron phosphide and 37-68% of phosphite) by Pasek and Block (2009) (Fig. 1.5a) and in a clay fulgurite (schreibersite, $(Fe, Ni)_3P$ - phosphide) by Hess et al. (2021) (Fig. 1.5b) indicate that fulgurites might be a potential host for reduced forms. However, these fulgurites were generated from no feasible early Earth material. Thus, the feasibility of the fulgurite hypothesis remains uncertain until this thesis.

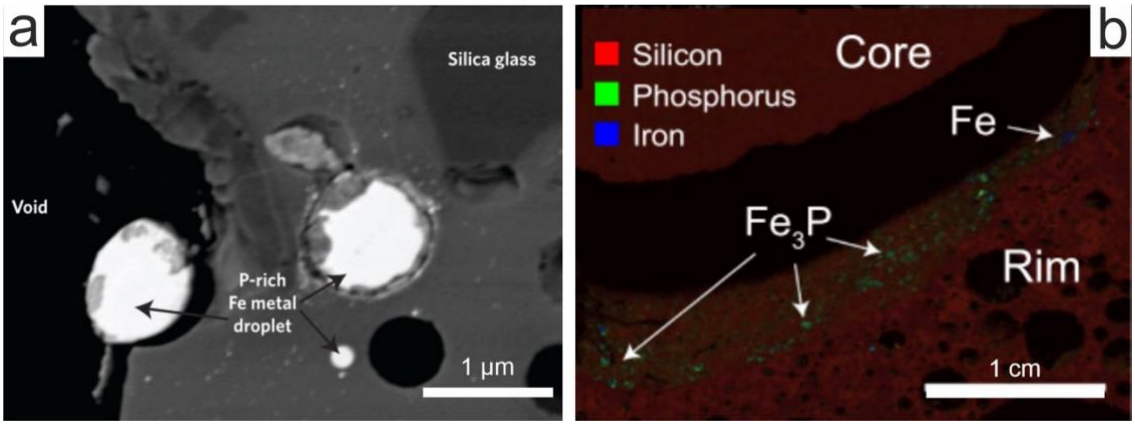

Figure 1.5: (**a**) Fe–P metal alloy spherules were detected in a fulgurite from York County, Pennsylvania (Pasek and Block, 2009). (**b**) Schreibersite (Fe_3P) and native iron (Fe) spherules were found in clay fulgurites from Glen Ellyn, Illinois (Hess et al., 2021).

1.6. Aims of this study

This study aimed to investigate fulgurites using a new experimental setup that closely mimics natural lightning discharges. In addition, this study focused on investigating the significance of fulgurites in a broader perspective. In pursuit of this objective, this thesis aimed to address the following research questions:

⇒ To what extent is it feasible to create fulgurites in an experimental setting?

⇒ Do experimentally produced fulgurites exhibit similar properties to natural fulgurites?

⇒ May fulgurites have played a significant role in pre-biotic chemistry?

Most fulgurite studies are based on natural sand fulgurites and are limited to morphological and chemical changes. However, the formation mechanism of the fulgurite has not been thoroughly explored, mainly due to technical limitations in simulating natural lightning. For this reason, the first part of this study (**Chapter 2**) focused on investigating the formation process of the fulgurites under a controlled environment via a realistically simulated lightning discharge in the high-voltage laboratory.

Furthermore, the study also aimed to determine whether experimentally produced fulgurites exhibit properties comparable to their natural counterparts. To address this question, we have used a natural fulgurite sample, its protolith material, and an experimental fulgurite generated using the protolith material of natural fulgurite via our experimental setup. A comprehensive comparison between natural and experimental fulgurites is detailed in **Chapter 3**. The analyses covered various aspects, including their physical properties, chemical composition, and structural features to seek similarities and differences of experimental and natural formation processes within the fulgurites. Furthermore, the lightning discharge parameters, which could potentially form natural fulgurite, were provided from the World Wide Lightning Location Network data.

Lightning discharges have been previously associated with chemical reactions on the ground materials, such as reducing elements due to their energetic nature. Previously, particular components like phosphite and schreibersite-reduced (reactive) Phosphorus were discovered in sand fulgurites. These components are significant for pre-biotic chemical reactions. However, the sand does not fit the geological setting of the early Earth. The formation of these components in the early Earth conditions remains a mystery. **Chapter 4** explored the possibility of creating the essential components for pre-biotic chemistry by utilizing a high-phosphorus content material (apatite) that was present in the early Earth environment.

Chapter 2: Experimental generation of fulgurite under realistic lightning discharge conditions

2.1. Abstract

Fulgurites have been documented in geological deposits from throughout Earth's history. They have also been assigned a potential role in prebiotic chemistry as a source of reactants. Fulgurites are generated in nature by cloud-to-ground lightning strikes. The unpredictability in space and time of the occurrence of lightning events has limited the investigation of both the mechanisms and the conditions under, which fulgurites form. A laboratory-based approach can mitigate these limitations. Here, we describe experimentally generated fulgurites generated from Laacher See volcanic ash. We employ a DC source with a trigger-pulse setup in a high voltage laboratory, whose capabilities enable experimental conditions that correspond closely to the electrical characteristics of natural lightning strikes. The experimentally generated fulgurites closely resemble naturally occurring fulgurites in both state and texture. These experimental investigations yield a high reproducibility of the characteristics of fulgurites generated under well-constrained conditions, enabling some inferences to be made regarding the processes involved in the generation of fulgurites in nature. This work provides a basis for a systematic characterization of experimental fulgurites and the characteristics of lightning discharges.

2.2. Introduction

Fulgurites, from the Latin word for lightning - fulgur, generally take the form of natural glassy irregular tubes generated by lightning strikes in the sand, soil, or rock. Natural fulgurites were first described (in sandy sediments) by Herman in 1706 (Rakov 2008), and the oldest fulgurite

found to date has been speculated, based on the fossiliferous Carboniferous rocks overlying the host, to be of Permian age (Harland and Hacker, 1966). The fulgurites present on Earth form from cloud-to-ground lightning strikes (by either thunderstorms or volcanic eruptions) or as a result of accidents involving electric transmission lines(Kassi et al., 2013; Martín-Ramos et al., 2019; Alte da Veiga et al., 2021). Natural fulgurites have been explored in terms of their morphological and chemical states(Essene and Fischer, 1986; Pasek et al., 2012; Stefano et al., 2020; Elmi et al., 2021), including the description of high-temperature mineralization (Ballhaus et al., 2017), reconstruction of paleoecology (Navarro-González et al., 2007), and evaluation of the availability of chemical sources for pre-biotic chemistry (Pasek et al., 2009; Hess et al., 2021).

Experimentally generated fulgurites have also been briefly described in some preliminary feasibility studies (Beudant et al., 1828; Butcher, 1907; Arai, 1969; Kumazaki et al., 1997; Elmi et al., 2018; Castro et al., 2020). These valuable pioneering scientific inquiries have generally not been subject to the standard protocols of the natural lightning research community and generally lack the reproducibility and precision of a systematic approach. The reasons generally lie in the experimental technologies employed. The current generated by the Leyden jar battery (ca. 20 - 60 kV) was, for example, insufficient to create fulgurites closely resembling natural ones (Beudant et al., 1828; Butcher, 1907). Subsequent experiment setups were missing inductivity (Arai, 1969), and/or they produced solely a first-return stroke component (the component of the lightning discharge vital for breaking down the dielectric field strength of the original material) (Kumazaki et al., 1997; Genareau et al., 2020). The pulse they generated using the sinusoidal waveform aids the dielectric breakdown of the sample, ultimately generating melting, but it is not sufficient to reproduce the typical morphology of fulgurites (Elmi et al., 2018). The produced current (50 A) by the electro melt simulator for 200 - 300 ms

used by Castro et al. (2020) was well below the current condition of natural lightning (~30 kA for negative polarity and ~300 kA for positive polarity flashes (Uman 2001)).

The experimental setup used in our study (DC source with trigger pulse) has been designed and constructed to ensure compliance with the lightning research community's recommendations for lightning strike studies (e.g., waveforms IEC 62305 (International Electrotechnical Commission [IEC] 2010)) and is located at the Universität der Bundeswehr (UniBw), Munich, Germany. A major advantage of this setup is that these experiments can be easily and very precisely reproduced.

Here, we use volcanic ash from the Laacher See, East Eifel volcanic field, Germany, as pristine material for the generation of the experimental fulgurites and systematically describe their formation mechanism and characteristics as a function of the varying conditions of the discharges.

2.3. Method

2.3.1. Sample preparation

To quantify the morphological properties of the fulgurite, all fulgurites were cut perpendicular to their long axis using a precision diamond wire saw. After that, half of each fulgurite sample, around 50 g of natural LSB, and synthesized LSB glass were ground in an agate mortar in a vibration mill below 63 µm for helium pycnometer analysis. Embedded epoxy mounts were also prepared from the other half of each fulgurite for further analysis.

2.3.2. Scanning electron microscope

The natural apatite and experimentally generated fulgurite were analyzed using a Hitachi SU 5000 scanning electron microscope (SEM) at the Department of Earth and Environmental Sciences of the LMU University of Munich. Backscattered electron images (BSE) of representative portions of the apatite and fulgurite were acquired at varying magnifications (i.e.,

100x, 200x, etc.). Data collection was conducted by Aztech (version 6.0, Oxford Instrument, AZtechEnergy Advanced EDX-System).

2.3.3. He-pycnometer analysis

The density of natural LSB, synthesized LSB glass, and all fulgurites were measured using a Quantachrome helium pycnometer at LMU University of Munich. Each fulgurite was cut in half longitudinally, and these half parts of the fulgurites were used for the measurements. All samples were crushed down to 63 µm to eliminate voids, especially the isolated porosity that can affect the density measurements. Each of the densities was measured at least ten times, and the values are presented in Appendix A.

2.3.4. Differential scanning calorimetry

The calorimetric glass transition temperatures have been measured using a Netzsch 404 C Pegasus. Samples between 50-60 mg were placed in a Pt-crucible and heated above the glass transition peak in a dynamic, high-purity Argon atmosphere. The samples were then cooled and subsequently reheated at a rate of 10 K/min. Peak glass transition temperatures were extracted from the reheating segments. Fig. 2.6 shows the DSC raw curves for the different samples. The samples have been shifted manually for clarity. A temperature correction of -4.2°C must be applied to all glass transition temperatures based on a temperature calibration using the melting points of indium, zinc, aluminum, and gold. The error of the temperature measurements is +/- 1°C.

2.4. Natural fulgurites

Here, we define some basic characteristics of natural fulgurites to facilitate the comparison of natural fulgurites with their experimental counterparts. Natural fulgurites may exhibit diverse compositions and colors, which depend on the pristine material chemistry, possible interactions and reactions, and chemical diffusion between phases in contact upon melting. Such fulgurites share some general morphological characteristics; commonly exhibiting sub-circular cross-

sectional structures characterized by a central void (either open, partially closed, or closed) which represents the path of lightning propagation into the target material. Their lengths vary from centimeters to several meters, with variable wall thickness. The geometry of the central void can reveal tortuous morphologies with branching reflecting secondary conductive paths along the main direction of propagation of the lightning discharge. The external surfaces of natural fulgurites typically display a rough texture and may be partially covered with the remains of pristine material and partially melted crystals adhering to the melted fulguritic mass. In contrast, the fulgurites' interior surfaces generally exhibit a vitreous smooth surface surrounding the central void. A remainder of partially melted crystals can be found on the surface of the glassy volume of the fulgurite. A representative natural fulgurite sample from the Sahara Desert in Africa (De Campos and Hess, 2021) and a general cross-sectional and longitudinal view illustrating the fundamental morphological features of a fulgurite are presented in Fig. 2.1.

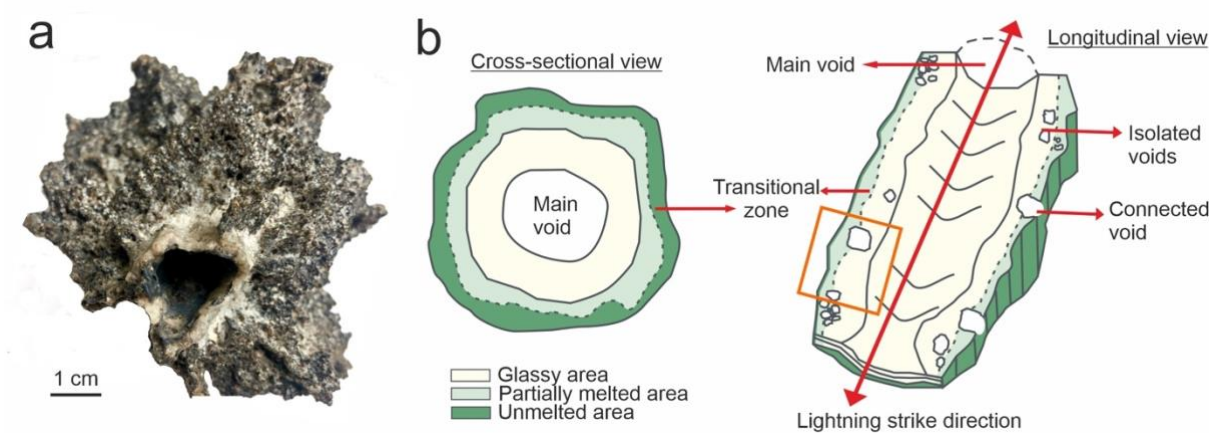

Figure 2.1: (**a**) An example of natural fulgurite (i.e., sand) from the Sahara Desert. (**b**) A representative cross-sectional and longitudinal view of a natural fulgurite with detailed morphological description. The orange square in the longitudinal view corresponds to the area where BSE images of the generated fulgurites in Fig. 2.4a-e are presented.

2.5. Experimental setup

We simulated lightning discharge in an insulated sample container by a DC source with a trigger-pulse setup (Fig. 2a). The DC setup simulates the effects of natural lightning current discharges within controlled and highly reproducible conditions. The main elements of the setup are a Marx-generator, a battery system (DC source) consisting of 60 silver-lead-acid batteries of 12 V connected in series (720V - 600 A), circuit breakers and switches, a switching controller and an extender safety circuit (Fig. 2.2a). The setup is designed to represent the main current components of natural lightning (Rakov and Uman, 2003), namely: (1) first return stroke, which has the highest current amplitudes – typically of the order of 10^3 A lasting up to several 100 µs; (2) subsequent return stroke, which is lower in amplitude and duration but often with a significantly higher current (up to a few 100 kA/µs); (3) the long-duration continuing current, which exhibits much lower current amplitudes of just a few 100' A (Aleksandrov et al., 2000), but of much longer duration (generally lasting up to 100 ms). In our setup, the first return stroke is initiated by a voltage impulse, using the Marx-generator (impulse currents of 1500-5000 A for approximately 100 µs) to trigger the spark gap between electrodes located in the insulated sample container, thus allowing the breakdown of the dielectric strength of the target material. Next, the DC source initiates the production of the long-duration continuing current. Two circuit breakers are arranged to stop this current at a pre-set time duration. In our experiments, we simulate positive lightning discharges by positively charging the top electrode while the bottom one is negatively charged. Negative discharges can also be simulated with the same setup and produce fulgurites showing no significant difference from those generated by positive discharges. Fulgurite generation by positive discharges is, however, preferred for practical reasons during the preparation of the experiments.

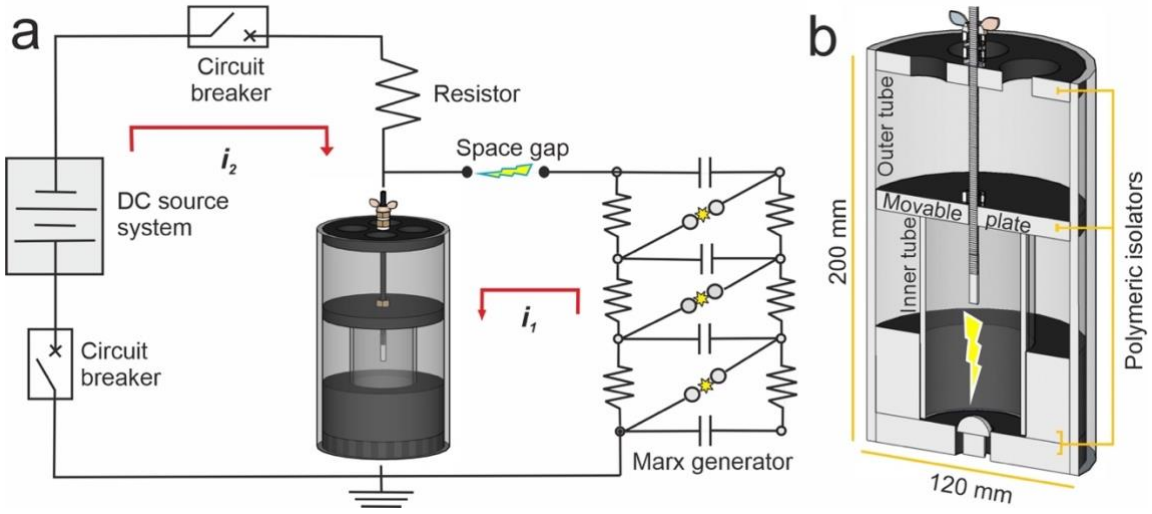

Figure 2.2: Schematic view of the experimental setup. (**a**) Circuit diagram of the DC source with trigger-pulse setup and 3D image of the sample container. The first return stroke (i_1) indicates the lightning first return stroke component and the long-duration continuing current (i_2) indicates the lightning continuous current component. (**b**) A sectional view of the cylindric sample container.

The insulated sample container has two coaxial cylindrical containers made of 3 mm thick plexiglass tubes: the inner tube (height (h): 200 mm and diameter (D): 120mm) contains the sample, while the outer tube (h: 60 mm and D: 60 mm) prevents mobilization and dispersion of the sample in the laboratory space when hit by the discharge (Fig. 2.2b).

Electrically non-conductive and mechanically resistant polymeric cylindrical disc plates are located at three positions within the sample container (top, middle, and bottom). The top and bottom plates are fixed, whereas the middle plate is designed to be movable, which enables the adjustment of the distance between electrodes to optimize experimental conditions and, thereby, the consequences of any abrupt mechanical shock in the container during the experiments. The lightning discharge is generated between two electrodes with different geometries: a bullet-shaped upper electrode (h: 27.42 mm and D: 13 mm) attached to the middle plate and a dome-shaped lower electrode (h: 19 mm and D: 46 mm) attached to the bottom plate.

All the experiments were conducted at atmospheric temperature and pressure. The environmental conditions in the laboratory were measured regularly by a GFTB 100 precision

Thermo-Hygrometer and Barometer, which showed a stable environment (T: ~19.2°C ± 0.2, P: ~946 hPa ± 10 and RHmean: ~50.0% ± 0.6) during the experiments.

Three test experiments were performed to adjust the distance between the electrodes and to determine the optimal amount of target material to fill the inner tube. Subsequently, six experiments were performed under similar experimental conditions (i_1: up to a few 100 kA/µs and i_2: 220 A - 350 A) but with varying durations (0, 100, 200, 300, 400, and 500 ms). The lowest duration time of continuing current allowed by our setup is 100 ms, which is also close to the average duration (nearly 150 ms) for long-duration continuing current produced by natural lightning, as claimed by Brook et al. (1962). From 200 ms to 500 ms, experiments were conducted to examine the duration of extremely prolonged continuing current effect on the fulgurites' structure. Hereafter, we will refer to the experiments as T0, T100, T200, etc., according to the characteristic duration of the continuing current phase. The T0 experiment was performed by striking the sample with the first return stroke alone with no continuing current phase. The inner tube was filled with 200 g of target material for each experiment, and all experiments were performed with new sample batches. The spacing of the electrodes was held constant at 50 mm for all the experiments. It is worth noticing that the fixed distance between the electrodes largely determines the maximum length of the experimental fulgurites. A schematic electrical waveform generated by the setup for each experiment duration can be seen in Fig. 2.3a (current waveforms with a digital oscilloscope: Appendix A).

2.6. Target material

As pristine material for the experiments, we used pre-sieved volcanic ash particles of Laacher See pumice, the "Laacher See Bimse" (hereafter LSB) deposits produced during the 13 ky eruption of Laacher See volcano (Eifel, Germany) provided by ROTEC GmbH. We use the fraction size of LSB particles between 90 and 300 µm with the addition of 3 wt.% of very fine ash (<63µm) (Gaudin and Cimarelli, 2019). The LSB is a multi-phase material consisting

mainly of vesiculated glass particles, lithic fragments, and loose crystals (Bogaard und Schmincke, 1985), which presents connected and isolated porosity (Fig. 2.3b). The juvenile material is phonolitic in composition (SiO_2 ~55 wt.%; Al_2O_3 ~20.5 wt.%; Na_2O ~11 wt.%; K_2O ~5.5 wt.%) and the main crystalline phases (5 - 8%) are quartz, plagioclase, sanidine, and clinopyroxenes (Wörner and Schmincke, 1984; Müller et al., 2021). The feldspar and quartz crystal grains are ~1 wt.% of the total bulk composition, and the average fraction size of these crystals is 250 µm. The average density of the LSB used here was measured as 2.42 ± 0.02 g/cm^3 by helium pycnometer (Springsklee et al., 2022). The LSB volcanic ash was chosen as a starting material as it has been extensively characterized and deployed in previous lightning discharge experiments (Gaudin and Cimarelli, 2019; Springsklee et al., 2022; Mueller et al., 2018; Stern et al., 2019). The grain size distribution of LSB approximates that of silt and sand sediments where fulgurites are often found. Moreover, its mineral assemblage contains quartz and feldspars, which are common minerals in sediments. Hence, this volcanic granular material offers the advantage of studying the physical and chemical modification of its glass and crystal grain components upon lightning-induced melting reactions.

2.7. Experimentally generated fulgurites

2.7.1. Morphology

We generated five fulgurites in 6 experiments. In the T0 experiment (100 µs impulsive current and no continuing current) was only found some partial melting and sintering of particle clusters. On the contrary, all experiments characterized by variably long-continuing currents (T100 and T200, etc.) did generate fulgurites (Fig. 2.3c-g). The exterior surface of all fulgurites exhibits the reddish-brown color of the pristine material. Most of the surface of each fulgurite is covered by remnants of pristine material and partially melted crystals. The fulgurites from T100 to T400 experiments have a similar length of 45 mm, while the T500 fulgurite has a length of 35 mm, i.e., 5 and 15 mm shorter than the distance between the electrodes, respectively. The

thicknesses of the unmelted and partially melted area of the fulgurites vary up to 0.6 mm and 0.5 mm, respectively, and the glass area exhibits variable thickness overall, regardless of the experiment duration. The main void also exhibits a variable diameter in different parts of the fulgurite, reflecting its irregular geometry. The average diameter of T100, T200, T300, and T500 fulgurites is around 25 mm, whereas T400 fulgurite is about 20 mm in diameter. All fulgurites exhibit a tube-like morphology, exception made for T500. The T100, T200, and T500 fulgurites display short apophyses (branches). An open central void is only observed in the T200 fulgurite. The total mass of the fulgurites (2.432 g - T100, 4.998 g - T200, 6.002 g -T300, 8.370 g - T400, and 9.589 g - T500) shows a gradual increment with increasing duration of the continuing current.

2.7.2. Mineralogy

All fulgurites have been sectioned longitudinally (i.e., parallel to the direction of lightning discharge). Cross sections from the glassy area (center) to the external area are shown in Fig. 2.4a,e. Partially melted crystals are detected in partially melted and glassy areas. They are mostly constituted by quartz with minor Fe-oxide and K-feldspar, while no residual pyroxene crystals were observed (Fig. 2.4h,j). The other oxides (i.e., Cupper and Wolfram composites) are also found, and their size ($< 10^3$ nm) is tiny to present and difficult to resolve in the BSE images. The size and the fraction of these crystals and oxides show no change with increasing experiment duration, nor do they exhibit a specific spatial distribution.

Voids are observed in all fulgurites. No correlation was found between their size, number, and spatial distribution with the duration of each experiment. They display complex shapes due to the presence of partially melted crystals. Some of the voids also appear as coalesced. They predominantly cluster to form a layer between the glassy and partially melted areas, but some voids are also detected within the glassy areas. The voids in the glassy area are up to 20 mm in

length, whereas the voids between the unmelted and partially melted areas are up to 0.7 mm in length. (Fig. 2.4c).

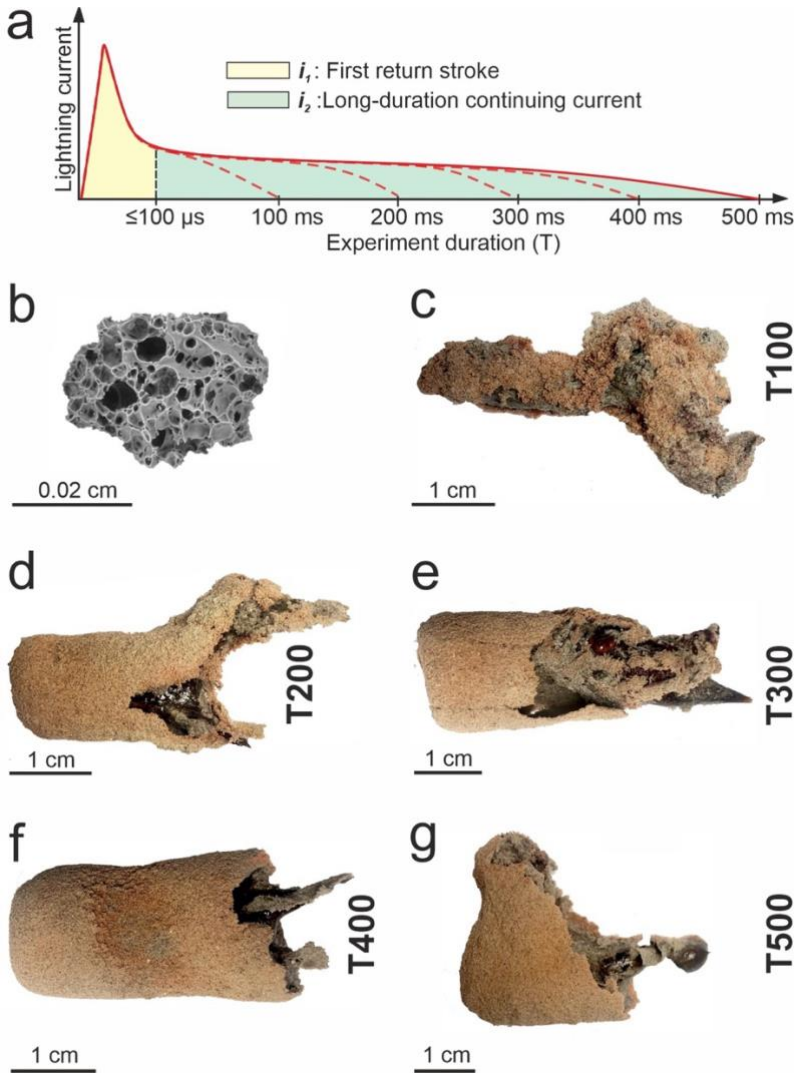

Figure 2.3: (**a**) Schematic composite electrical waveform of the experimental lightning components i_1 and i_2 for different experiment durations in µs and ms. (**b**). A SEM-BSE image of a pristine clast of the LSB. (**c-g**) Pictures of experimentally generated fulgurites under the variable long-duration continuing current (100-500 ms). The left end of each fulgurite corresponds to the portion adhering to the lower electrode in the experimental setup.

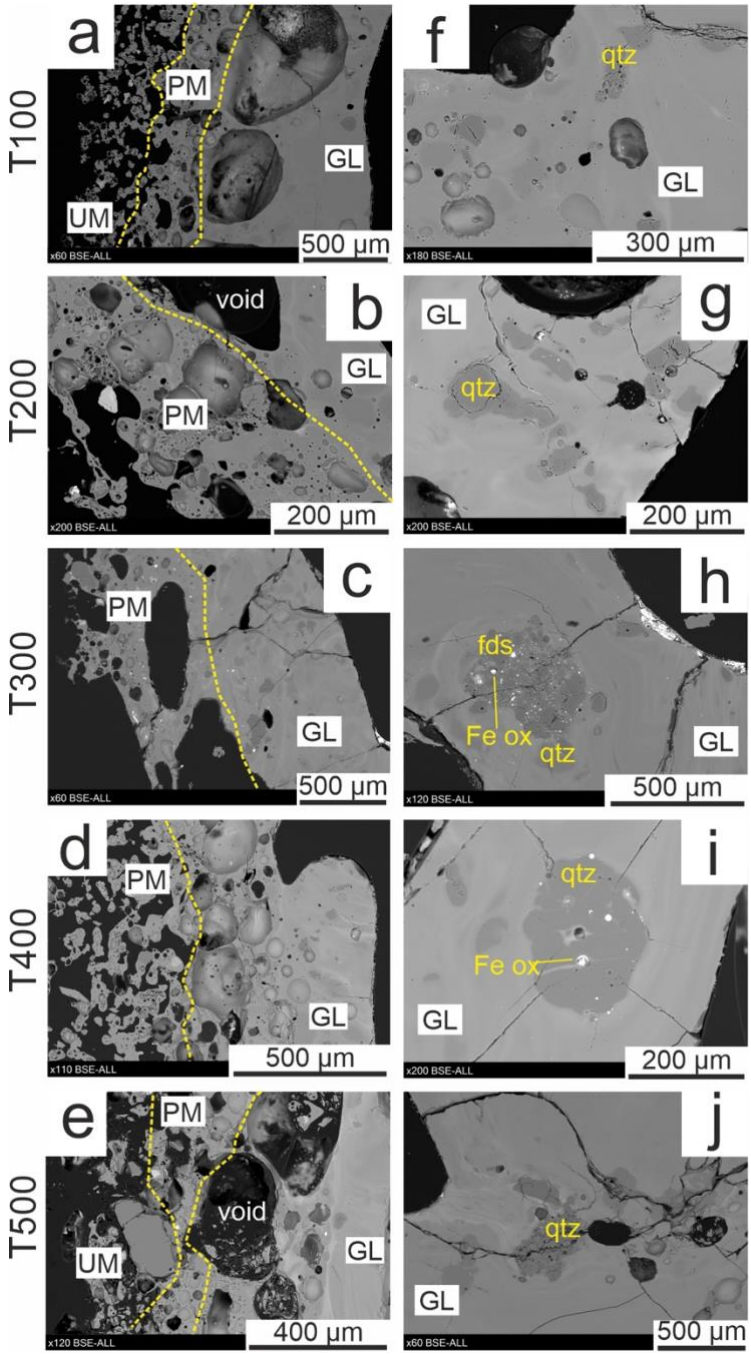

Figure 2.4: (**a-e**) BSE images of half face of each cut fulgurite as referred to in Fig. 2.1b. Yellow dashed lines on the images mark the transitions between textural domains. (**f-j**) Images of the partially melted crystals in the glassy area of the fulgurites. Quartz: qtz, Feldspar: fds, and Iron-oxides: FeO. GL: Glassy area, PM: Partially melted area, and UM: Unmelted area.

2.7.3. Density and porosity

In order to quantify the density and porosity as a function of melting duration, we used 2D image (BSE) analysis as representative of the 3D vesicularity combined with helium pycnometry data (Fig. 2.5a,b; Appendix A). The density of the pristine material (glass + multiphase crystals) is 2.42 ± 0.02 g/cm^3 (Springsklee et al., 2022). Firstly, all pristine materials adhering to the solid fulgurite were cleaned by brushing before being crushed to ≤ 63 µm for the correct evaluation of the analyses. The fulgurites (glass and partially melted crystals, possibly minor unmelted crystals) exhibit a density value of around 2.48 ± 0.02 g/cm^3. The T300 is the least dense among all fulgurites, with around 2.46 ± 0.007 g/cm^3. The density value (2.42 ± 0.004 g/cm^3) of the synthesized LSB glass (glass and possible minor microcrystals) was also measured to compare with all fulgurite samples to see the expansion ratio of fulgurites. The fulgurites indicate a slightly higher density than LSB and synthesized LSB glass.

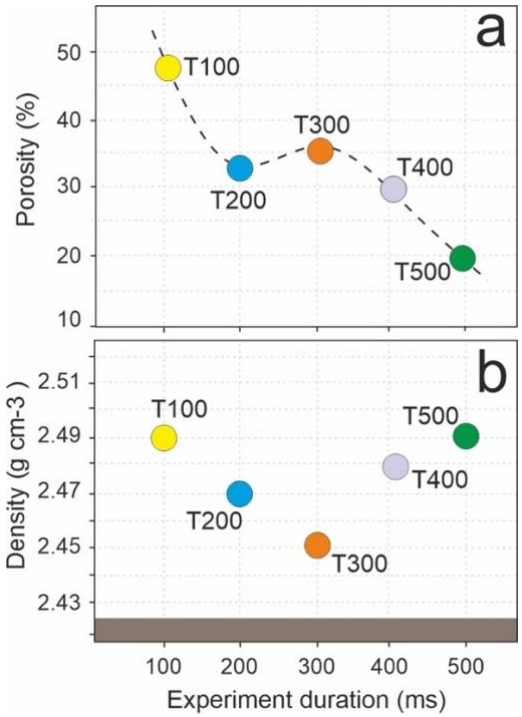

Figure 2.5: (**a**) The porosity calculation from 2D image analysis of all fulgurites. (**b**) Density measurements of LSB, synthesized LSB glass, and all fulgurites. The brown area represents LSB (2.42 ± 0.02 g/cm^3) and synthesized LSB glass (2.42 ± 0.004 g/cm^3)densities for

comparison. The error of the calculated and measured values for each experimental run is within the size of the symbols.

A mosaic of the BSE image of each fulgurite is used to estimate the porosity ratio. We exclude the voids among the pristine particles in the unmelted area to match the density measurement. It is found that the porosity ratio of the fulgurites (glassy + partially melted area) reduces from ~47% in T100 to ~18% in T500.

2.8. Discussion

We successfully generated five fulgurites using natural volcanic ash samples of phonolitic composition and consistent grain size (<300 μm) distribution by exposing the ash to high-current impulsive transients and variable duration of continuing current. Although our setup does not allow direct observation of the formation of the fulgurites, the videography of the experiments and detailed characterization of the resulting fulgurites, together with the imposed experimental conditions, allow insight into the fulgurite formation. Our fulgurites present a tube-like shape with a thick glass wall and are coated with thin pristine particles (crystals + glass) and partially melted crystals. These fulgurites do not fit into the fulgurite classification (Type I-sand, II-soil, III-caliche, VI-rock, and V-droplet) proposed by Pasek et al. (2012). Although that classification scheme tackles the difficult task of ordering the complex nature of fulgurites, it does not include fulgurites from volcanic protoliths. Material composition as well as the size and nature of its components -especially when the protolith consists of incoherent sediments or clastic rocks- play a crucial role in the morphology, density, porosity, and glass proportion of the fulgurite considering the variations in the current flow and duration of the lightning strike.

In the high current and high voltage (up to a few 100 kA and 150 kV) experiment, the starting material was exposed to a highly energetic event only for a very short time (100 μs), and some partial melting of particle clusters was found. Fulgurites were generated only in the high voltage

and current impulse experiments with a continuing current (220 A - 350 A) of variable duration (100 ms to 500 ms) (Fig. 2.3c-g). Results of the high current impulse experiments by Genareau et al. (2020) also support our finding that the initial high current impulse alone is insufficient to produce enough melting to generate a fulgurite body. The addition of a prolonged continuing current phase, instead, allows the necessary energy (heat) transfer required to sustain the melting process of the pristine material and is often associated with lightning-ignited fires (Latham and Williams, 2001; Pineda et al., 2014; Pérez-Invernón et al., 2022). Measured continuing currents in natural lightning have revealed variable durations and have been referred to as very short (3-10 ms), short (10-40 ms), and long (>40 ms) by Lapierre et al. (2014). Studies show that, although infrequent, continuing current following return strokes can last longer than 100 ms and can exceed 350 ms (Lapierre et al., 2014; Saba et al., 2006). In our study, the minimum continuing current duration at which substantial melting is first observed is 100 ms (experiment T100). This is also the shortest continuing current duration that can be achieved with our setup; hence, we cannot exclude that melting may be already produced by shorter continuing currents, other parameters (i.e., composition, grain size distribution, and electrodes' gap) kept constant. A striking difference in the structure of the fulgurite is observed between experiments with no continuing currents and a continuing current of 100 ms (i.e., experiments T0 and T100, respectively). Exposure of the pristine material to longer continuing currents (i.e., T200 and T300) does not produce substantial structural and chemical changes in the experimental fulgurites relative to T100.

The state of the pristine material and the lightning discharge characteristics have a strong influence on the formation process of the fulgurites. Silicate glasses are more suitable target materials for fulgurite generation due to the lower melting temperature of glass as compared to the melting temperatures of silicate minerals. The presence of organic matter (i.e., lichen, roots) in the pristine material can also create a local positive electrostatic charge to which the lightning

can attach (Elmi et al., 2019). Burnt organic matter might thus increase the opportunity to find elements in their reduced form (i.e., phosphorus) in the fulgurite composition (Elmi et al., 2017; Wasserman et al., 2002). These elements are also referred to as a substantial matter for the organic forms (Pasek et al., 2012), which makes fulgurite attractive for the emergence of life studies. The presence of organic matter in our pristine samples is to be excluded as the grains are obtained by fresh rock exposures. However, some levels of chemical weathering cannot be excluded a priori.

Additional experiments by our group (not presented here) and Teixeira (2019), run under similar electrical conditions (constant experiment duration - 500 ms), have also revealed that increasing the proportion of larger grains in the target material plays a vital role in the fulgurite formation process, independently on the mineral phase composition. A prevalence of the larger grains (>300 µm) in the pristine material seems to prevent the shaping of the fulgurite in its form, while they seem not to prevent the shaping of the fulgurite when in moderate to low amounts. However, as shown in this study, larger grains undergo thermal deformation from their outer boundaries (Fig. 2.4f-j). On the other side, Teixeira (2019) indicates that smaller grains (40-150 µm – quartz) were completely melted in the formation of the fulgurite. Wadsworth et al. (2017) also support our finding in that the edges of the smaller (nearly 310 µm) volcanic ash particles would round up in the ionized lightning channel for heating durations of 3 ms and temperature exceeding 3000 K, while larger grains would retain their original shape. Elmi et al. (2017) show that an uncrushed holocrystalline rock (an unaltered block of granitic rock sample) exposed to the AC source voltage (up to 150kV) with 26.5 cm distance of electrodes did also not generate any melt. This indicates that after the grain size exceeds a certain limit, the formation of a fulguritic mass is greatly inhibited.

The morphology of the fulgurite is highly associated with the state of the pristine material. For instance, the homogeneous target material content decreases the likelihood of branch formation

due to the low resistive root for the lightning discharges, while the heterogenous content of the target material increases the least resistance root, and generated fulgurites might present several branches in different sizes. Therefore, there are almost no branches found on our fulgurites, which are generated from homogeneous material. (Fig. 2.3e,f).

The average length of all fulgurites is measured as nearly 45 mm, except T500 - 35 mm. It is seen that the length of fulgurites is limited to the gap between the specified electrodes (50 mm). The ratio of the average diameter between the fulgurite (in total nearly 25 mm) and the main central void (around 5 mm) is 5, and it is similar for all the experimental fulgurites, except experiment 500 ms. It is clear that a longer time (continuing current) applied to heat on the target material under the same distance of the electrodes does not change the tube geometry of fulgurite until the density of the molten material is capable of maintaining a unique form during cooling. Once we exceed this point, which is 500 ms in the present study on the particular composition, the tube structure collapses, destroying the main voids. On the other hand, we know from other trial experiments that increasing the distance of the electrodes has an effect on reducing the diameter of the central void, regardless of the composition of the target material. The bulk mass of the fulgurites increases with the duration of the continuing current; however, the density of the fulgurites varies in a very narrow range (around 2.48 ± 0.01 g/cm^3). That can be explained by the stabilization of the overall volume due to the decrease in porosity (Fig. 2.5a,b). A longer time of heat transfer (i.e., longer continuing currents) increases the chances for voids to coalesce and eventually collapse, hence reducing the overall porosity. It is thus expected that longer duration experiments would show a bulk density, which progressively increases. T300 is the best example of the inversely proportional relationship between porosity and density. In general, the density value of the fulgurites is higher than the pristine LSB (2.42 ± 0.02 g/cm^3) and the synthesized LSB glass (nearly 2.42 ± 0.004 g/cm^3). For this particular composition, the pycnometry result shows some inconsistencies, which could be due to a

number of reasons: 1) the microporosity of the pristine vesiculated material hindering the repeatability of the density measurements; 2) the limited availability of small fulgurite fragments (< 1g) with respect to the volume of the pycnometer measurement cell; the amount of pristine and partially melted particles of crushed pieces from fulgurites. Nonetheless, the density values of the investigated specimens are very close to each other. Therefore, we conclude that the variations observed may be considered negligible and within the experimental error.

The dielectric field strength of the target material, directly related to the composition, constrains the current, which must be reached by the lightning discharge to kick start the melting. The glass transition temperature (peak) has been determined as ~ 718°C for the natural LSB sample (glass + crystals), at ~ 694°C for the experimental fulgurite (glass + possible minor amount of partially melted crystals) and at ~ 693°C for the remelted LSB glass (Fig. 2.6). The fulgurite sample and synthesized LSB glass temperatures are identical within the bounds of error (+/- 1°C). The glass transition in fulgurite provides a constraint of sample deformation during the lightning strike. The estimated glass transition peak indicates the required temperature for softening the glass of the natural LSB. Despite technical limitations preventing us from determining the possible temperature reached by the plasma, earlier research indicates that it might attain temperatures up to 32,000 K in microseconds (Kieu et al., 2020). It is noteworthy that 1600°C represents the lower limit of our simulated arc plasma's minimum temperature, as a thin melt layer coats some residual quartz crystal, which is the most refractory crystal of the pristine mineral assemblage, with a melting point near 1600°C at atmospheric pressure (Deer et al., 1966). The distribution of the glassy and crystalline area in the fulgurites demonstrate also the presence of a notable thermal gradient towards the external surface of all fulgurites. The structure of the grains as a remnant of initial material in the fulgurite might be used relatively to estimate the mean duration of the energy transfer through lightning discharge.

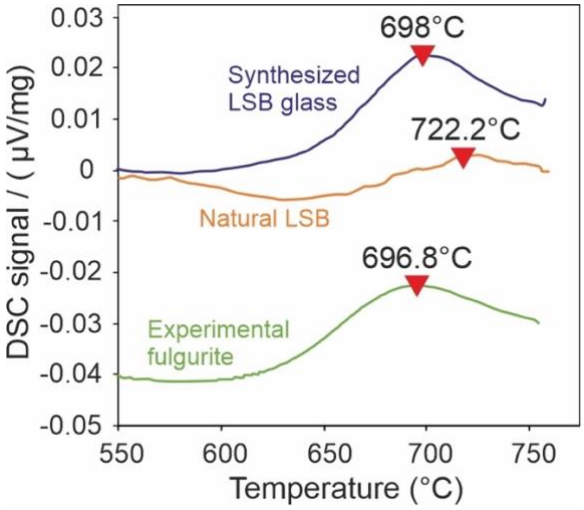

Figure 2.6: Simultaneous thermal analyses of the experimental fulgurite, synthesized LSB glass, and natural LSB specimens (raw data). The reverse triangles refer to the estimated peak glass transition temperature for each sample.

2.9. Conclusion

The experimentally generated fulgurites produced in this study demonstrate a notable similarity with fulgurites found in nature. Thus, our experimental setup and implemented protocol provide a valid pathway that approximately well natural fulgurite formation. Most remarkably, we find that the presence of a continuing current phase in the discharge allows the necessary heat transfer to produce melting of the pristine material.

With these results, we can begin to build a calibration for inferring the parameters of the lightning discharges from the characteristics of natural fulgurites. Determination of a minimum temperature of the lightning strike should be possible based on phase melting. The dielectric strength of the target material, directly related to the composition, constrains the current that must be reached by the lightning discharge to generate melting. The forms of the grains as remnants of initial material in the fulgurite can be used to estimate the average duration of the energy transfer via lightning discharge.

Finally, this reconnaissance study of the relationship between lightning and fulgurite formation will hopefully provide an opportunity in the near future to study the significance of this process in generating reactants for prebiotic chemistry on early Earth.

Chapter 3. Experimental vs. natural fulgurite: A comparison and implications for the formation of process

3.1. Abstract

Fulgurites are glassy structures formed when lightning strikes the ground, causing ground material (e.g., rocks, sediments, or soil) to melt and fuse. While fulgurites are relatively rare, they provide valuable insights into paleoecology and may play a key role in prebiotic chemistry. Despite their significance in nature, understanding the conditions underlying the formation of fulgurites poses severe challenges, as the physical parameters and timing of the fulgurite-generating lightning event still need to be discovered.

Here, we use a unique opportunity from the recent *in situ* discovery of a natural fulgurite still embedded in its protolith. Using a high voltage setup, we further compare this natural fulgurite with the experimentally generated fulgurite obtained from the original protolith. The natural and experimental fulgurites exhibit evidence of similar melting sequences and post-melting recrystallization structures. Using Raman spectroscopy applied to the quartz phase transition, we estimate the thermal gradient present in the fulgurite during formation to be a minimum of 1600°C at the inner wall of the fulgurite and ca. 600°C at the outer wall of the fulgurite. The natural fulgurite-generating event is also accessible via World Wide Lightning Network data. Those findings suggest that the current responsible for the cloud-to-ground lightning discharges that generated the natural fulgurite lay in the range of 11.960 kA to 14.473 kA. The state of the experimental fulgurites matched that of the natural fulgurite, validating the experimental option for studying fulgurite generation.

Keywords: Fulgurite, Lightning discharge, Experiment, WWLLN, ENTLN

3.2. Introduction

Fulgurites are irregular, glassy, tube-shaped formations that occur when lightning discharges (specifically cloud-to-ground or CG) melt the Earth´s surface at peak temperatures, followed by rapid cooling. They typically contain a large glass fraction hosting some initial unmelted lithologies and often exhibit some quench crystallization.

Only one-third of thundercloud lightning discharges are estimated to reach the ground, potentially generating fulgurites (Rakov 2016). Despite the limited number of examples, it has been proposed that fulgurites may offer valuable data for paleoecology reconstructions (Navarro-González et al., 2007; Ballhaus et al., 2017) and demonstrate the existence of rare essential prebiotic chemical reactants, such as phosphite (e.g., Pasek and Block, 2009; Hess et al., 2021; Çalışkanoğlu et al., 2023a; Bindi et al., 2023).

Previous fulgurite research has predominantly focused on natural examples (e.g., Pasek et al., 2012; Ende et al., 2012; Stefeno et al., 2020; Karadag et al., 2022), with very few experimental studies to date (e.g., Castro et al., 2020; Genareau et al., 2017). Those pioneering experimental studies were severely limited in their ability to mimic natural lightning due to constraints arising from technical aspects of the experiments, such as the absence of a trigger or a continuing current. They, therefore, largely fail to replicate accurately the conditions of fulgurite petrogenesis. In contrast, the high current and voltage experimental setup (see detail in Çalışkanoğlu et al., 2023b) employed here enables the accurate simulation of lightning discharges responsible for fulgurite formation.

Here, we compare a natural fulgurite (Eastern Türkiye) and an equivalent experimentally generated fulgurite obtained using the *in situ* adjacent protolith as a starting material. The experimental fulgurite, generated under variable well-controlled experimental conditions, yields new insights into the textural evolution of the natural fulgurite and about temperature gradients during melting and recrystallization at high cooling rates. Simultaneously, we report

the first detailed measurements of lightning discharge parameters that we infer led to the formation of the natural fulgurite, thereby effectively constraining the electrical conditions necessary for fulgurite formation.

3.3. Methods

3.3.1. Sample preparation and analytical techniques

The target material was thoroughly cleaned to remove any potential macroscopic organics (plants). The most comprehensive possible range of macroscopically distinct clasts was selected and roughly crushed to less than 10 mm, and a mixture of them was embedded in epoxy for further analytical analyses.

Several 10 mm chips of fulgurites (both natural and experimental) were embedded in their respective epoxy mounts for microtextural analyses.

The surfaces of further chips of both natural and experimental fulgurites were examined using a Keyence 3D Laser Scanning Confocal Microscope (LSCM) VK-X1000 with a 5x objective lens (WD 22.5) in the Department of Earth and Environmental Sciences at Ludwig-Maximilians-Universität (LMU), Munich - Germany.

BSE images of the target material, natural and experimental fulgurite samples, were collected using Scanning Electron Microscopy (SEM) at LMU - Munich with an accelerating voltage of 20 kV under a low vacuum. Semi-quantitative chemical composition data collection at the SEM was conducted through EDS using an Oxford Instrument Aztech software (AztechEnergy Advanced EDS-System) on the natural fulgurite, its protolith, and the experimental fulgurite.

We used the confocal HORIBA Jobin Yvon XploRa micro-Raman spectrometer at the Mineralogical State Collection Munich (SNSB) to identify mineral phases. The instrument was calibrated with a silica standard, and the spectra were acquired with a green Nd: YAG-Laser (532 nm wavelength), focused through the 100LWD objective lens, with 0.9 μm laser spot diameter. Grating of 1800T, a confocal hole of 300 μm, a slit of 100 μm, and an exposure time

of 30 s three times acquired were applied. The backscattered Raman radiation was collected between 100 - 1500 cm^{-1}, with an error of ±1.5 cm^{-1}, to include the low and high wavenumber regions.

3.3.2. Fulgurite synthesis experiment

We simulated natural lightning discharges in the high voltage laboratory at Universität der Bundeswehr (UniBw) in Germany, utilizing a DC source with a trigger-pulse setup to synthesize a fulgurite. The setup was designed based on recommendations from the lightning research community, such as the waveforms specified in IEC 62305 (International Electrotechnical Commission [IEC] 2010) derived from studies of natural lightning phenomena.

The lightning strikes are conducted between two electrodes placed inside a cylindrical sample container, which is connected to an electrical apparatus consisting of two parts: a Marx generator (which produced the trigger pulse) and a DC source (which acted as a prolonged current generator). The container was filled with approximately 250 g of target material. Initially, the Marx generator generated ca. 135 kA for ca. 100 microseconds, creating a conductive path between the electrodes, which were 5.7 cm apart. This high voltage and current initiated the melting of the target material. Subsequently, the DC source was kept constant between ca. 280 A and ca. 320 A for ca. 500 milliseconds, simulating the long duration of a natural lightning discharge (Rakov and Uman, 2003; Lapierre et al., 2014). This prolonged current promoted the melting of more material and facilitated the formation of a fulguritic mass. Several experimental trials were conducted to establish the setup conditions and comprehend the material's behavior under high current and voltage conditions. All experiments were carried out at atmospheric temperature and pressure. In the first experiment, the target material was utilized in its natural form (fragments ranging from 32 µm to a few cm), but no melted pieces or fulguritic structures were observed. Simulated lightning is characterized by a lower peak

current than natural lightning, thus preventing larger grains from melting. To ameliorate this discrepancy, ca. 50% of the coarse fraction (> 10 mm) was removed, and the experiment was repeated under the same electrical parameters as above, resulting in the formation of a fulgurite. The waveform of the experimental current was recorded using a Measurement Impulse Analyzer System (MIAS) at an 800-1000 ms time interval.

3.3.3. Field lightning monitoring

ENTLN comprises more than 1800 sensors deployed across more than 100 countries, which detect broad-spectrum electric field signals originating from intracloud (IC) and CG lightning events (Liu and Heckman, 2011). The CG lightning data is obtained from the World Wide Lightning Location Network (WWLLN) to enhance ENTLN detection capabilities. The WWLLN detects, locates, and timestamps lightning strikes worldwide with a spatial accuracy of 10 km and a temporal accuracy of 10 μs (Abreu et al., 2010; Holzworth et al., 2019; Hutchins et al., 2012, 2013; Rodger et al., 2004, 2005). We utilized WWLLN data to identify natural lightning events, which might have generated our natural fulgurite.

We focused on the period of April 1-15, 2021. Our search area was limited to an 8 km radius around the location where the natural fulgurite was found. We detected one IC and two CG lightning events (CG-1 and -2) within the focused area and time frame by using ENTLN data (Table 3.1 and Fig. 3.1a). IC events do not generate fulgurite; thus, the IC data is neglected in the present study. Both CG-1 and CG-2 lightning strokes showed a “downward negative” direction (the most common for global CG lightning, Rakov and Uman (2003)). The CGs were ordered according to the time of occurrence, with the location estimates CG-1 and CG-2 illustrated in Fig. 3.1a. It should be noted that due to the technical limitations of the antenna network, the designated locations of the CGs are, within error, equivalent to the fulgurite location (i.e., WWLLN - Rodger et al. (2005); ENTLN - Zhu et al. (2022)). Considering the

data from the WWLLN, we propose that one of these occurrences generated the investigated natural fulgurite.

Table 3.1: WWLLN data around the sampling area of the natural fulgurite.

Type of lightning	Date	Time	Location	Peak current [kA]	IC height [km]	Number sensors
IC	01.04.20	12:25:32	38º15'01.2"N 44º18'32.7"E	5.113	18.917	5
CG-1	01.04.20	17:27:14	38º11'04.6"N 44º17'19.3"E	-14.473	0	6
CG-2	01.04.20	17:29:41	38º14'22.2"N 44º16'47.3"E	-11.960	0	5

3.4. The natural fulgurite

A sample of natural fulgurite and its adjacent protolith were obtained from a private seller who discovered the fulgurite in north-west Van-Türkiye (38°13'17.6"N 44°15'55.9"E) in mid-April 2021 (Fig. 3.1a,b) after a thunderstorm of April 1st, 2021. The investigated natural fulgurite part will be detailed in the Result section. The CG lightning associated with that thunderstorm has been detected by radio-frequency antennas of Earth Networks Total Lightning Network (ENTLN; Zhu et al., 2022). In addition to the approximate location of the lightning discharge, the antennas provide the magnitude of the current associated with each lightning event. This discovery provides us with a unique opportunity to evaluate natural fulgurite formation versus experimental fulgurite formation from the protolith using independent control of lightning parameters under realistic conditions.

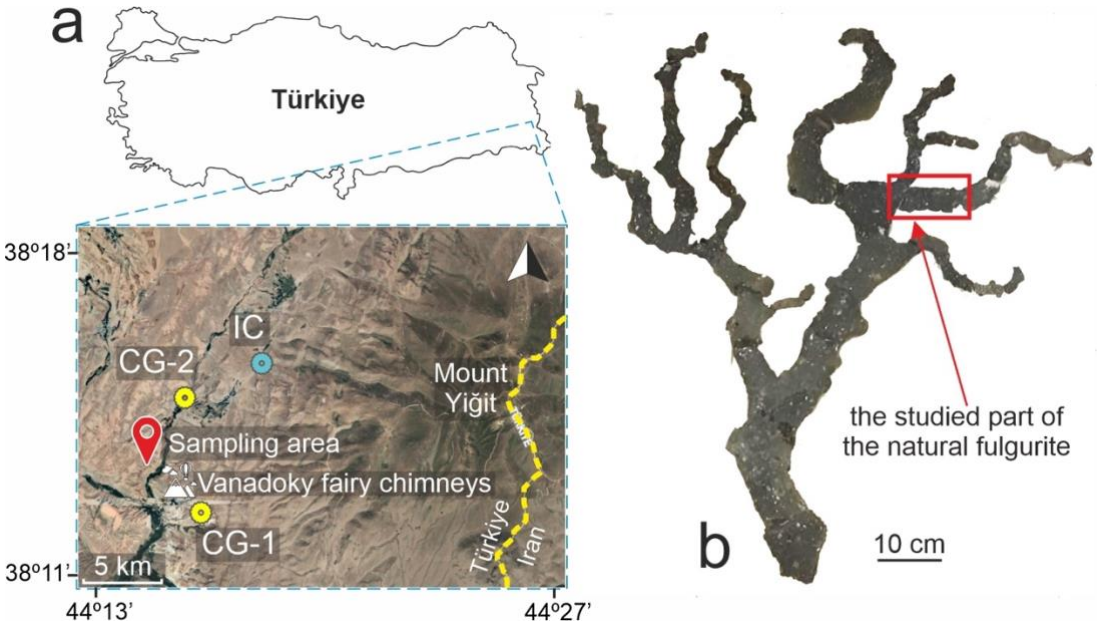

Figure 3.1: Sampling area and general image of the natural fulgurite. (**a**) The fulgurite was found northwest of the Vanadoky fairy chimneys in Van, Türkiye. The ENTLN detected two CG and one intracloud (IC) lightning discharges. The topographic image is taken from Google Maps (2023). (**b**) A photographic image of the natural fulgurite is shown. The red rectangle indicates the portion of the natural fulgurite object of this study.

3.5. The target (protolith) material

The protolith (a soil-bearing epiclastic sediment), collected from an area immediately adjacent to the natural fulgurite (Fig. 3.1a), was used as a target material for the fulgurite synthesis experiments. The remote location means no nearby communication poles might have accidentally generated the fulgurites "artificially" (e.g., Kassi et al., 2013).

The local geology consists of several geological units from oldest to youngest: 1) pre-Neogene pyroclastic deposits (pumice, tuff, and ignimbrites) and intermediate (andesite/trachyandesite) deposits from Mount Yiğit (Türkecan 2017), 2) Neogene clastic rocks (conglomerate, sandstone, marl, and - locally - tuff and lava blocks), 3) Pliocene sedimentary deposits (Şenel et al., 1984) and basaltic lava flows, which represent the latest stage of Mount Yiğit volcanism (1.87 ± 0.07 My; Allen et al., 2011). The protolith used as experimental target material was collected from where the Neogene clastic rocks crop out (Fig. 3.2a).

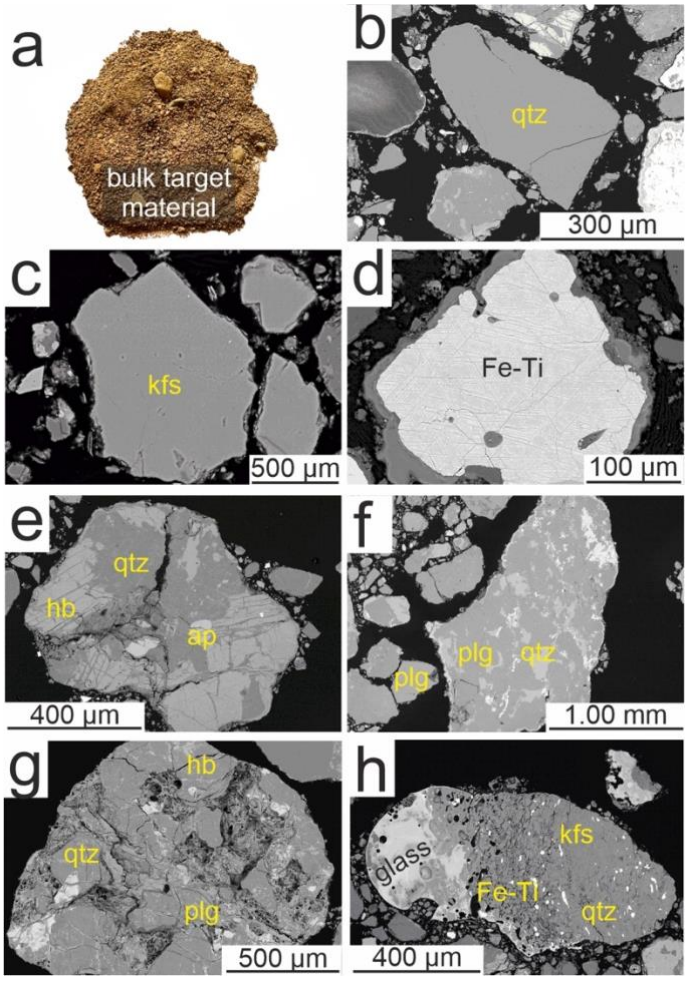

Figure 3.2: Target material and detailed BSE images of its heterogeneous grains. (**a**) An image of the protolith of natural fulgurite. (**b-f**) Mono- and polymineralic grains of the target material. These grains represent the sampling area's clastic rock unit (Şenel et al., 1984). Quartz: qtz, Alkali feldspar: kfs, Oxides: Fe-Ti, Hornblende: hbl, Apatite: ap, Plagioclase: plg.

The protolith appears yellowish-brown and is composed of rock fragments of varying sizes, ranging from ca. 30 µm to a few centimeters, consisting of mono- and polymineralic grains. The rock fragments exhibit sub-rounded to rounded edges. Energy-dispersive X-ray spectroscopy (EDS) analysis reveals that the monomineralic grains include quartz, plagioclase, and alkali feldspar, along with minor Fe- and Ti-oxides (Fig. 3.2b,c,d). The polymineralic grains exhibit diverse compositions, but plagioclase, quartz, and alkali feldspar are the most common minerals, with minor hornblende, biotite, apatite, zircon, Fe- and Ti-oxides (Fig. 3.2d,e). Most clasts are fully crystalline (Fig. 3.2e-g), but some exhibit up to 20% glass (Fig.

3.2h). Backscattered Electron (BSE) images reveal no evidence of lightning-induced effects in the protolith used subsequently as experimental target material.

3.6. Results

3.6.1. Natural fulgurite

The natural fulgurite is ca. 112 cm long and ca. 105 cm wide (Fig. 3.1b). It displays several small branches connected to two main branches. An available piece of this fulgurite was obtained commercially and investigated in the present study (Fig. 3.3a,b). Hereafter, we refer to this sample as the "natural fulgurite". The natural fulgurite is ca. 17 cm in length and has a diameter of ca. 6 cm. It appears darker than the protolith. The outer surface of the natural fulgurite has a rough texture with several unmelted grains remaining from the protolith (Fig. 3.2a). In contrast, the central portion of the natural fulgurite is entirely glassy. Vesicles of variable shapes and sizes are present. The "main void" is the largest vesicle (ca. 2.5 cm in size) in the natural fulgurite, as shown in Fig. 3.3b. Immediately adjacent to the glassy region is a zone of large vesicle concentration. Smaller vesicles are distributed from the glassy region to the unmelted protolith. (Fig. 3.3c). The fulgurite wall thickness varies from ca. 1 cm to 3 cm. The fulgurite contains unmelted to partially-melted, angular, and sub-angular grains (up to a few millimeters) and a fully-melted glassy region. Unmelted grains are common on the outer wall of the fulgurite, whereas partially melted grains are typically scattered in the glassy mass. BSE images show no sharp transition between unmelted and partially-melted grains. The glassy mass is composed of a heterogeneous mingling of molten materials (Fig. 3.3d).

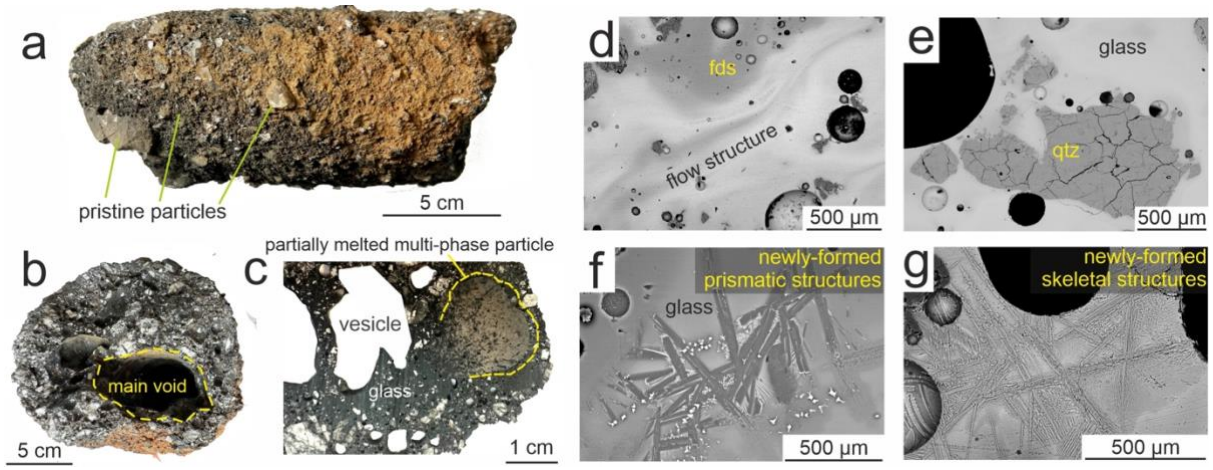

Figure 3.3: Detailed optical and BSE images of the natural fulgurite. (**a**) A photo of the studied part of the fulgurite specimen in detail. (**b**) A section view of the natural fulgurite exhibits the "main void". (**c**) An optical image of a segment of a section of the natural fulgurite captured by 3D LSCM, showing vesicles of varying sizes and shapes. (**d**) The heterogeneous glass mass displays a flow structure within the glass mass. (**e**) BSE images reveal fractured quartz crystals. (**f**) Newly-formed prismatic-tabular structures exhibit enrichment in SiO_2, Al_2O_3, Na_2O and K_2O. **(g)** Newly-formed skeletal structures present MgO enrichment. Feldspar: fds.

Natural fulgurite grains are mono- and polymineralic, occurring in unmelted and partially-melted states. Monomineralic grains are typically alkali feldspar, plagioclase, and quartz or minor Fe- and Ti-oxides. Melts apparently derived from feldspar mingle with the matrix-derived melts, as evidenced by heterogeneity in the glass, in the form of flow structures (Fig. 3d). Partially-melted quartz crystals are commonly fractured (Fig. 3.3e). The phase change from alpha (α) quartz (crystals located in the outer zone of the fulgurite) to cristobalite (crystals located close to the inner wall) was also detected.

Post-melting recrystallization structures with different compositions were detected, as shown in Table 3.2. No orientation is apparent in the growth pattern of these structures. Their size reaches a maximum of 1 mm. Prismatic-tabular structures, which are enriched in SiO2, Al2O3, CaO, and Na_2O, are observed (Fig. 3.3f). Skeletal structures, which are enriched in MgO, are (Fig. 3.3g). Other structures (i.e., cross, spherical and another skeletal) have notably high FeO contents (Fig. 3.4a-c). The cross and spherical structures are found in proximity to one another

and appear to be formed sequentially. These structures' considerably smaller size (<1 µm) prevents accurate composition measurements because of SiO_2 and Al_2O_3 contamination from the surrounding material. However, their compositions appear similar to those of the Fe-containing phases.

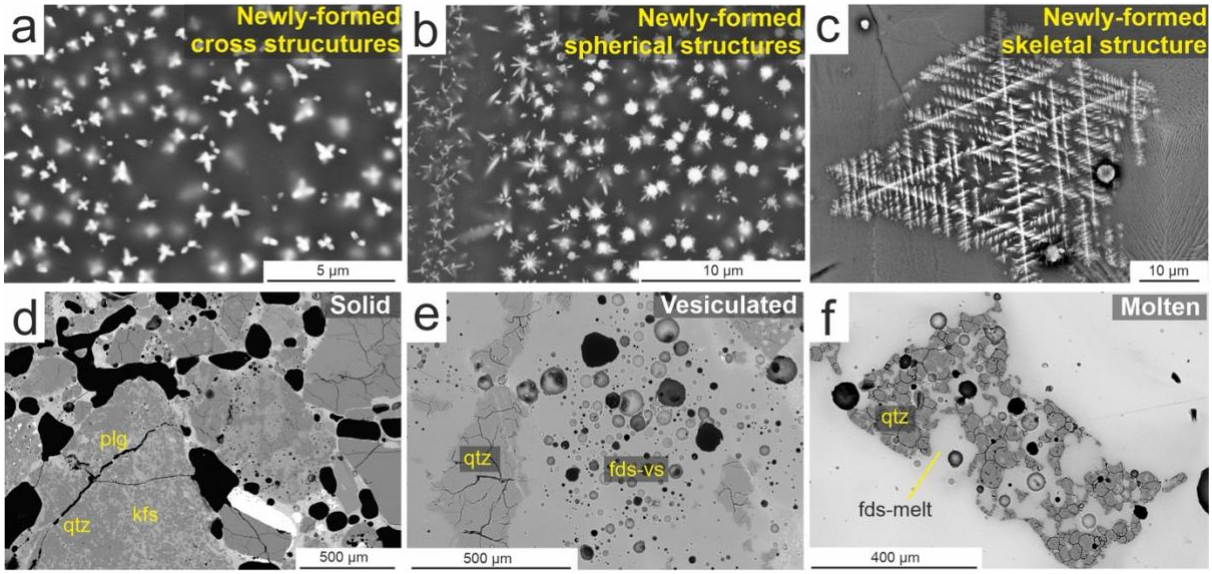

Figure 3.4: Post-melting recrystallization structures and melting morphologies of the main crystals (feldspar) in the natural fulgurite are shown in (**a-c**) and (**d-f**), respectively. Fe-rich recrystallization structures grew in different forms, such as cross (**a**), spherical (**b**), and skeletal (**c**). (**d**) Unmelted polymineralic grains are named "solid". (**e**) Feldspar displays vesicles due to high-temperature interactions in the "vesiculated". (**f**) The "molten" exhibits complete melting of the feldspar. Vesicle: vs.

The polymineralic grains in the natural fulgurite consist mainly of quartz, plagioclase, and alkali feldspar, with minor biotite, hornblende, apatite, zircon, and oxides (Fe and Ti). These grains are found in both unmelted and partially-melted regions. The volume fraction of unmelted grains is much lower than that of partially-melted grains in the glassy region. Feldspar crystals exhibit three morphologies: "solid," "vesiculated", and "molten". The solid morphology represents the feldspar crystals (either alkali feldspar or plagioclase) that do not show any chemical and physical changes (i.e., unmelted) (Fig. 3.4d). These crystals are only found in the outer wall of the natural fulgurite. The vesiculated morphology indicates crystals containing mainly rounded vesicles (Fig. 3.4e). They are mostly found in the middle of the natural fulgurite wall. The chemical composition of this region is enriched in SiO_2, Al_2O_3, Na_2O, and K_2O. The

Na_2O and K_2O values are variable depending on the volume ratio of plagioclase and alkali feldspar in the primary grains. The molten morphology may result from feldspar crystals melting completely in the presence of some other minor phases, such as Fe-oxide (Fig. 3.4f).

Table 3.2: Chemical composition of natural fulgurite (SEM-EDS normalized data).

	Natural fulgurite									
		Melting morphologies of feldspar				Post-melting crystallization structures				
	Glass mass	Solid		Vesiculated	Molten	Fe-rich phases			Prismatic -tabular	Mg-rich skeletal
		Plagioclase	Alkali feldspar			Cross	Spherical	Skeletal		
Si_2O	60.11	66.07	64.69	67.24	69.21	57.31	42.29	3.60	56.89	54.07
Al_2O_3	17.01	21.45	18.82	20.76	17.41	13.50	11.45	2.12	25.94	4.89
FeO	9.91	0.17	0.14	0.19	2.99	22.92	35.21	91.23	2.14	12.76
CaO	3.29	1.85	0.06	0.69	1.95	0.78	0.81	0.01	8.63	2.22
K_2O	2.61	0.96	14.63	3.53	3.30	0.37	0.31	0.02	0.60	0.36
Na_2O	3.09	9.31	1.58	7.35	3.63	2,41	4.16	0.18	5.13	0.56
MgO	2.49	0.1	0.02	0.09	1.20	1.63	2.02	0.50	0.34	24.19
TiO_2	1.26	0.04	0.02	0.03	0.24	1.01	3.15	1.86	0.22	0.47
MnO	0.19	0.02	0.01	0.03	nd	0.05	0.13	0.03	0.04	0.28
Cr_2O_3	0.04	nd	0.02	0.02	nd	0.02	0.02	0.06	0.07	0.02
W	nd	Nd	nd	nd	nd	nd	0.45	0.19	nd	0.09
Cu	nd	0.03	0.01	nd	0.08	nd	nd	0.02	nd	nd

3.6.2. Experimental fulgurite

The experimentally-generated fulgurite is also tube-like without branches (Fig. 3.5a) and appears dark brown. It is approximately 7 cm in length and 1 cm in width, with a main void diameter of approximately 7 mm (Fig. 3.5b). The thickness of the fulgurite wall is ca. 2 mm. The distribution of unmelted and partially-melted grains, as well as the glassy region, is found to be quite similar to that of the natural fulgurite, and there is no sharp transition between unmelted and partially-melted grains at the outer edge of the experimental fulgurite. However,

the proportion of the unmelted grains in the glassy region is much lower than in the natural fulgurite, presumably due to the finer grain size of the target material. The average grain size of both the unmelted and partially-melted grains is approximately 0.5 mm. Several vesicles, ranging up to 1 mm in size (rounded and sub-rounded), are highly concentrated between unmelted and partially-melted regions (Fig. 3.5c).

The experimental fulgurite contains mono- and polymineralic grains in both unmelted and partially-melted forms. Quartz and feldspar crystals are the two monomineralic grains. Feldspar crystals are mingled in the glassy region, resulting in the flow structures observed (Fig. 5d). Quartz crystals are ca. 0.5 mm in size (Fig. 3.5e), and they exhibit physical deformation such as fractures (Fig. 3.5f) and have been identified as α-quartz via Raman spectroscopic analysis. Three distinct post-melting recrystallization structures are observed. They are numbered 1, 2, and 3 based on their structural differences from right to left on a BSE image (Fig. 3.5g). They exhibit strong FeO enrichment together with high SiO_2 and Al_2O_3 contents (Table 3.3). Structure 1 displays a cross-formed shape, as observed in the natural fulgurite (Fig. 3.4a). In structure 2, radial arms extend from a central point to form spherulites. Structure 3 displays a symmetric skeletal form. The structures 1 and 3 cover a larger area of the fulgurite than the structure 2. Analysis of these small Fe-rich suffers from contamination (i.e., SiO_2 and Al_2O_3) originating from the surrounding glass.

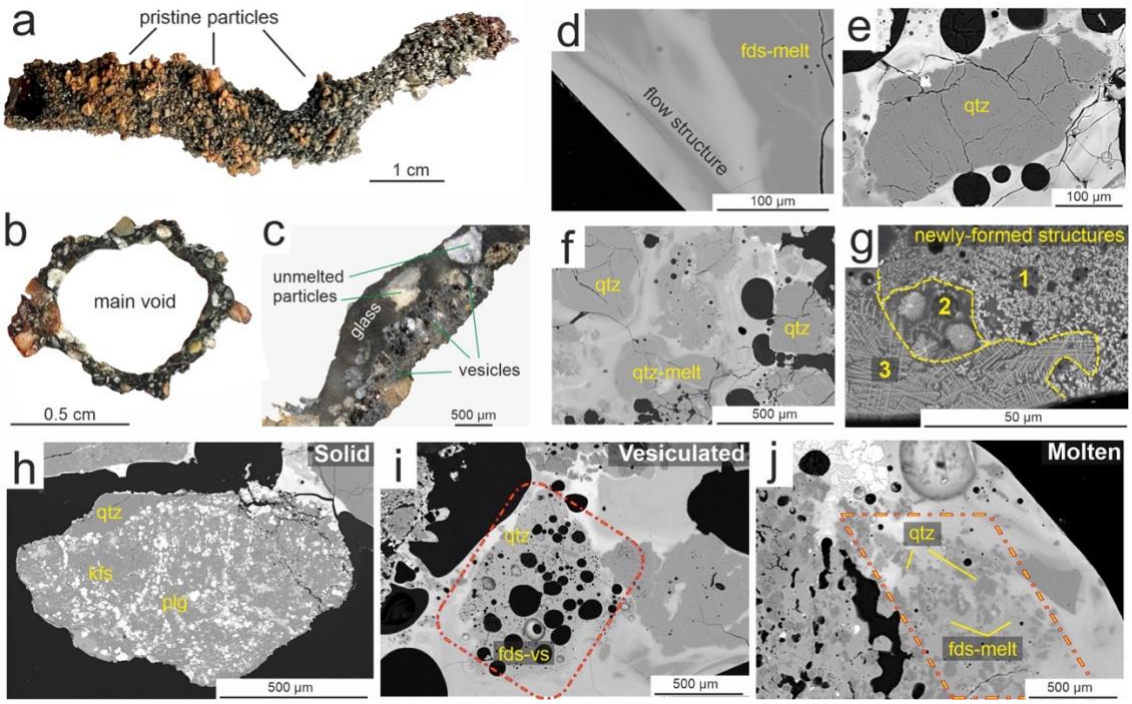

Figure 3.5: Optical and BSE images of the experimental fulgurite. (**a**) A photo of the experimentally generated fulgurite. (**b**) A sectional view of the experimental fulgurite. (**c**) An optical image of the fulgurite shows unmelted and partially-melted mono- and polymineralic grains in a glassy mass. (**d**) Partially-melted feldspar crystals, which have mingled with the glass mass. (**e**) A BSE image of a monomineralic partially-melted quartz. (**f**) Partially-melted quartz and alkali feldspar crystals. (**g**) Newly formed structures grew in different forms (i.e., spherical and skeletal). The feldspar crystals exhibit a "solid" (**h**), "vesiculated" (**i**), and "molten" morphologies (**j**) in the polymineralic grains.

The polymineralic grains consist mainly of quartz, plagioclase, and alkali feldspar. Hornblende, apatite, and minor Fe and Ti. These minor phases are solely detected in the partially melted grains near the outer wall of the experimental fulgurite. Quartz crystals have retained their general form with numerous fractures and show no notable chemical changes. In contrast, feldspars exhibit chemical and mechanical changes. They show the same textural morphologies (solid, vesiculated, molten) (Fig. 3.5h-j) as described for the natural fulgurite (Fig. 3.4d-f). Feldspar crystals (alkali feldspar and plagioclase) in the solid morphology are detected in the outer wall of the experimental fulgurite (Fig. 3.5h). They exhibit enhanced vesiculation (Fig. 3.5i). In the molten morphology, feldspars appear entirely molten without any recognizable morphological crystal form close to the interior fulgurite wall, and they are surrounded by fractured quartz crystals (Fig. 3.5j). EDS measurements on the well-mixed glassy region

indicate that the glass composition of the experimental fulgurite is quite similar to that of the natural fulgurite (Table 3.2).

Table 3.3. Chemical composition of experimental fulgurite (SEM-EDS normalized data).

	Experimental fulgurite							
		Melting morphologies of feldspar				Post-melting crystallization structures		
		Solid						
	Glass mass	Plagioclase	Alkali feldspar	Vesiculated	Molten	Fe-rich phases		
						Structure 1	Structure 2	Structure 3
Si_2O	64.11	65.48	63.77	66.07	63.98	21.53	21.61	42.07
Al_2O_3	17.78	21.87	18.89	19.14	24.42	nd	8.31	14.42
FeO	6.71	0.92	0.24	2.35	0.38	77.13	65.26	31.52
CaO	3.57	0.65	0.07	0.52	0.88	nd	1.26	1.73
K_2O	1.91	1.94	16.68	8.05	2.82	0.07	0.42	1.94
Na_2O	2.28	8.38	0.22	3.27	7.20	1.12	0.80	2.33
MgO	1.52	0.31	0.08	0.5	0.16	nd	1.03	2.78
TiO_2	1.18	0.10	nd	nd	nd	0.04	1.04	2.98
MnO	0.11	0.25	0.02	nd	0.39	nd	0.08	0.20
Cr_2O_3	nd	0.10	nd	nd	0.55	0.10	0.17	nd
W	0.72	0.35	nd	nd	0.06	0.01	nd	nd
Cu	nd	nd	0.03	0.01	0.10	nd	0.04	nd

3.7. Discussion

Fulgurite was experimentally generated from the protolith recovered adjacent to a natural fulgurite. The formation of a fulgurite is confirmed to be a complex process that depends on several factors, including the lightning parameters (i.e., temperature and current), as well as the composition and the state of the host rock. Even though the current intensities of the natural lightning discharge, ca. 13.000 kA ± 1.250 (Table 3.1), and the experiment, ca. 300 A are vastly different, our results reveal that the fulgurites generated in nature and experiments resemble each other closely. A notable exception is that the higher natural current does lead to a higher

degree of melting of coarser grains. A possible explanation for this scale-invariant character may lie in the intrinsic fractal nature of lightning discharges (Niemayer et al., 1984; Wiesmann and Zeller, 1986). Previous work from Çalışkanoğlu et al. (2023b) indicates that the continuing current of a lightning strike has a noticeable effect on the formation of fulgurite, indicating a threshold of ca. 100 ms for fulgurite formation. We confirm here that a 300 A current and a prolonged duration of discharge (ca. 100 ms) facilitates the formation of fulgurite from the silicate protolith (Maurer 2021), as it has been previously demonstrated for non-silicate (Çalışkanoğlu et al. 2023a) protolith.

Temperature gradients and grain size distribution both exert first-order influences on fulgurite texture. The temperature of natural lightning discharges typically ranges between 10.000 to 28.000 K (Paxton et al., 1986). Based on melting temperatures, we observe that our simulated lightning discharge generates a minimum of ca. 2000 K (Çalışkanoğlu et al., 2023a-b). Regions experiencing lower temperatures, due to their distal location to the lightning plasma and higher concentration of coarse grain sizes, exhibit a higher proportion of partially-melted and unmelted grains in the fulgurite, yielding distinct regions whose textures are systematically defined by their degrees of melting (e.g., Hess et al., 2021; Kenny and Pasek, 2021; Çalışkanoğlu et al., 2023a-b). In both nature and experiment, coarse grains that have been partially melted exhibit distinctive flow structures in their glassy products, indicating that such melts are not homogenized during fulgurite formation (c.f. Lavallée et al., 2015). In contrast, the homogeneous glassy (fully remelted) regions of experimental and natural fulgurites exhibit similar chemistry as determined by SEM/EDS (Table 3.2 and 3.3).

Quartz crystals (initially both mono- and polymineralic grains) undergo a phase change (Fig. 3.6a,b) with increasing temperature, resulting in a fractured structure. Folstad et al. (2023) indicate that cracks in quartz are commonly observed in two temperature ranges. The first range, approximately 300-600°C, primarily arises from volume changes in impurity regions, uneven

surfaces of quartz, and/or the presence of fluid inclusions. The second range, ca. 1300-1600°C, is likely a consequence of the phase transformation of quartz from β-quartz to β-cristobalite. As noted above, the natural fulgurite exhibits α-quartz in the outer wall and β-cristobalite in the inner wall. This implies the presence of a strong temperature gradient across ca. 1 cm. In contrast, the experimental fulgurite exhibits no cristobalite. Possible reasons for this discrepancy include (1) the simulated lightning may not have reached the equivalent temperature range and/or (2) the pressure generated by simulated lightning may be lower.

Feldspar crystals situated in proximity to the lightning plasma undergo complete melting, whereas those subjected to lower temperatures display partial melting with vesicle formation. This distinction within the feldspar crystals supports the strong temperature gradient extending from the inner wall (adjacent to the plasma) to the outer wall of the fulgurite.

Upon cooling, both the natural and experimental fulgurites reveal the presence of multiple coexisting crystalline structures (i.e., spherical and dendritic) (Fig. 3f-g, 4a-c and 5g). Similar crystal structures have also been reported in other rapidly quenched glasses, such as impactites, meteorites, and chondrules (e.g., Kumler and Day, 2021). Skeletal structure (magnetite) has previously been documented in fulgurites by Ablesimov et al. (1986) and Grapes and Müller-Sigmund (2010). To the best of our knowledge, this study marks the first documented occurrence of spherical Fe-rich forms within natural and experimental fulgurites. The juxtaposition of distinct growth patterns and crystal sizes might reflect locally varying melt compositions and/or different cooling rates determined by proximity to the lightning plasma and heterogeneous composition.

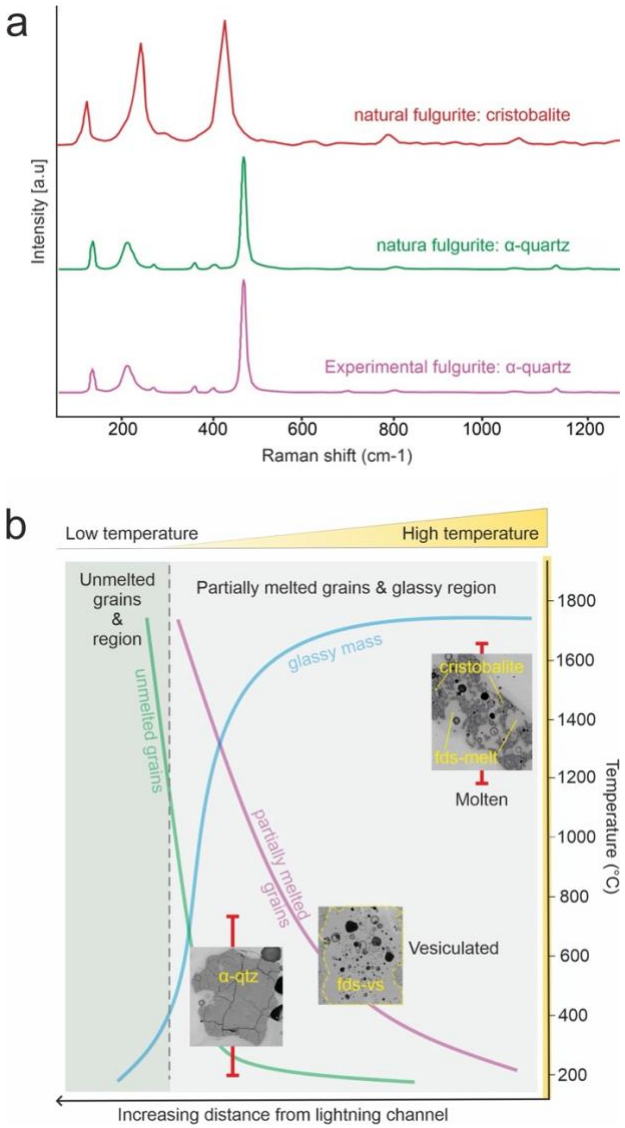

Figure 3.6: Micro-Raman spectroscopy of quartz crystals and a schematic diagram illustrating the evolution of grains in the fulgurites. (**a**) The Raman spectra of quartz crystals in fulgurites from each fulgurite's inner and outer walls. The experimental fulgurite exhibits only α-quartz and natural fulgurite displays both α-quartz and cristobalite. (**b**) The textural evolution of the fulgurites concerning temperature development during lightning discharge. The textural evolution among the defined morphologies (i.e., solid, vesiculated, and molten) is scaled in temperature using the α-β transition (Folstad et al., 2023) and cristobalite stability (Wagstaff 1969).

3.8. Implications

This work demonstrated a realistic comparison between natural and experimental fulgurites for the first time, revealing a remarkable similarity in their textural and mineralogical evolution.

This validates that the state of the experimental fulgurite matched that of the natural fulgurite using the DC source trigger-pulse setup as a lightning simulator. This work also further documents the physical parameters (maximum voltage and current) of lightning strikes that likely generated the natural fulgurite. Our results interestingly suggest a scale-invariant character of the experimental fulgurites concerning the natural one, whereby the lower voltage and current values used in the experiments allow the reproduction of identical textures observed in the natural fulgurite. As shown in previous experiments, we confirm the importance of long-duration (100's ms) continuous currents in favoring extensive melting and, ultimately, the fulgurite formation. This work introduces a novel methodology for reproducible fulgurite generation through laboratory experiments. This opens up possibilities for systematic petrogenetic analysis of fulgurite formation with broader geological implications, providing researchers with a controlled environment to explore and understand the processes involved.

Chapter 4. Reactive phosphorus via simulated lightning discharge: A role for fulgurites in pre-biotic chemistry

4.1. Abstract

Apatite is the most common phosphorus-bearing mineral in primary igneous rocks. Despite its early and ubiquitous presence in such rocks at the Earth's surface, its phosphorus exhibits a low reactivity in prebiotic chemosynthesis. This situation may change radically upon the transformation of phosphorus from orthophosphates to pyrophosphates or phosphides, which are, in contrast, highly reactive in such scenarios. Pyrophosphates and phosphides are today; however, scarce on Earth, generally not being stabilized in rock-forming processes. Noticeable exceptions are lightning-struck rocks (i.e., fulgurites).

Here, we present the first evidence of reactive phosphorus (P) in a fulgurite, which has been experimentally generated under controlled conditions from natural apatite. Crushed apatite was transformed into a fulgurite through the application of controlled high voltage electrical discharges. We document both the apatite (pre-experiment) and the fulgurite (post-experiment) texture, state, and chemistry. ^{31}P and ^{19}F nuclear magnetic resonance spectroscopy reveals the presence of a reactive P phase (pyrophosphate) in the fulgurite. Our results support the speculation that frequent lightning activity under early Earth conditions may have provided more than 100-10.000 kg/yr of reactive P on early Earth through the generation of reactive P-bearing fulgurites. Their presence may have enabled the chemosynthesis of vital prebiotic components such as RNA and lipids for the emergence of life on Earth.

Keywords: Fulgurite, Lightning discharge, Phosphorus, Experiment

4.2. Introduction

Phosphorus (P) is a key element in the evolution of life because it is pivotal in the biological coding of information (DNA and RNA), in metabolism (as ATP), and in cellular structure (as phospholipids). In magmatic systems from the Hadean up to today, the minor element P is present virtually exclusively in the oxidized state (orthophosphate: PO_4^{3-}) in phases such as apatite, monazite, and whitlockite (Hazen 2013). Apatite is also known as the highest P crustal reservoir (Smith 1981; Walton et al., 2021). Thus, phosphate minerals on Earth have almost certainly been witnesses to the prebiotic path to life. The common phosphate minerals are however highly stable and relatively unreactive, leading to the so-called phosphate problem (Orgel 1989; Benner et al., 2012; Pasek 2017). Reduced P compounds (e.g., phosphites, hypophosphites) have, in contrast, been proposed as a source of P for primitive biological systems (White and Metcalf, 2007). This is because phosphide minerals (e.g., schreibersite, $(Fe, Ni)_3P$) are thermodynamically unstable on the Earth´s surface and thus more reactive than phosphate minerals, reacting with water to yield energetic phosphites (Pasek and Lauretta, 2005; Bryant and Kee, 2006; Pasek et al., 2007; Gull et al., 2015). Phosphides are common accessory phases in chondritic meteorites, interplanetary dust particles, and comets (Buchwald 1984; Papike 1998) but extremely rare on the Earth's surface (c.f., Disko Island, Greenland (Pedersen 1981), Sulu terrain, China (Yang et al., 2005), Hatrurim formation in Levant (Britvin et al., 2015)). It has been postulated that reactive P phases might be readily available on the early Earth due to (i) heavy meteorite bombardments (Pasek and Lauretta, 2005; Bryant and Kee, 2006; Pasek et al., 2007; Bryant et al., 2009), (ii) low-temperature metamorphic heating (Herschy et al., 2018) and (iii) the reduction of phosphate to phosphite via lightning discharge (Essene and Fisher, 1986; Pasek and Block, 2009; Pasek et al., 2012; Hess et al., 2021). Here, we concentrate on the latter.

To date, studies on the lightning discharge origin of reactive P compounds have been based almost exclusively on the analysis of natural fulgurite samples composed of non-prebiotic materials (i.e., sand) (Essene and Fisher, 1986; Pasek and Block, 2009; Pasek et al., 2012; Hess et al., 2021). Exceptions are provided by Glindemann et al. (1999) and De Graaf and Schwartz (2000), who exposed powdered apatite placed in a quartz tube sealed with a tungsten wire to a low-power electric current in a domestic microwave oven.

Here, we present the first successful generation of a reactive P phase in fulgurite generated experimentally by lightning discharges on natural apatite. Importantly, in the controlled environment of the experiments presented here, we employ a continuing current effect, a crucial component of natural fulgurite genesis. The experimental apparatus used in this study has been designed and constructed to ensure compliance with the lightning research community's recommendations for lightning strike studies (e.g., waveforms IEC 62305) and thus can be easily compared and reproduced by other groups. We document experimentally for the first time the lightning-induced generation of reactive P phase in generated fulgurite using ^{31}P solid/liquid-state nuclear magnetic resonance (NMR) spectroscopy. The results demonstrate the feasibility of the fulgurite hypothesis for a repository of a reactive P-bearing phase on the early Earth.

4.3. Methods

4.3.1. Fulgurite synthesis experiment

The fulgurite sample was experimentally generated via a DC source with a trigger-pulse setup in the high voltage laboratory at the Universität der Bundeswehr (UniBw), Germany. A schematic diagram of the setup can be seen in Appendix B.

The laboratory setup was built considering the similarity of natural lightning currents, and the study procedure was based on the electrical inputs developed for standard lightning tests. Lightning currents are essentially unidirectional and are studied as a sum of different

component effects. The main current components are first return stroke, subsequent return stroke, and long-duration continuing current. The first return strokes have the highest current amplitudes, typically of the order of 103 A, lasting up to several 100 microseconds. The subsequent return strokes are lower in amplitude and duration but often with a significantly higher current steepness di/dt of up to a few 100 kA/µs. The long-duration continuing currents exhibit much lower current amplitudes of just a few 100 A, but last much longer (in the range of 100 to 500 milliseconds).

Our experiment setup consists of a Marx-generator, DC-source system, circuit breaker, inductor, and cylindrical sample container (Appendix B). The Marx-generator is used as a trigger-pulse to override the dielectric field strength of the target material, producing currents with a 500 - 5000 A peak over ca. 100 µs, in a first stroke effect. Next, the DC source produces a long-duration continuing current (60 batteries of 12 V, 720 V). These modules are connected to a cylindrical sample container (Fig. 4.1), yielding lightning strikes in a highly controlled environment. A circuit breaker is used to control the current flow at pre-determined conditions by lightning standards.

In our setup, the inner tube is filled with approx. 250 g of crushed powder as we knew that particle size plays a role in the generation of fulgurite from our previous experimental observations. The dielectric field strength of the material is overridden with the help of a Marx generator, igniting the arc channel to start the melting process with an impulse duration of around 100 µs. Next, a DC-source generator produces a long-duration continuing current on the material in pre-set time - 500 ms, which is within the limits of natural lightning, to melt more mass around the arc. All melted mass is rapidly cooled down and creates ca. 4 g of fulgurite. The long-duration continuing current characteristic used for the experimentally generated fulgurite is presented in Appendix B.

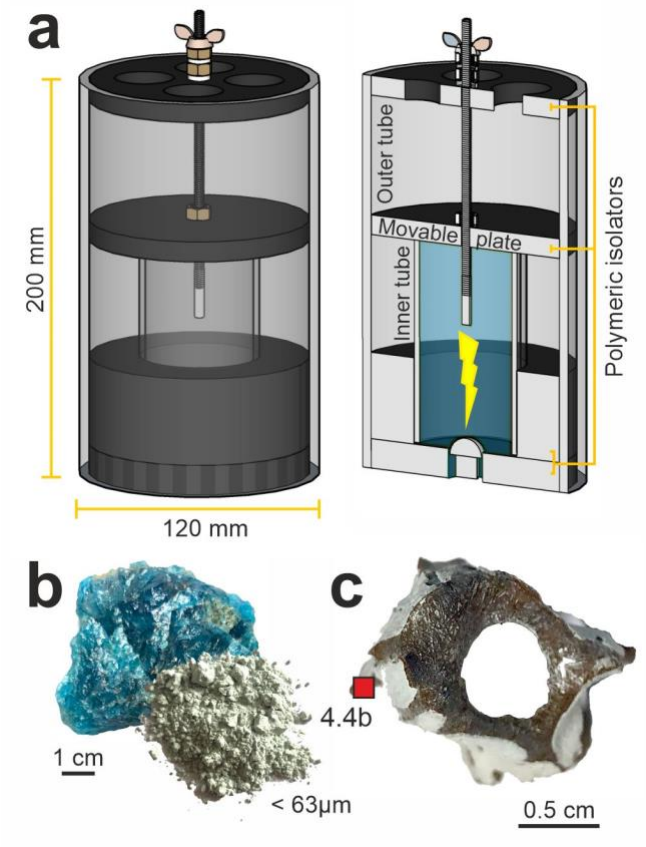

Figure 4.1: Experimental apparatus, natural apatite (target material), and experimentally generated fulgurite. (**a**) 3D image and sectional view of the sample container. The outer plexiglass tube is used as a protective shell for a possible explosion, and the inner tube holds a controlled volume of the target material. (**b**) Hand specimen of apatite and its crushed powder. (**c**) Experimentally generated fulgurite; the red square represents the area sampled for ^{19}F MAS NMR analyses (Fig. 4.4b).

4.3.2. Sample preparation

250 g of natural apatite were ground in an agate mortar in a vibration mill down to 63 µm for a lightning discharge experiment. Additionally, a sample of natural apatite (length/width: 3 cm /3 cm) was embedded in an epoxy mount for further analytical analysis.

The generated fulgurite sample was embedded into Crystalbond 509, a semi-permanent transparent mounting medium, to prevent possible mechanical disruption of the fulgurite sample during cutting. To quantify the morphological properties of the fulgurite, the sample was cut perpendicular to its long axis using a precision diamond wire saw. After cutting the

specimen, it was heated to 80°C for ca. 1 minute to remove most of the Crystalbond, followed by immersion in acetone for ca. 30 seconds to complete the cleaning process. Next, the surface was checked with a binocular microscope to verify that the Crystalbond was removed completely. A mount (epoxy resin) was prepared from one-half of the fulgurite.

4.3.3. Laser scanning confocal microscopy

The fulgurite was examined under a Keyence 3D Laser Scanning Confocal Microscope (LSCM) VK-X1000 with 5x objective lens (WD 22.5) in the Department of Earth and Environmental Sciences at Ludwig-Maximilians-Universität (LMU), Munich - Germany in order to examine the inner and outer surface of the tube-like fulgurite sample.

4.3.4. X-ray fluorescence spectroscopy

Major and trace element analyses on natural apatite were conducted using a Malvern Panalytical Axios Fast X-ray fluorescence spectrometer (XRF) at the University of Mainz, Germany. The major element analyses were carried out on fused glass discs, whereas the trace element analyses were carried out on compacted powder pellets. The typical accuracy of the analyses of the standard references was nearly 1% relative (RMS) for major elements and around 4% relative (RMS) for trace elements.

4.3.5. Scanning electron microscopy

The natural apatite and experimentally generated fulgurite were analyzed using a Hitachi SU 5000 Scanning Electron Microscope (SEM) at LMU Munich. Backscattered electron images (BSE) of representative portions of the apatite and fulgurite were acquired at 100x magnification. Data collection was conducted using Oxford Instrument (AZtechEnergy Advanced EDX-System) Aztech software.

4.3.6. Electron probe microanalysis

The quantitative chemical compositions of the apatite and the fulgurite were analyzed using a Cameca SX 100 electron microprobe at LMU Munich. The apatite and fulgurite samples were examined under the same conditions and standards for accurate comparison of these two

samples. The operating conditions were an accelerating voltage of 15 kV and an electron beam diameter of 10 µm with a current of 20 nA. The following standards were used: orthoclase (Al, K), albite (Na, Si), Durango fluorapatite (P, Ca, and F), anhydrite (S), vanadinite (Cl), thorium oxides (Th), rutile (Ti), $LaPO_4$ (La), $CePO_4$ (Ce), $NdPO_4$ (Nd), copper (Cu), tungsten (W).

4.3.7. X-ray diffraction spectroscopy

Qualitative phase determinations of natural apatite and fulgurite were obtained using a GE X-ray diffractometer (XRD 3003 TT) at LMU Munich. In order to determine the amorphous content (glass), approximately 17 wt.% of silicon (Alpha Aesar Silicone powder, -325 mesh, 99.5%) was added as internal standard and mixed in agate mortar until well-mixed visually homogeneous powder was obtained. Mineral indexing patterns were interpreted using Profex 10.13 software.

4.3.8. ^{31}P and ^{19}F NMR spectroscopy

^{31}P and ^{19}F NMR experiments were conducted on a solid-state NMR spectrometer at TU-Darmstadt. Direct-polarization (DP) and ^{19}F/^{31}P cross-polarization (CP) experiments were conducted under magic angle spinning (MAS) conditions. The spectrometer was equipped with a 400 MHz wide-bore Magnet, Bruker Avance II+ console, and a Bruker 3.2 mm H/F/X/Y MAS probe. Samples were spun in 3.2 mm zirconia rotors. MAS frequencies were set to 18 kHz for DP experiments, ^{31}P and ^{19}F, and 10 kHz for CP experiments, respectively. Background suppression was utilized for 19F DP spectra (Bruker zgbs sequence), with a 90° pulse of 3.9 µs. The relaxation delay was set to 10 s to ensure thermal equilibrium conditions for each scan. The tip angle for ^{31}P DP was set to 22°, the relaxation delay to 9 s, and ^{19}F decoupling was applied during data acquisition. The parameters for the ^{19}F/^{31}P cross CP. Experiments were; a 3.5 ms contact time for long-range cross-polarization, 100 µs for short-range cross-polarization, VACP sequence with 50% ramp on the ^{19}F channel, 10 s relaxation delay, and ^{19}F decoupling

during data acquisition. External standards for referencing were phosphoric acid (0 ppm) for ^{31}P spectra and solid Barium Fluoride (-14.3 ppm to $CFCl_3$) for ^{19}F spectra, respectively.

Solutional ^{31}P NMR spectroscopy was performed on a Unity INOVA spectrometer at the University of South Florida (operating at 161.84 MHz). 200 mg samples of the unaltered powdered apatite and the artificial fulgurite were separately extracted by a Na4EDTA (0.025 M) solution for one week in closed vials, and the resulting supernatant was then filtered and dried down, and rehydrated in D_2O. NMR then analyzed the solutions for 5000 scans using previously described methods (Gull et al., 2020).

4.4. Results

4.4.1. Starting material

Crushed natural apatite from Ipirá Complex, Bahia (Brazil) (<63 µm mesh size) was used as a starting material for our experiments instead of a rock containing apatite, which might highly cause mineral contaminations. The natural apatite and crushed powder are illustrated together in Fig. 4.1b. The apatite was analyzed for bulk composition using XRF (Table 4.1). The morphology and state of the apatite were investigated using SEM, EPMA, XRD, and ^{31}P solid/liquid-state NMR.

In terms of morphology and mineral chemistry, the apatite sample represents a typical polycrystalline blue apatite specimen from the Ipirá complex (Fig. 4.1b). Its mineral formula has been calculated using the method provided by Ketcham (2015) as $(Ca_{5.133}Sr_{0.002}Ce_{0.0142}La_{0.009}Mn_{0.002}Fe_{0.002})$ $(P_{2.824}Si_{0.130}O_{12})$ $(F_{0.857}Cl_{0.033}OH_{0.108})$. The presence of minor uranium and thorium was also detected. The EPMA data are confirmed by "bulk" XRF analyses (Appendix B). The apatite sample contains minor microscopic subhedral to anhedral calcite grains (<5 µm) (Fig. 4.2a-c). It can be classified as a fluorapatite in composition and crystalline structure, as confirmed by an XRD analysis (Fig. 4.2d). As expected, a complete absence of any amorphous material in the structure of the pristine apatite has been confirmed

by ^{19}F magic-angle spinning (MAS) NMR spectroscopy (Fig. 4.2e). According to Vyalikh et al. (2015), -88 and -100 ppm peaks may be attributed to isolated water in this spectrum.

Table 4.1: Major and trace element composition of natural apatite from Ipirá Complex, Bahia (Brazil), determined using XRF.

Major elements (wt.%)		Trace elements (ppm)	
SiO_2	1.49	Sc	2
Al_2O_3	0.01	Co	2
Fe_2O_3	0.04	Ni	28
MnO	0.04	Zn	7
MgO	bd	Ga	3
CaO	54.76	Sr	566
Na_2O	bd	Y	bd
K_2O	bd	Zr	bd
TiO_2	bd	Nb	bd
P_2O_5	38.14	Cs	94
F	3.1	Ba	7
Cl	0.229	La	2500
Cr_2O_3	bd	Ce	3800
NiO	0.0012	Nd	1800
SO_3	1.034	V	32
LOI	0.29	Rb	bd
Total	99.229	Cu	6
		Cr	15
		W	33
		Pb	85
		Th	3251
		U	118

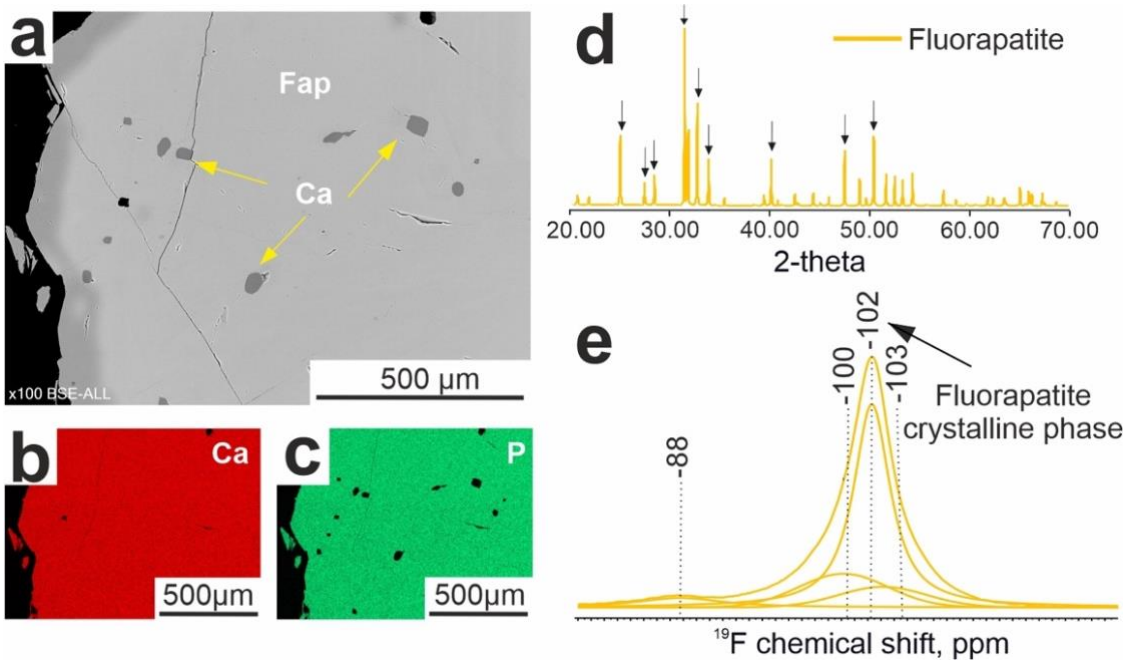

Figure 4.2: Morphological and chemical properties of natural apatite. (**a**) BSE image revealing calcite (Ca) crystals in a fluorapatite (FAp) mass. (**b**) EDS element mapping of Ca (**c**) EDS element mapping of P. (**d**) XRD pattern of the natural apatite. Fitted spectra shows the crystalline fluorapatite phase and some of the main peaks are indicated by arrows. (**e**) ^{19}F MAS (18 kHz) NMR spectrum of natural apatite. The Y-axis shows intensity (a.u.).

4.4.2. Experimentally generated fulgurite

The experimentally generated fulgurite is dark brown in color, and its outer surface is finely dusted by a loose greenish powder of pristine apatite (Fig 4.1c). It is nearly 1.5 cm in length and 2 cm in width (Fig. 4.3a) and displays a 0.7 cm diameter longitudinal central void, a common feature of natural fulgurites. Despite having been melted, the fulgurite exhibits a high degree of crystallinity, which clearly represents a recrystallized apatite mass wholly different in texture from the natural apatite. This is in contrast to the common observation of a glassy state of silicate fulgurites (Purdom 1966; Frenzel and Ottemann, 1978; Merrill 1886; Frenzel and Stähle, 1982-1984; Frenzel et al., 1989; Clocchiatii 1990; Pasek et al., 2012) and likely results from the poor glass-forming ability of molten oxyfluorides. Newly-formed euhedral semi-transparent apatite crystals (ca. 0.4 mm) were detected via LSCM (Fig 4.3b). The size of the newly recrystallized apatite crystals increases to ca. 0.6 mm at the inner surface of the

fulgurite (Fig. 4.3c). Pristine crystals adhering to the outer surface exhibit sub-rounded edges, a morphological modification generated during the high temperature excursions of the experimental lightning strikes (Figure 4.3d). XRD data confirm that the bulk of this crystalline mass is fluorapatite (Fig. 4.4a) and coherent with the common fluorapatite spectrum (Silva et al. 2021).

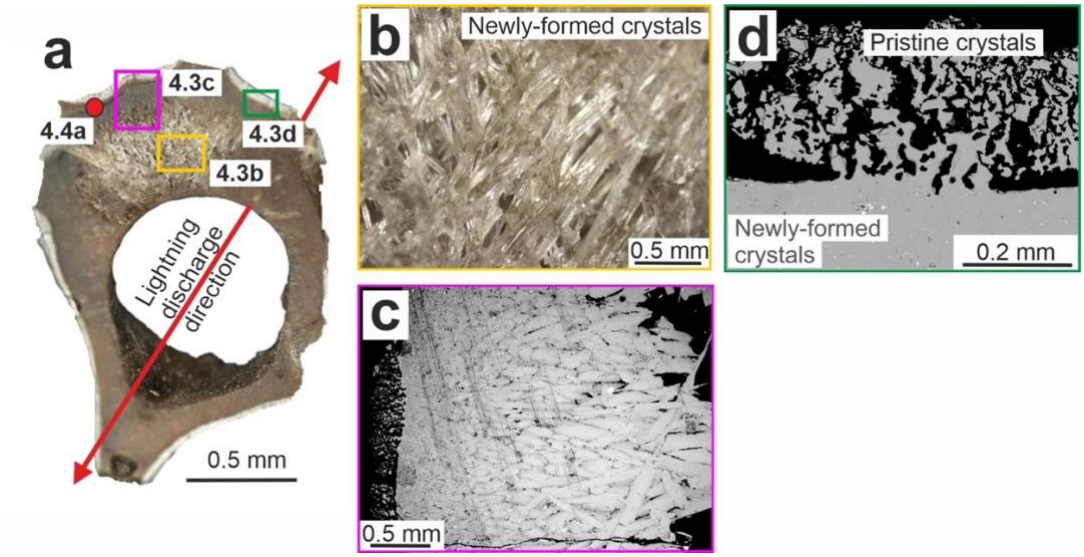

Figure 4.3: Morphological properties of experimentally generated fulgurite. (**a**) Transverse image of fulgurite in the 3D LCSM. The double arrow shows the lightning discharge direction, which symbolizes that lightning can initiate from the upper or lower electrodes. (**b**) Optical image of newly-formed semi-transparent fluorapatite crystals via 3D LCSM and (**c**) BSE image. (**d**) A BSE image of residual crystals and newly-formed crystals on the outer edge of the fulgurite.

^{19}F MAS NMR has been performed to examine the state of fluorine in the fulgurite. A single peak dominates the NMR spectrum at -102 ppm, attributed to PO_4^{3-} groups in crystalline fluorapatite. Additional peaks have resolved at -99 ppm, -105 ppm, and -108 ppm. The -99 ppm and -105 ppm peaks can be assigned to amorphous phases. The -108 ppm peak might be assigned as Ca···-F interactions (-108 ppm) like in crystalline CaF_2 (Massiot et al., 2001) or Ca_3F by Vyalikh et al. (2015). However, we could not identify the presence of CaF_2 and Ca_3F in corresponding to our XRD data (Fig. 4.4b). Further, the phase diagram of apatite-fluorite

contains thermal maxima that would appear to exclude the formation of CaF_2 from an apatite starting material. The EPMA data of the fulgurite reveal a homogeneous chemical composition for the fluorapatite. The pristine crystals on the outer surface of the fulgurite show slight morphological differences, presumably due to thermal effects, but no major shifts in chemical composition. The newly-formed apatite crystals are depleted in F. Increased concentrations of W and Cu at trace levels are also observed in the newly-formed crystals and the interstitial phases. The interstitial phases also appear to be enriched in Th and REEs. Unfortunately, point measurements via EPMA involve an excitation volume significantly exceeding the size of the interstitial phases, and thus, there may be some convolution of the volumes of minor phases whose dimensions are ca. 3 µm. All chemical data are summarized in Appendix B.

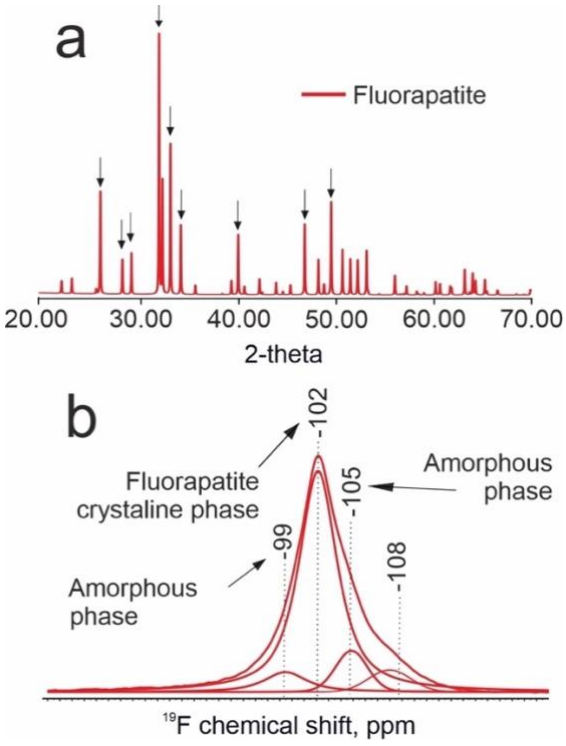

Figure 4.4: Chemical properties of experimentally generated fulgurite. (**a**) XRD pattern of the studied area on the fulgurite. Fitted spectra show the crystalline fluorapatite phase. Some major peaks are indicated by arrows. (**b**) ^{19}F MAS (18 kHz) NMR spectrum of fulgurite detected using direct polarization. The Y-axis shows intensity (a.u.).

^{31}P solid/liquid-state NMR have been performed to examine the structural differentiation between natural apatite and experimentally generated fulgurite (Fig. 4.5a-b). The main difference between pre- and post-experimental samples is the presence of the phosphate dimer pyrophosphate ($P_2O_7^{4-}$, PPi) in the fulgurite sample at a -4.5 ppm peak. This finding thus confirms the presence of a reactive P-bearing phase at a concentration of 5% at a 4 ppm peak via ^{31}P solid-state MAS NMR measurement (Fig. 4.5c). This is the first experimental evidence for the presence of a reactive phase of P in an experimentally generated fulgurite composed of natural fluorapatite.

4.5. Discussion

Based on the observations presented above, we interpreted the synthesis process of this experimental fulgurite, generated from natural apatite, as one in which the entire sample within the domain of fulgurite generation has wholly melted and then massively recrystallized to a variably fine-grained apatite upon cooling. This recrystallization generates F- (and possibly Cl-) depleted apatite crystals accompanied by the nucleation and growth of interstitial phases, which presumably capture some of the F, together with Th and REEs. Phosphide minerals (e.g., schreibersite, $(Fe, Ni)_3P$) have yet to be explicitly detected in these fulgurites. It must, however, be noted that our attempts at detection using XRD, EPMA, and SEM were likely complicated due to the low Fe and Ni content of the initial material and the nano-crystallinity of potential phosphide phases. Despite these potential analytical limitations, a minor amorphous phase was detected in the bulk of fulgurite by ^{19}F MAS NMR (Fig. 4.4b).

The rate of fulgurite-forming lightning discharge and the phosphorus content of the sample in which the lightning strike plays a crucial role in the estimation of the reactive phosphorus source from fulgurite in the early Earth. Hess et al. (2021) estimate the amount of reduced phosphorus created by each strike by assuming an average fulgurite mass (250 gr), average phosphorus contents (0.0065 - 0.044 wt.%), and the percent of phosphorus that is reduced (10-20% highly

reduced, 25-50% mildly reduced). Based on these values, the amount of reactive phosphorus is calculated as 0.224% to 3.08%:

$$(0.0064 \text{ to } 0.044)\times[(0.1+0.25) \text{ to } (0.2+0.5)]=0.224\% \text{ to } 3.08\%.$$

In this work, we measured the total amount of reactive phosphorous in the fulgurite to be around 5% by NMR analysis, which is higher than the upper limit (0.224% to 3.08%) based on the assumed values by Hess et al. (2021). Apatite as a monomineralic rock is rare in nature, and hence, in the presence of further rock-forming phases, it may be different in detail. Our work here should be viewed as an important basis on which to build towards multiphase rocks. Multi-phase rocks might behave differently under lightning discharge, and the possible reactive phosphorus amount may vary depending on the phosphorus content of the rock (Yamagata et al., 1991). Additionally, the rate of cloud-to-ground lightning discharge during the early Earth environment and target material physical features are other significant factors. It has been observed in our unpublished study that the target material with a small grain size supports the formation of fulgurite. It is thought that the presence of suitable target material with a higher lightning discharge fraction may increase the reactive phosphorus source.

The importance of abiotic P redox changes, such as those demonstrated here in the lightning-generated reactive phase of P in experimentally generated fulgurite, for prebiotic chemosynthesis has been a central point of discussion (Gulick, 1955; Schwartz, 1977; Glindemann et al., 1999; De Graaf and Schwartz, 2000; Pasek and Lauretta, 2005; Pasek, 2008; Pasek and Block, 2009; Pasek et al., 2012; Pasek et al., 2013; Pasek et al., 2017; Herschy et al., 2018; Hess et al., 2021). The thermodynamic study of Pasek and Block (2009) indicates that phosphate (as $CaHPO_4$) can be reduced to phosphite (as $CaHPO_3$) at about 2,000 K and oxygen fugacity of about 10^{-5} in natural fulgurites. In local environments, the proportion of the reduced P species may also exhibit enrichment under reduced atmospheric conditions (De Graaf and Schwartz, 2000). Here, the newly-formed crystals are proof that we have exceeded the melting

point of fluorapatite (around 1644℃) and that the minimum temperature of the simulated plasma is close to the reduction temperature range (about 2000 K) referred to by Pasek and Block (2009). The temperature might be significantly higher; however, we cannot measure the temperature in the experiment setup due to current technical limitations.

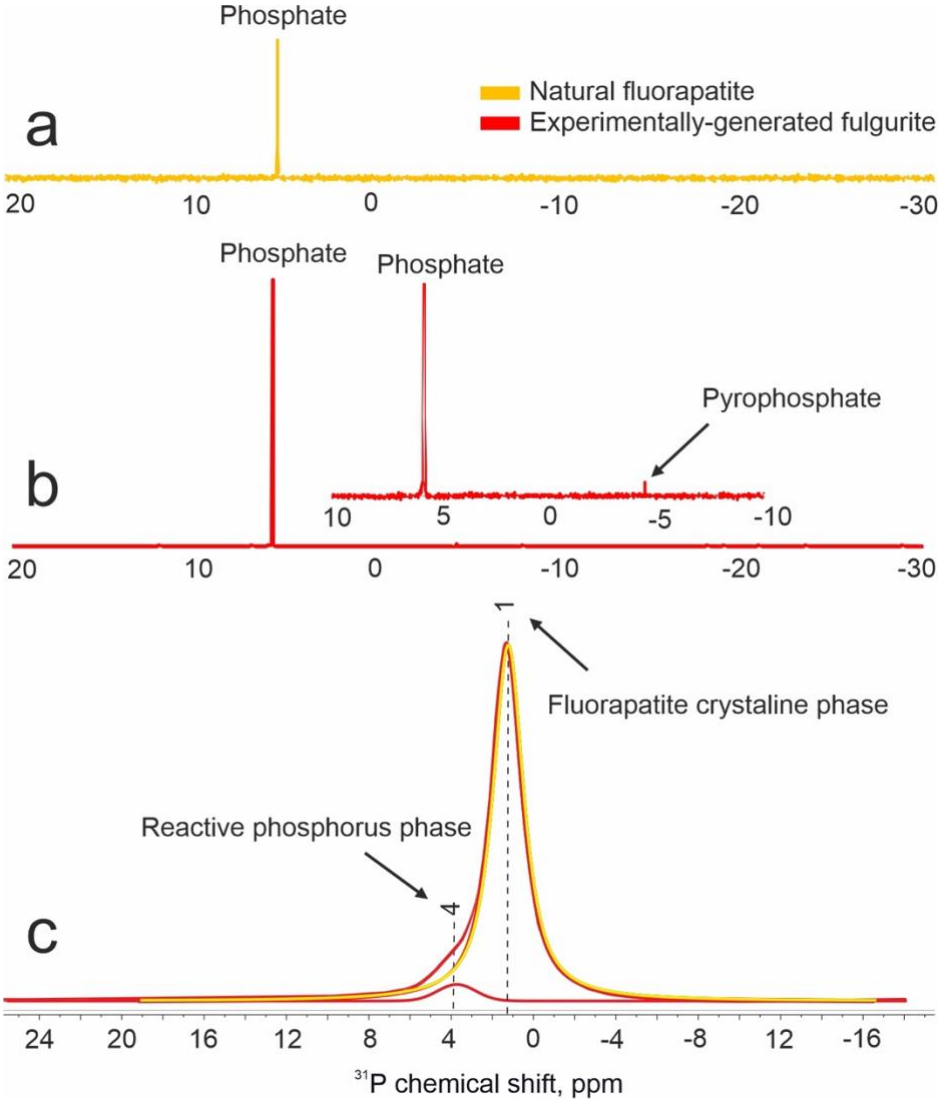

Figure 4.5: ^{31}P NMR spectra of natural fluorapatite and experimentally generated fulgurite extract. (**a**) A solution state natural fluorapatite sample exhibits a single phosphate peak. (**b**) A solution state experimentally generated fulgurite displays an additional peak at -4.5 ppm consistent with the presence of pyrophosphate. (**c**) ^{31}P solid-state MAS NMR spectrum presents approx. 5% reactive phosphorus on the 4 ppm peak in the bulk of experimentally generated fulgurite. Spectra are normalized to a maximum intensity. The Y-axis shows intensity (a.u.).

The formation of reduced P requires high energy inputs. Meteorite impacts may have delivered substantial quantities of P to the early Earth system (Russell et al., 2014; Pasek 2017; Ritson et al., 2020). However, we note that its relatively chaotic environment may have destroyed potential prebiotic reagents and would have generally created inappropriate conditions for prebiotic synthesis. Further, some P species (e.g., phosphide minerals) carried to Earth by meteorite impacts also require survival through delivery followed by aqueous alteration to generate a reactive P phase.

As noted at the outset, lightning strikes have also been suggested as a terrestrial source of reduced P species in natural fulgurites (Essene and Fisher, 1986; Pasek and Block, 2009; Pasek et al., 2012; Hess et al., 2021). Notably, these previously-studied fulgurites are all modern and bear a lithology influenced by modern biogeochemistry. For instance, Essene and Fisher (1986) link the production of phosphides and other reduced phases in their fulgurite to the combustion of a tree root during a lightning strike. In the absence of biologically-derived concentrated carbon for reduction, we show that lightning discharge still facilitates phosphate activation through the formation of pyrophosphate. While not a reduced oxidation state P species, pyrophosphate still bears appreciable phosphorylating power and can phosphorylate sugars and other simple substrates to generate critical organophosphates (Pasek 2020). Lightning strikes at the Earth's surface might generate environments in which prebiotic reagents can survive once generated and participate in the crucial formation steps of proto-life. On the early Earth, lightning activity may have been far more common than today. The successful generation of reactive P-bearing species in experimentally generated fulgurite under controlled conditions represents a crucial step in constraining the P problem, providing a readily reactive P source on the early Earth.

4.6. Conclusions

A natural fulgurite recently found *in situ* in Eastern-Türkiye provided the opportunity to compare it to an experimentally generated fulgurite derived from adjacent protolith. The natural and experimental fulgurites exhibit a high degree of similarity in their textural and mineralogical evolution. This implies that experimental fulgurites can serve as valid proxies for studying natural fulgurites, enabling the inference of natural conditions during fulgurite generation.

Amongst the further implications of this work for natural fulgurite formation is the first observation of lightning discharge parameters associated with the recovery of a pristine natural fulgurite. These parameters, obtained from the WWLLN data range from 11.960 kA to 14.473 kA. Thus, for the first time, a link between natural fulgurite, fulgurite experiments, and lightning monitoring data has been established.

The careful observations of evolving mineralogical textures in the experimental fulgurites generated here have led to the interpretation of the equivalent textures of the natural fulgurites, leading to a better understanding of the geological and environmental consequences of lightning strikes, ultimately enhancing our ability to assess and mitigate potential risks associated with lightning events, thereby opening up a new subfield of experimental geosciences.

Chapter 5. Conclusions and outlook

This thesis explored the formation and significance of fulgurites experimentally. A DC source trigger-pulse setup generated fulgurites under controlled conditions from different compositions, aligning with the experimental objectives.

Experimental fulgurites have been generated using various techniques and setups (Beduent et al., 1828; Butcher 1907; Arai 1969; Kumazaki et al., 1997; Elmi et al., 2018; Castro et al., 2020). Unfortunately, these setups could not fully replicate natural lightning conditions due to technical limitations. Realistic simulations of lightning discharges are necessary to understand fulgurite formation mechanisms and conditions. Therefore, the DC source trigger-pulse setup is designed to align with the ISO standards for lightning effects and protection. This guarantees the reproducibility of tests and physical parameters of the discharges as close as possible to the natural phenomena. This setup comprises two essential components: a Marx generator and a DC source. The Marx generator provides a high current for a few microseconds. This current aids in breaking the dielectric field strength of the target material stored in a sample container. Subsequently, the DC source generates a prolonged continuous current for a pre-determined time range, typically lasting tens of hundreds of milliseconds. It is found that these two steps are critically crucial for fulgurite synthesis because the heat transferred to the target material by the first stroke alone would be insufficient for substantial melting and fulgurite formation. Remarkably, increasing the duration of the prolonged continuous current (i.e., > 100 ms) has no significant effect on the formation mechanism.

It is essential to compare the physical and textural features of experimental and natural fulgurites to understand the similarities and differences in how they are formed. A natural

fulgurite was recently discovered *in situ* Eastern-Türkiye, providing an opportunity to compare it with an experimental fulgurite generated from a co-sampled protolith using the DC source with trigger-pulse setup.

Additionally, the natural fulgurite discovered following a thunderstorm provided a temporal reference point for its formation. Thus, using the World Wide Lightning Location Networks monitors, two cloud-to-ground lightning discharges were determined during this period. These findings, for the first time, indicate the parameters of lightning discharge that may have created the natural fulgurite.

Trial experiments on the protolith of the natural fulgurite indicate that the particle size distribution significantly influences the fulgurite formation. Coarse particles limit the melting due to their high electrical resistivity features. Although the natural lightning overcomes the current (around 11.960 kA and 14.473 kA) generated by the experimental setup by order of magnitude, remarkable similarities are found between the natural and experimental fulgurite. Both fulgurites present similar morphological and chemical features (exhibiting the same sequence of mineral melting and the formation of new structures). This demonstrates the fulgurite synthesis method closely mimics its natural counterpart.

Lightning discharges are provided as an alternative way to reduce the phosphorus in pre-biotic chemistry studies because some reduced (reactive) phosphorus minerals were found in fulgurites. However, it is important to note that these studies have predominantly focused on fulgurites formed from geological materials, such as sand, which may not accurately represent the conditions of early Earth's environment.

To bridge this gap and gain insights into the potential phosphorus reduction mechanisms on the early Earth, I conducted fulgurite synthesis experiments using apatite, a mineral abundant in phosphorus and as a possible P source in the early Earth's mineralogy. These experiments were

carried out under atmospheric conditions since the high voltage laboratory was not designed to use multiple gases during experimentation. However, the primary objective of these experiments was to elucidate the fundamental mechanisms behind phosphorus reduction during fulgurite formation. The extreme temperatures generated during lightning strikes induce both partial and complete melting of the materials involved, followed by recrystallization within the resulting fulgurites. The generated fulgurite presents a high amount of reactive phosphorus relative to its apatite protolith. Thus, this study has shown that fulgurites can be an alternative source of reduced phosphorus, which is involved in the structure of basic building blocks.

This thesis provided a methodology for accurately mimicking lightning discharges with a carefully designed setup to synthesize fulgurites. Based on their chemical and morphological features, generated fulgurites closely resemble their natural counterparts. Furthermore, the influence of different compositions and particle sizes of target materials on fulgurite formation warrants further exploration, as does the potential role of newly formed mineral structures in understanding crystallization sequences in geological systems.

In addition, investigating the phosphorus-bearing rocks might behave differently under replicated atmospheric conditions of early Earth. The atmospheric composition during that period may vary, and this uncertainty opens up the possibility that these rocks could exhibit distinct behaviors. Such variations in atmospheric conditions may influence chemical reactions in both favorable and unfavorable ways.

In essence, this thesis has not only unraveled the mysteries of fulgurite formation but has also opened doors to many exciting research avenues, offering a promising glimpse into the complex interplay between lightning, minerals, and pre-biotic chemistry.

Appendix A

Experimental generation of fulgurite under realistic lightning discharge condition

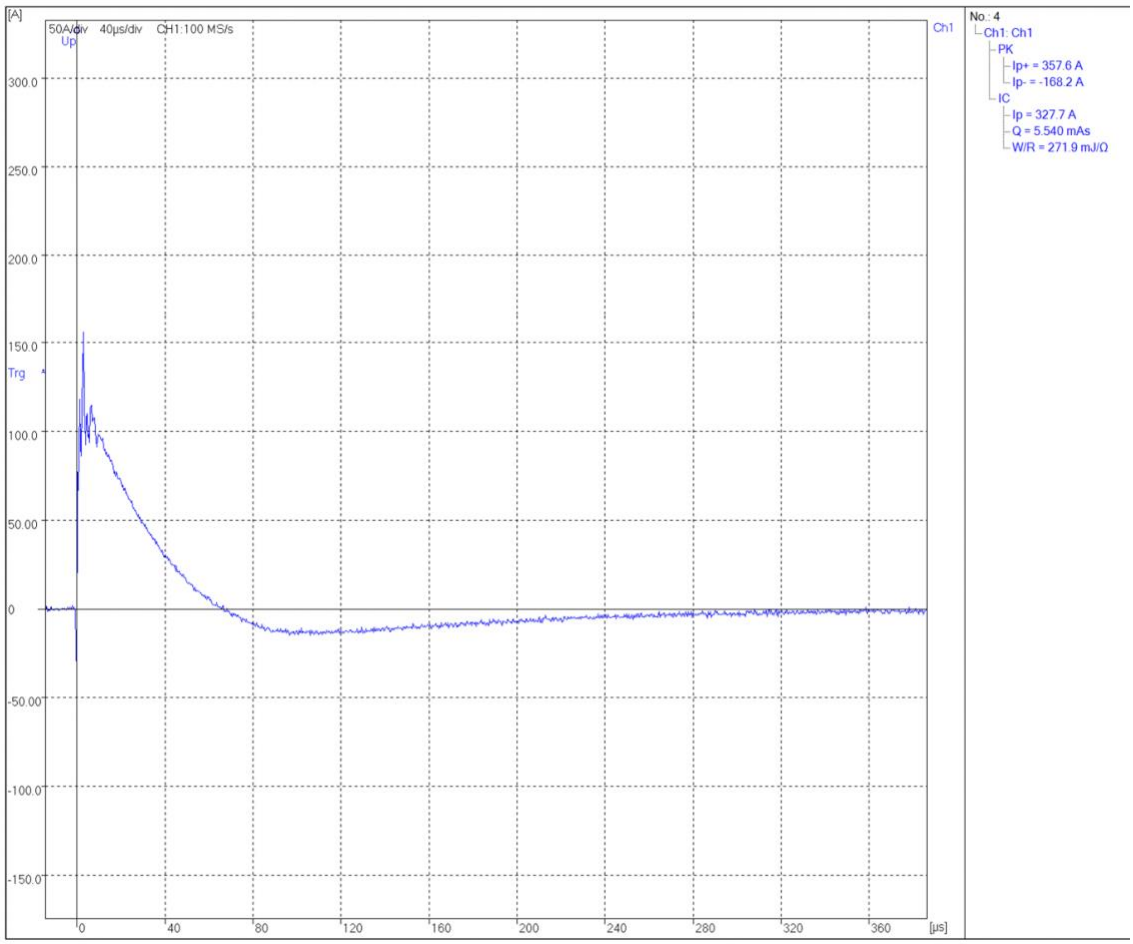

Figure A.1. Electrical waveform of T0. The target material was exposed only in the first stroke with no continuing current phase.

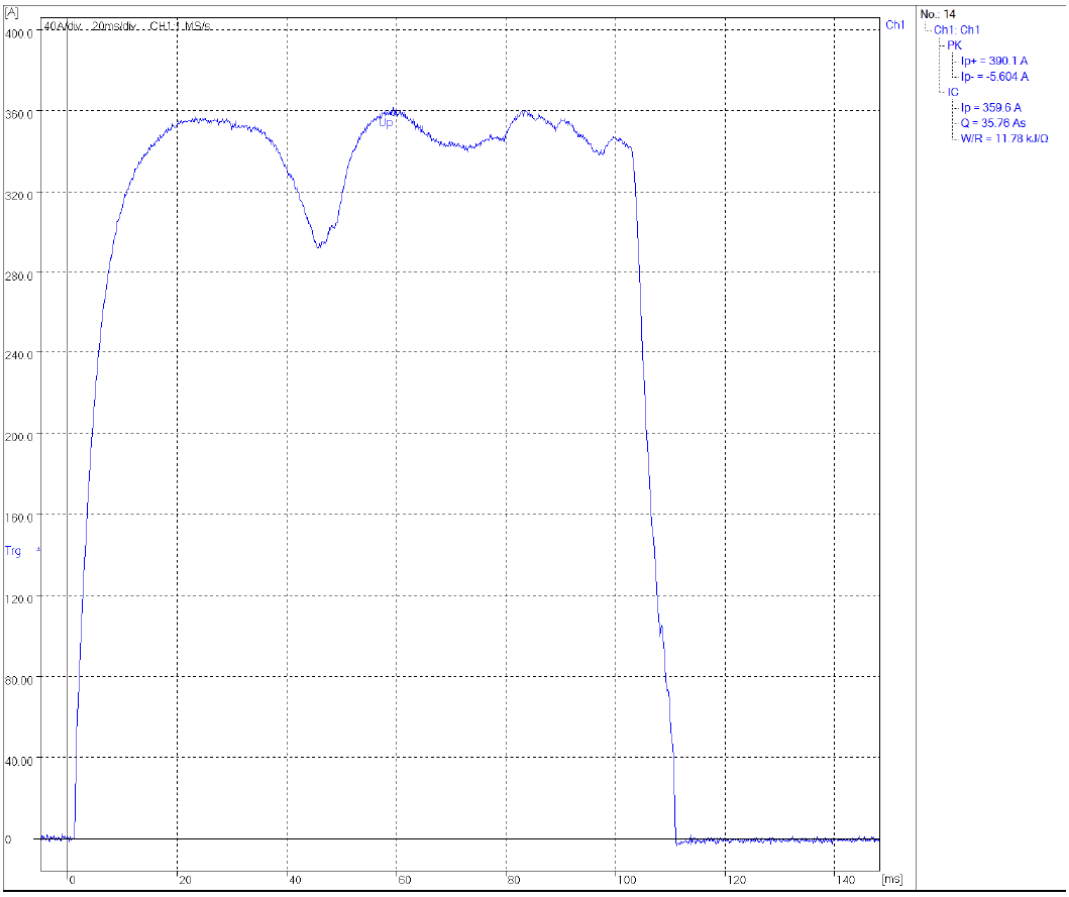

Figure A.2. Electrical waveform of T100 fulgurite. The experiment was performed by striking the target material with the first stroke and continuing the current around 100 ms.

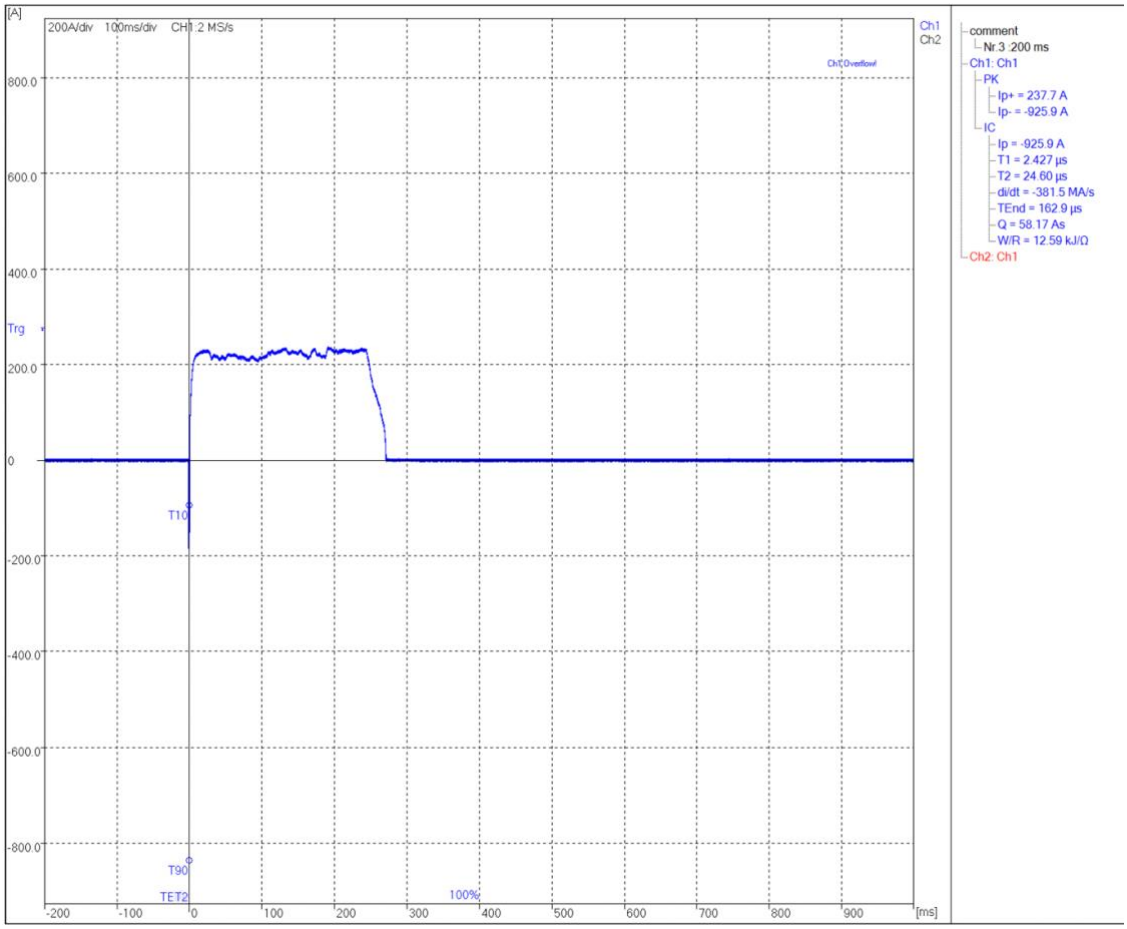

Figure A.3. Electrical waveform of T200 fulgurite. The experiment consisted of striking the target material with an initial stroke and then maintaining a current for approximately 200 ms.

Figure A.4. Electrical waveform of T300 fulgurite. The experiment was initiated striking the target material with a first stroke, followed by continuing current for approximately 300 ms.

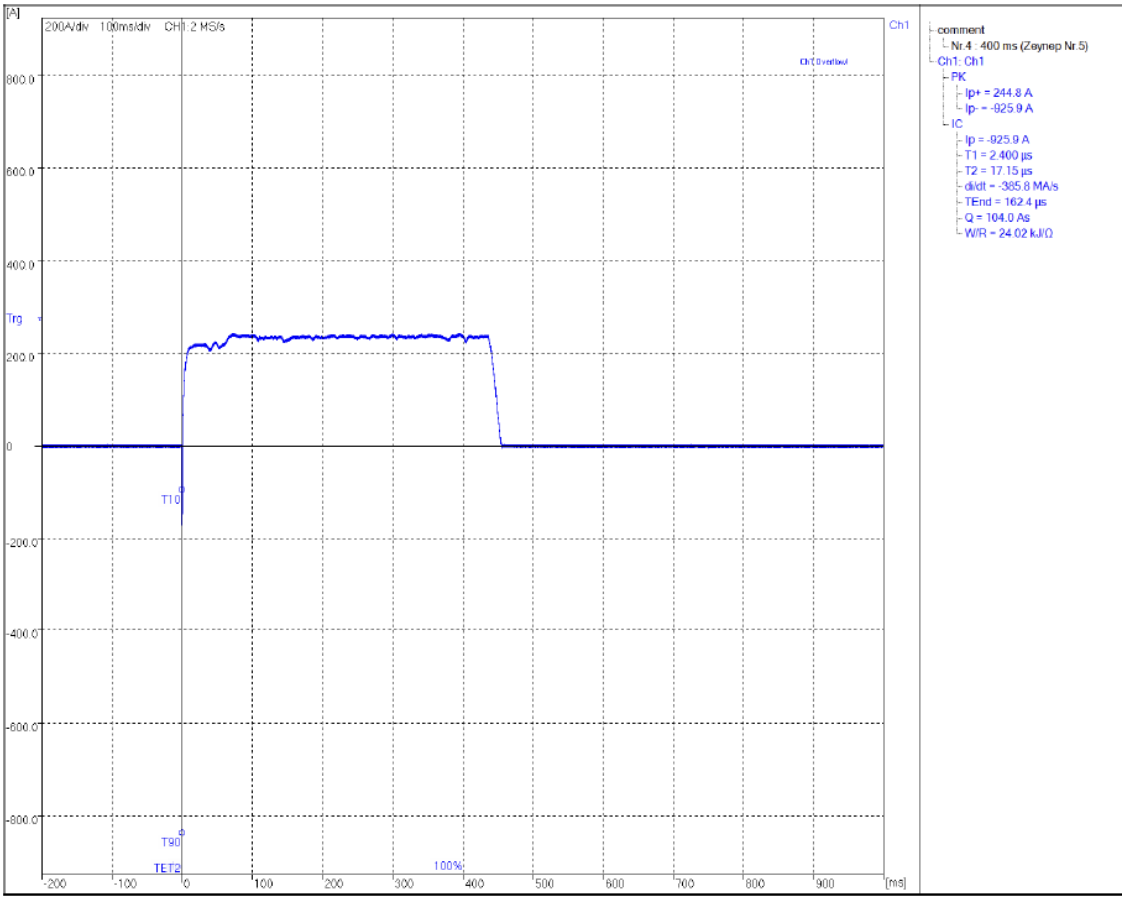

Figure A.5. Electrical waveform of T400 fulgurite. The experiment was performed by striking the target material with the first stroke and continuing the current around 400 ms.

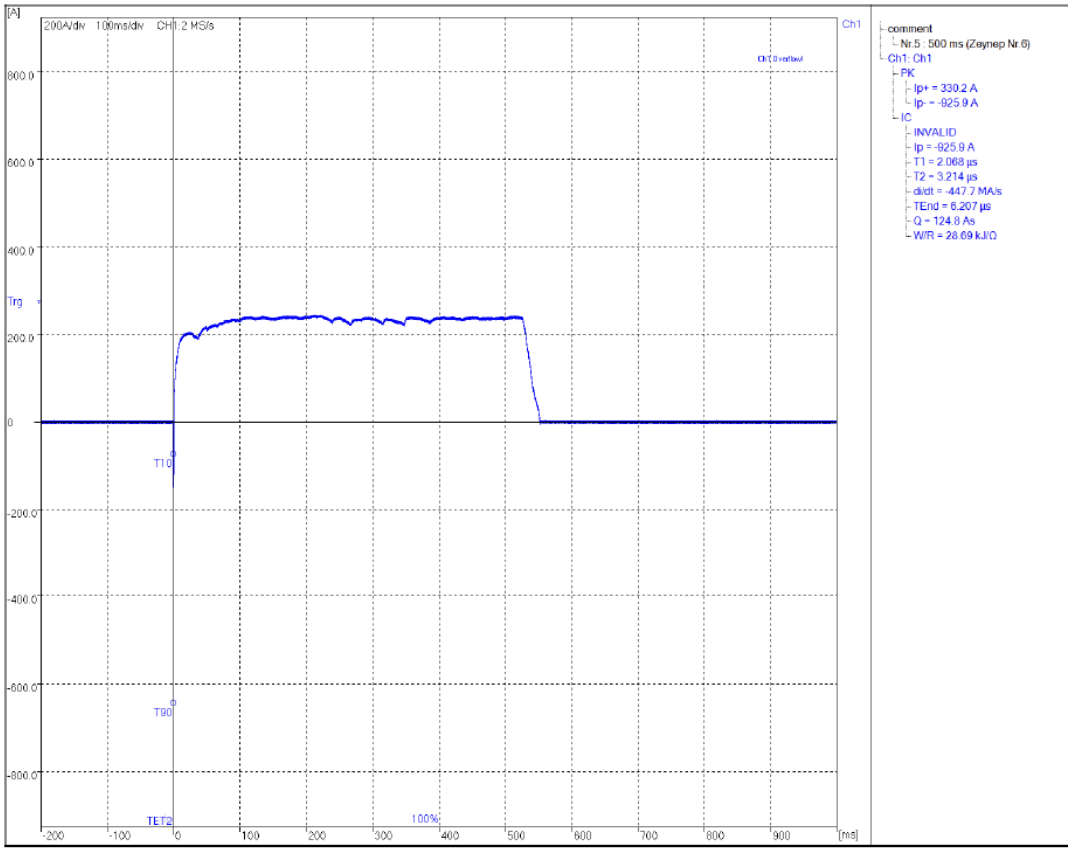

Figure A.6. The electrical waveform of T500 fulgurite. The experiment consisted of striking the target material with an initial stroke and then maintaining a current for approximately 500 ms.

Table A.1. The data of Helium pycnometer analysis. The name LSB refers to the Laacher See Bims deposit in Germany.

	Experimentally generated fulgurites										Synthesized LSB glass	
	T100		T200		T300		T400		T500			
Run	Volume cm3	Density g cm-3	Volume cm3	Density g cm-3	Volume cm3	Density g cm-3	Volume cm3	Density g cm-3	Volume cm3	Density g cm-3	Volume cm3	Density g cm-3
1	0.638	2.488	0.636	2.482	0.644	2.459	0.647	2.476	0.640	2.458	0.629	2.423
2	0.637	2.490	0.640	2.467	0.644	2.458	0.642	2.494	0.628	2.501	0.628	2.428
3	0.636	2.494	0.635	2.486	0.611	2.468	0.641	2.497	0.629	2.498	0.628	2.429
4	0.638	2.488	0.637	2.478	0.641	2.469	0.641	2.498	0.630	2.496	0.629	2.424
5	0.638	2.486	0.638	2.472	0.641	2.468	0.643	2.489	0.630	2.496	0.630	2.422
6	0.638	2.487	0.639	2.469	0.641	2.468	0.644	2.488	0.627	2.505	0.629	2.424
7	0.637	2.491	0.638	2.472	0.644	2.459	0.643	2.490	0.629	2.498	0.630	2.419
8	0.637	2.491	0.637	2.477	0.644	2.458	0.645	2.484	0.618	2.502	0.629	2.424
9	0.637	2.491	0.638	2.472	0.645	2.452	0.645	2.484	0.633	2.481	0.630	2.419
10	0.637	2.492	0.639	2.470	0.645	2.454	0.646	2.479	0.634	2.479	0.630	2.422
Average	0.637	2.490	0.638	2.475	0.640	2.461	0.644	2.488	0.630	2.491	0.629	2.423

Appendix B

Reactive phosphorus via simulated lightning discharge:

A role for fulgurites in pre-biotic chemistry

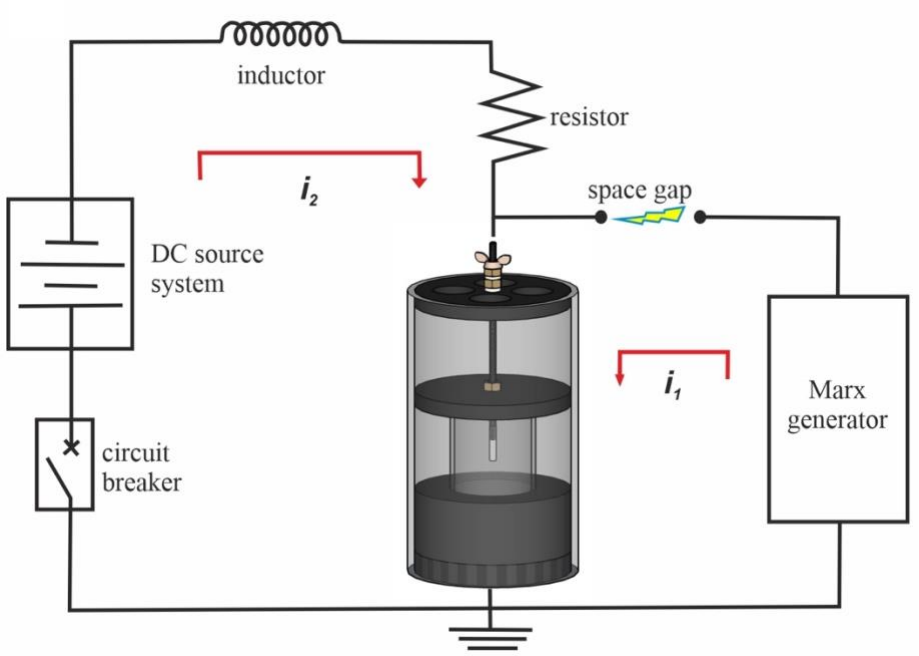

Figure B.1. Schematic view of the DC-trigger impulse setup. The main apparatus of the setup consists of the Marx-generator, DC source system, circuit breaker, inductor, resistor, and insulated sample container. i_1: First return stroke and i_2: Long-duration continuing current.

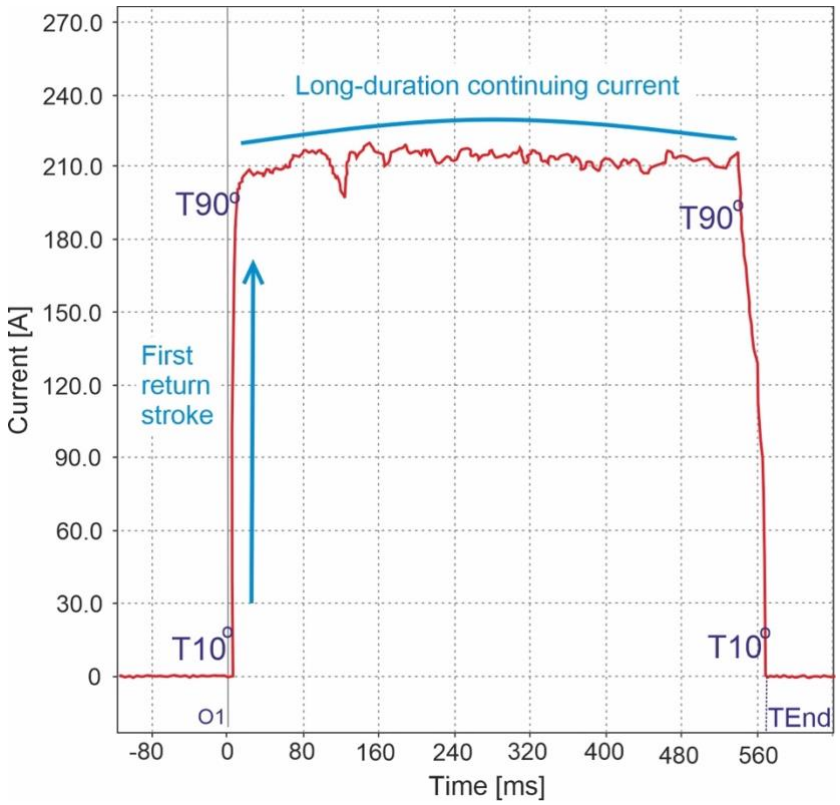

Figure B.2. The long-duration continuing current characteristic used for the fulgurite synthesis experiment.

Table B.1. Major elements concentrations of natural apatite in EPMA data.

	1	2	3	4	5	6	7	8	9	10
Na_2O	0.04	0.04	0.03	0.02	0.05	0.02	0.02	0.05	0.00	0.03
SiO_2	1.36	1.39	1.34	1.36	1.45	1.39	1.34	1.38	1.36	1.40
Al_2O_3	0.00	0.00	0.00	0.00	0.00	0.00	0.02	0.01	0.00	0.00
P_2O_5	38.14	38.26	39.07	37.38	37.75	38.12	37.85	38.41	37.86	38.28
SO_3	0.78	0.79	0.74	0.76	0.79	0.71	0.69	0.68	0.74	0.67
Cl	0.13	0.16	0.13	0.15	0.15	0.15	0.15	0.14	0.14	0.15
ThO_2	0.42	0.34	0.26	0.34	0.33	0.34	0.33	0.37	0.41	0.31
CaO	53.70	54.20	54.45	54.19	53.63	53.90	54.29	54.35	54.09	53.67
K_2O	0.00	0.02	0.02	0.00	0.00	0.00	0.00	0.00	0.01	0.00
TiO_2	0.00	0.00	0.00	0.00	0.00	0.00	0.00	0.00	0.00	0.00
FeO	0.01	0.00	0.02	0.01	0.00	0.00	0.00	0.00	0.00	0.00
F	3.93	3.56	3.33	3.19	3.67	3.69	3.03	3.33	3.67	3.38
La_2O_3	0.35	0.31	0.30	0.28	0.36	0.28	0.37	0.32	0.36	0.34
Ce_2O_3	0.62	0.68	0.68	0.72	0.67	0.56	0.68	0.71	0.68	0.67
Nd_2O_3	0.13	0.25	0.23	0.24	0.15	0.13	0.24	0.20	0.22	0.21
CuO	0.00	0.00	0.03	0.03	0.00	0.00	0.00	0.00	0.00	0.01
WO_3	0.00	0.07	0.16	0.05	0.05	0.00	0.00	0.03	0.09	0.06
SrO	0.11	0.07	0.07	0.06	0.10	0.08	0.08	0.04	0.07	0.05
Total	99.71	100.13	100.86	98.78	99.15	99.35	99.09	100.02	99.70	99.23

Table B.2. Major elements concentrations of natural apatite in EPMA data (continuous).

	11	12	13	14	15	16	17	18	19	20
Na_2O	0.04	0.02	0.02	0.03	0.05	0.05	0.02	0.03	0.04	0.02
SiO_2	1.42	1.38	1.33	1.40	1.42	1.41	1.41	1.40	1.31	1.36
Al_2O_3	0.01	0.01	0.01	0.00	0.01	0.00	0.00	0.00	0.00	0.00
P_2O_5	35.31	37.64	38.47	37.89	38.20	38.23	38.47	37.97	38.11	37.61
SO_3	0.80	0.71	0.63	0.68	0.66	0.63	0.62	0.67	0.65	0.67
Cl	0.20	0.15	0.16	0.13	0.14	0.16	0.16	0.13	0.16	0.15
ThO_2	0.34	0.32	0.19	0.33	0.29	0.32	0.23	0.35	0.22	0.38
CaO	56.81	54.09	54.02	53.92	53.59	53.69	53.95	53.75	54.01	54.42
K_2O	0.00	0.01	0.01	0.02	0.00	0.01	0.00	0.00	0.00	0.00
TiO_2	0.00	0.00	0.00	0.00	0.00	0.00	0.00	0.00	0.00	0.00
FeO	0.00	0.00	0.01	0.00	0.02	0.00	0.00	0.02	0.00	0.00
F	3.52	3.55	3.45	3.61	3.55	3.61	3.83	4.04	3.20	3.38
La_2O_3	0.31	0.25	0.30	0.28	0.16	0.25	0.16	0.37	0.23	0.28
Ce_2O_3	0.61	0.62	0.49	0.52	0.61	0.59	0.54	0.66	0.62	0.49
Nd_2O_3	0.24	0.14	0.20	0.14	0.25	0.25	0.27	0.18	0.18	0.19
CuO	0.00	0.02	0.01	0.01	0.00	0.00	0.03	0.01	0.00	0.00
WO_3	0.07	0.00	0.02	0.00	0.10	0.00	0.02	0.09	0.00	0.00
SrO	0.10	0.09	0.09	0.07	0.09	0.05	0.10	0.07	0.07	0.06
Total	99.77	98.99	99.42	99.02	99.14	99.25	99.81	99.73	98.81	99.00

Table B.3. Major elements concentrations of pristine materials in EPMA measurements of experimentally generated fulgurite.

	1	2	3	4	5
Na_2O	0.02	0.03	0.00	0.01	0.01
SiO_2	1.49	1.46	1.40	1.52	1.59
Al_2O_3	0.00	0.00	0.01	0.00	0.00
P_2O_5	3.95	37.86	38.27	37.88	37.58
SO_3	1.09	1.08	0.62	0.81	0.87
Cl	0.21	0.26	0.12	0.16	0.18
ThO_2	0.44	0.41	0.61	0.39	0.33
CaO	53.93	54.09	53.96.	54.23	53.88
K_2O	0.01	0.00	0.00	0.00	0.00
TiO_2	0.00	0.00	0.00	0.00	0.00
FeO	0.03	0.02	0.02	0.02	0.01
F	2.84	2.76	2.95	3.15	3.02
La_2O_3	0.20	0.37	0.38	0.34	0.35
Ce_2O_3	0.61	0.62	0.84	0.61	0.70
Nd_2O_3	0.20	0.23	0.24	0.21	0.26
CuO	0.06	0.04	0.00	0.05	0.04
WO_3	0.09	0.07	0.11	0.00	0.00
SrO	0.06	0.05	0.09	0.09	0.06
Total	99.27	99.43	99.70	99.52	98.93

Table B.4. Major elements concentrations of newly-formed crystals in EPMA measurements of experimentally generated fulgurite.

	1	2	3	4	5	6	7	8	9	10
Na_2O	0.01	0.01	0.00	0.01	0.00	0.00	0.00	0.00	0.00	0.01
SiO_2	1.59	1.76	1.54	1.72	1.63	1.68	1.43	1.67	1.60	1.44
Al_2O_3	0.00	0.00	0.01	0.01	0.00	0.00	0.00	0.00	0.00	0.00
P_2O_5	39.61	38.70	39.53	39.31	39.70	39.67	39.47	39.18	39.17	40.09
SO_3	0.01	0.00	0.02	0.05	0.03	0.03	0.02	0.00	0.00	0.00
Cl	0.10	0.11	0.12	0.13	0.11	0.09	0.15	0.11	0.15	0.14
ThO_2	0.22	0.20	0.11	0.21	0.13	0.21	0.12	0.22	0.17	0.14
CaO	54.56	55.40	54.55	54.66	54.25	54.77	54.70	54.58	54.74	54.69
K_2O	0.00	0.02	0.00	0.00	0.00	0.01	0.00	0.00	0.00	0.00
TiO_2	0.00	0.00	0.00	0.00	0.00	0.00	0.00	0.00	0.00	0.00
FeO	0.03	0.00	0.02	0.00	0.00	0.02	0.04	0.04	0.00	0.04
F	2.42	2.29	2.33	2.45	2.39	2.50	2.53	2.24	2.40	2.29
La_2O_3	0.27	0.30	0.24	0.26	0.28	0.22	0.25	0.28	0.30	0.20
Ce_2O_3	0.41	0.49	0.38	0.38	0.55	0.43	0.39	0.43	0.44	0.43
Nd_2O_3	0.21	0.14	0.26	0.17	0.19	0.29	0.10	0.22	0.21	0.21
CuO	0.09	0.15	0.12	0.02	0.12	0.11	0.04	0.00	0.05	0.04
WO_3	0.07	0.09	0.06	0.00	0.04	0.00	0.06	0.00	0.00	0.00
SrO	0.08	0.06	0.08	0.05	0.08	0.04	0.08	0.07	0.08	0.06
Total	99.69	99.72	99.38	99.42	99.51	100.07	99.38	99.06	99.32	99.78

Table B.5. Major elements concentrations of interstitial phases in EPMA measurements of experimentally generated fulgurite.

	1	2	3	4	5	6	7	8	9	10
Na_2O	nd	0.02	0.01	0.00	0.04	0.00	0.00	0.00	0.04	0.01
SiO_2	0.49	0.88	1.19	0.58	0.42	0.94	0.74	1.83	0.99	1.41
Al_2O_3	0.00	0.00	0.00	0.00	0.02	0.02	0.00	0.09	0.16	0.06
P_2O_5	14.43	29.79	22.14	35.35	2.78	38.59	29.94	34.94	4.09	29.26
SO_3	0.11	0.11	0.10	0.03	0.09	0.08	0.29	0.11	0.10	0.19
Cl	0.07	0.17	0.15	0.08	2.18	0.16	0.13	0.35	0.23	0.10
ThO_2	19.02	0.14	0.55	30.05	0.58	4.74	27.12	7.44	19.01	0.10
CaO	20.29	45.12	35.94	43.67	58.30	54.18	40.89	52.59	45.42	39.97
K_2O	0.01	0.15	0.00	0.00	0.04	0.00	0.00	0.00	0.00	0.00
TiO_2	0.00	0.00	0.00	0.00	0.00	0.00	0.00	0.00	0.00	0.00
FeO	0.00	0.03	0.00	0.00	0.10	0.03	0.00	0.28	0.12	0.04
F	2.21	2.57	2.24	1.75	29.27	2.36	2.23	2.13	1.20	0.00
La_2O_3	3.74	2.06	0.87	0,39	0.89	0.21	0.74	1.13	1.76	0.15
Ce_2O_3	34.79	0.39	0.59	14.21	3.49	2.55	9.04	6.57	13.70	0.28
Nd_2O_3	1.27	0.27	0.13	1.64	0.78	0.45	0.88	1.18	1.97	0.07
CuO	0.00	0.12	0.00	0.00	0.93	0.00	0.14	2.75	0.62	61.41
WO_3	0.22	0.00	0.05	0.00	0.15	0.04	0.08	0.33	0.48	0.00
SrO	0.06	0.05	0.09	0.05	0.02	0.06	0.08	0.02	0,.03	0.06
Total	96.72	81.88	64.04	127.81	100.08	104.42	112.31	111.73	89.93	133.11

Bibliography

1. Ablesimov, N.Y., Tsyurupa, A.I. and Lipatov, V.G. (1986) Phase and element ratios upon fulguritization of basalt. Trans (Dokl) USSR Acad. Earth Sci. 290, 161–164.
2. Abreu, S.F., Chandan, D., Holzworth, R.H. and Strong, K. (2010) A performance assessment of the World Wide Lightning Location Network (WWLLN) via comparison with the Canadian Lightning Detection Network (CLDN). Atmos. Meas. Tech. 3, 1143-1153. https://doi.org/10.5194/amt-3-1143-2010.
3. Aleksandrov, N.L., Bazelyan, É.M. and Shneider, M.N. (2000) Effect of continuous current during pauses between successive strokes on the decay of the lightning channel. Plasma Phys. Rep. 26, 893–901. https://doi.org/10.1134/1.1316830.
4. Allen, B.M., Mark, F.D., Kheirkhah, M., Barfod, D., Emami, H.M. and Saville, C. (2011) $^{40}Ar/^{39}Ar$ dating of Quaternary lavas in northwest Iran: constraints on the landscape evolution and incision rates of the Turkish–Iranian plateau. Geophys. J. Int. 1-14. https://doi.org/10.1111/j.1365-246X.2011.05022.x.
5. Alte da Veiga, N.M.S., Martín-Gil, F.J., Martín-Gil, J., Gomes, E.M.C. and Martín-Ramos, P. (2021) Physico-chemical study of an exogenic fulgurite from a thunderstorm on 10th August 2013 in Dallas, TX. Phys. Chem. Miner. 48, 1-15. https://doi.org/10.1007/s00269-021-01134-w.
6. Anderson, A.E. (1925). Sand fulgurites from Nebraska: Their structure and formative factors. Nebraska State Museum Bulletin. 1(7), 49-86.
7. Arai, B. (1969) The preliminary experiment on the Artificial Fulgurite: Science reports of the Yokohama National University 15, 17-24.
8. Ballhaus, C., Wirth, R. Fonseca, R.O.C., Blanchard, H., Pröll, W., Bragagni, A., Nagel, T., Schreiber, A., Dittrich, S., Thome, V., Hezel, D.C., Below, R. and Cieszynski, H.

(2017) Ultra-high pressure and ultra-reduced minerals in ophiolites may form by lightning strikes. Geochem. Perspect. Lett. 5, 42-46. https://doi.org/10.7185/geochemlet.1744.

9. Bazelyan, E.M. and Raizer, Y.P. (2000) Lightning physics and lightning protection. CRC Press.
10. Benner, S.A., Kim, H.J. and Carrigan, M.A. (2012) Asphalt, water, and the prebiotic synthesis of ribose, ribonucleosides, and RNA. Acc. Chem. Res. 45, 2025-2034. https://doi.org/10.1021/ar200332w.
11. Beudant, F.S., Hachette, J.N.P. and Savart, F. (1828) Expérience sur la formation des tubes fulminaires. Ann. Chim. Phys. 37, 319-321.
12. Bidin, N., Sanagi, M.M., Farah, M., Razali, M.N. and Khamis, J. (2018) Laser-induced artificial fulgurites. Laser Phys. Lett. 15 (7), 076001. doi:10.1088/1612-202X/aaada4.
13. Bindi, L., Feng, T. and Pasek, M.A. (2023) Routes to reduction of phosphate by high-energy events. Commun. Earth Environ. 4, 70. https://doi.org/10.1038/s43247-023-00736-2.
14. Bogaard, P. and Schmincke, H.U., (1985) Laacher See Tephra: A widespread isochronous late Quaternary tephra layer in central and northern Europe. Geol. Soc. Am. Bull. 96, 1554-1571. https://doi.org/10.1130/0016-7606(1985)96<1554:LSTAWI>2.0.CO;2.
15. Britvin, S.N., Murashko, M.N., Vapnik, Y., Polekhovsky, Y.S. and Krivovichev, S.V. (2015) Earth's Phosphides in Levant and insights into the source of Archean prebiotic phosphorus. Sci. Rep. 5, 1-5. https://doi.org/10.1038/srep08355.
16. Brook, M., Kitagawa, N. and Workman, E.J. (1962) Quantitative study of strokes and continuing currents in lightning discharges to ground. J. Geophys. Res. 67(2), 649-659. https://doi.org/10.1029/JZ067i002p00649.

17. Bryant, D.E. and Kee, T.P. (2006) Direct evidence for the availability of reactive, water-soluble phosphorus on the early Earth. H-Phosphonic acid from the Nantan meteorite. Chem. Commun. 22, 2344-2346. https://doi.org/10.1039/B602651F.

18. Bryant, D.E., Greenfield, D., Walshaw, R.D., Evans, S.M., Nimmo, A.E., Smith, C.L., Wang, L., Pasek, M.A. and Kee, T.P. (2009) Electrochemical studies of iron meteorites. Phosphorus redox chemistry on the early Earth. Int. J. Astrobiology 8, 27–36. https://doi.org/10.1017/S1473550408004345.

19. Buchwald, V.F. (1984) Handbook of iron meteorites. Univ. of California Press, Berkeley, CA, 1.

20. Butcher, D. (1907) Experiments on Artificial Fulgurites. Proc. Pyhs. Soc. Lond. 21, 254-260. https://doi.org/10.1088/1478-7814/21/1/315.

21. Castro, J.M., Keller, F., Feisel, Y., Lanari, P., Helo, C., Mueller, S.P. Schipper, C.I. and Thomas, C. (2020) Lightning-induced weathering of Cascadian volcanic peaks. Earth Planet Sci. Lett. 552, 116595. https://doi.org/10.1016/j.epsl.2020.116595.

22. Clocchiatii, R. (1990) Les fugurites et roches vitrifiées de l'Etna. Eur. J. Mineral. 2, 479–494.

23. Daly, T.K., Peter R.B., Peter, W. and Charles F.L. (1993) Fullerenes from a fulgurite. Science 259(5101), 1599-1601. https://doi.org/10.1126/science.259.5101.1599.

24. De Campos, C.P. and Hess, K.U. (2021) Geological Glasses. Encyclopedia of Glass Science, Technology, History and Culture 2, 215-829. https://doi.org/10.1002/9781118801017.ch7.2.

25. Deer, W., Howie, R.A. and Zussman, J. (1966) An introduction to the rock-forming minerals. London, UK: Longman 457. https://doi.org/10.1180/DHZ.

26. De Graaf, R.M. and Schwartz, A.W. (2000) Reduction and activation of phosphate on the primitive earth. Orig. Life Evol. Biosph. 30, 405-410. https://doi.org/10.1023/A:1006700512902.

27. Essene, E.J. and Fisher, D.C. (1986) Lightning strike fusion: extreme reduction and metal- silicate liquid immiscibility. Science 234, 189–193. https://doi.org/10.1126/science.234.4773.189.

28. Elmi, C., Chen, J., Goldsby, D. and Gieré, R. (2017) Mineralogical and compositional features of rock fulgurites: A record of lightning effects on granite. Am. Min. 102, 1470-1481. https://doi.org/10.2138/am-2017-5971.

29. Elmi, C., Chen, J., Goldsby, D. and Gieré, R. (2018) Mineralogical and compositional features of rock fulgurites: A record of lightning effects on granite. Am. Min. 102, 1470-1481. https://doi.org/10.2138/am-2017-5971.

30. Elmi, C., Cipriani, A., Lugli, F. and Sighinolfi, G. (2021) Insights on the Origin of Vitrified Rocks from Serravuda, Acri (Italy): Rock Fulgurite or Anthropogenic Activity? J. Geosci. 11, 493. https://doi.org/10.3390/geosciences11120493.

31. Ende, M., Schorr, S., Kloess, G., Franz, A. and Tovar, M. (2012) Shocked quartz in Sahara fulgurite. Eur. J. Mineral. 24, 499-507. https://doi.org/10.1127/0935-1221/2012/0024-2188.

32. Folstad, M.A., Yu, H., Wang, H. and Tangstad, M. (2023) Disintegration of six different quartz types during heating to 1600°C. Minerals 13, 132. https://doi.org/10.3390/ min13020132.

33. Frenzel, G. and Ottemann, J. (1978) Über Blitzgläser vom Katzenbuckel, Odenwald, und ihre Ähnlichkeit mit Tektiten. Neues Jahrb. für Mineral. Monatshefte 10, 439-446.

34. Frenzel, G. and Stähle, V. (1982) Fulgurite glass on peridotite from near Frankenstein near Darmstadt. Chem. Erde 41, 111-119.

35. Frenzel, G. and Stähle, V. (1984) Über Aluminosilikatglas mit Lechatelierit-Einschlüssen von einer Fulguritrühre des Hahnenstockes (Glarner Freiburg, Schweiz). Chem. Erde 43, 17-26.

36. Frenzel, G., Irouschek-Zumthor, A. and Stähle, V. (1989) Stobwellenmetamorphose, Aufschmelzung and Verdampfung bei Fulguritbildung an exponierten Berggipfeln. Chem. Erde 49, 265-286.

37. Galliot, M.P. (1980) Petrified lightning: a discussion of sand fulgurites. Rocks & Minerals 55, 13–17.

38. Gaudin, D. and Cimarelli, C. (2019) The electrification of volcanic jets and controlling parameters: A laboratory study. Earth. Planetary Sci. Lett. 513, 69-80. https://doi.org/10.1016/j.epsl.2019.02.024.

39. Genareau, K., Gharghabi, P., Gafford, J. and Mazzola, M. (2017) The elusive evidence of volcanic lightning. Sci. Rep. 7, 1-9. doi: 10.1038/s41598-017-15643-8.

40. Genareau, K., Gharghabi, P. and Klüss, J. (2020) Influence of shock propagation on lightning evidence in volcanic ashfall deposits. Earth Planetary Sci. Lett. 535, 116124. https://doi.org/10.1016/j.epsl.2020.116124.

41. Glindemann, D., De Graaf, R.M. and Schwartz, A.W. (1999) Chemical reduction of phosphate on the primitive Earth. Orig. Life Evol. Biosph. 29, 555-561. https://doi.org/10.1023/a:1006622900660.

42. Grapes, R.H. and Müller-Sigmund, H. (2010) Lightning-strike fusion of gabbro and formation of magnetite-bearing fulgurite, Cornone di Blumone, Adamello, Western Alps, Italy. Mineral. Petrol. 99, 67-74. https://doi.org/10.1007/s00710-009-0100-3.

43. Gulick, A. (1995) Phosphorus as a factor in the origin of life. Am. Sci. 43, 479-489.

44. Gull, M., Mojica, M.A., Fernández, F.M., Gaul, D.A., Orlando, T.M., Liotta, C.L. and Pasek, M.A. (2015) Nucleoside phosphorylation by the mineral schreibersite. Sci. Rep. 5. https://doi.org/17198.10.1038/srep17198.

45. Gull, M., Omran, A., Feng, T. and Pasek, M.A. (2020) Silicate-, Magnesium Ion-, and Urea-Induced Prebiotic Phosphorylation of Uridine via Pyrophosphate; Revisiting the Hot Drying Water Pool Scenario. Life 8, 122. https://doi.org/10.3390/life10080122.

46. Harland, W.B. and Hacker, J.F. (1966) Fossil lightning strikes 250 million years ago. Adv. Sci. 22, 663 -665.

47. Hazen, R.M. (2013) Paleomineralogy of the Hadean Eon: a preliminary species list. Am. J. Sci. 313, 807-843. https://doi.org/10.2475/09.2013.01.

48. Herschy B., Chang, S.J., Blake, R., Lepland, A., Abbott-Lyon, H., Sampson, J., Atlas, Z., Kee, T.P. and Pasek, M.A. (2018) Archean phosphorus liberation induced by iron redox geochemistry. Nat. Commun. 9, 1346. https://doi.org/10.1038/s41467-018-03835-3.

49. Hess, B.L., Piazolo, S. and Harvey, J. (2021) Lightning strikes as a major facilitator of prebiotic phosphorus reduction on early Earth. Nat. Commun. 12, 1-8. https://doi.org/10.1038/s41467-021-21849-2.

50. Holzworth, R.H., McCarthy, M.P., Brundell, J.B., Jacobson, A.R. and Rodger, C.J. (2019) Global distribution of superbolts. Geophys. Res. Atmos. 124, 9996-10005. https://doi.org/10.1029/2019JD030975.

51. Hutchins, M.L., Holtzworth, R.H., Rodger, C.J. and Brundell, J.B. (2012) Far-field power of lightning strokes as measured by the World Wide Lightning Location Network. Atmos. Ocean. Technol. 29, 1102-1110. https://doi.org/10.1175/jtech-d-11-00174.1.

52. Hutchins, M.L., Jacobson, A.R., Holzworth, R.H. and Brundell, J.B. (2013) Azimuthal dependence of VLF propagation. J. Geophys. Res. Space Phys. 118, 5808-5812. https://doi.org/10.1002/jgra.50533.

53. International Electrotechnical Commission (IEC). (2010) Protection against lightning - Part 1: General Principles (2nd ed.), ISBN 978-2-88912-280-6.

54. Jones, B.E., Jones, K.S., Rambo, K.J., Rakov, V.A., Jerald, J. and Uman, M.A. (2005). Oxide reduction during triggered-lightning fulgurite formation. Atmos. Sol. Terr. Phys. 67(4), 423-428. https://doi.org/10.1016/j.jastp.2004.11.005.

55. Karadag, A., Kaygisiz, E., Nikitin, T., Ongen, S., Ogruc Ildiz, G., Aysal, N., Yilmaz, A. and Fausto, R. (2022) Micro-Raman Spectroscopy and X-ray Diffraction Analyses of the Core and Shell Compartments of an Iron-Rich Fulgurite. Molecules 27, 3053. https://doi.org/10.3390/molecules27103053.

56. Kassi, A.M., Kasi A.K., Friis, H. and Kakar, D.M. (2013) Occurrences of rock fulgurites associated with steel pylons of the overhead electric transmission line at Tor Zawar, Ziarat District and Jang Tor Ghar, Muslim Bagh, Pakistan. Turk. J. Earth Sci. 22, 1010-19. doi:10.3906/yer-1207-6.

57. Kenny, G.G. and Pasek, M.A. (2021) The response of zircon to the extreme pressures and temperatures of a lightning strike. Sci. Rep. 11, 1560. https://doi.org/10.1038/s41598-021-81043-8.

58. Ketcham R.A. (2015). Technical Note: Calculation of stoichiometry from EMP data for apatite and other phases with mixing on monovalent anion sites. Am. Min. 100 (7), 1620–1623. https://doi.org/10.2138/am-2015-5171.

59. Kieu, N., Gordillo-Vázquez, F.J., Passas, M., Sánchez, J., Pérez-Invernón, F.J., Luque, A., Montanjá, J. and Christian, H. (2020) Sub microsecond spectroscopy of lightning-

like discharges: Exploring new time regimes. Geophys. Res. Lett. 47 (15). https://doi.org/10.1029/2020GL088755.

60. Kumazaki, K., Naito, K. and Horii, K. (1997) Production of artificial fulgurite by utilizing rocket triggered lightning. IEEJ Trans. Fundam. Mater. 117, 1013-1020. https://doi.org/10.1541/ieejfms1990.117.10_1013.

61. Kumler, B. and Day, J.M.D. (2021) Trace element variations generated by magmatic and post-crystallization processes in eucrite meteorites. Cosmochim. Acta. 301, 211-229. https://doi.org/10.1016/j.gca.2021.03.002.

62. Kuo, L.W., Smith, S.A.F., Chen, C.C., Ku, C. S., Chiang, C. Y., Brown, D., Negrini, M. Huang, W.J. and Chen, T.Y. (2021) Lightning-induced high temperature and pressure microstructures in surface and subsurface fulgurites. Sci. Rep. 11, 22031. https://doi.org/10.1038/s41598-021-01559-x.

63. Lapierre, J.L., Sonnenfeld, R.G., Edens, H.E. and Stock, M. (2014) On the relationship between continuing current and positive leader growth. J. Geophys. Res. Atmos. 119, 12-479. https://doi.org/10.1002/2014JD022080.

64. Latham, D. and Williams, E. (2001) Lightning and forest fires in: Forest Fires. Academic press. 375-418. https://doi.org/10.1016/B978-012386660-8/50013-1.

65. Lavallée, Y., Hirose, T., Kendrick, J.E., Hess, K.U. and Dingwell, D.B. (2015) Fault rheology beyond frictional melting. Proceedings of the National Academy of Sciences, 112(30), 9276-9280. https://doi.org/10.1073/pnas.1413608112.

66. Libby, C.A. (1986) Fulgurite in the Sierra Nevada. California Geology 39, 262.

67. Liu, C. and Heckman, S. (2011) The application of total lightning detection and cell tracking for severe weather prediction. In Proceedings of the 91st American Meteorological Society Annual Meeting, Seattle, WA, USA. 23-27.

68. Martín-Ramos, P., Gil, F.P., Martín-Gil, F. and Martín-Gil, J. (2019) Characterization of exogenic fulgurites from an archaeological site in Tiedra, Valladolid, Spain. Geol. Mag. 156, 1455-1462. https://doi.org/10.1017/S0016756819000438.

69. Massiot, D., Fayon, F., Capron, M., King, I., Le Calvé, S., Alonso, B., Durand, J.O., Bujoli, B., Gan, Z. and Hoatson, G. (2001) Modelling one- and two-dimensional solid-state NMR spectra. Magn. Reson. Chem. 40, 70-76. https://doi.org/10.1002/mrc.984.

70. Maurer, B. (2021) Lightning induced olivine spherules. Experimental generation and structural and chemical characterization of crystalline and glassy particles generated by artificial lightning. [MS.c. Thesis]: Luswig-Maximilians-Universität, 71.

71. Mazur, V. (2016). Principles of lightning physics. IoP Publishing.

72. Merrill, G.P. (1886) On fulgurites: Proceedings of the United States National Museum 9, 83-91. https://doi.org/10.5479/si.00963801.9-554.83.

73. Mohling, J.W. (2004). Exogenic fulgurites from Elko County, Nevada: A new class of fulgurite associated with large soil-gravel fulgurite tubes. Rock. Mineral 79, 334-340.

74. Mueller, S.P., Helo, C., Keller, F., Taddeucci, J. and Castro, J.M. (2018) First experimental observations on melting and chemical modification of volcanic ash during lightning interaction. Sci. Rep. 8(1), 1389. https://doi.org/10.1038/s41598-018-19608-3.

75. Müller, D., Hess, K.H., Kueppers, U., Lokachari, S., Dingwell, D.B., Wolf, G., Rokicki, P. and Nowotnik, A. (2021) Rheological and chemical interaction between volcanic ash and thermal barrier coatings. Surf. Coat. Technol. 412, 127049. https://doi.org/10.1016/j.surfcoat.2021.127049.

76. Navarro-González, R., Mahan, S.A., Singhvi, A.K., Navarro-Aceves, R., Rajot, J.L., McKay, C.O., Coll, P. and Raulin, F. (2007) Paleoecology reconstruction from trapped gases in a fulgurite from the late Pleistocene of the Libyan Desert. Geology 35, 171-174. https://doi.org/10.1130/G23246A.1.

77. Niemeyer, L., Pietrono, L. and Wiesmann H.J. (1984) Fractal dimension of dielectric breakdown, Phys. Rev. Lett., 52(12), 1033–1036, doi:10.1103/PhysRevLett.52.1033.

78. Orgel, L.E. (1968) Evolution of the genetic apparatus. J. Mol. Biol. 38, 381-393.

79. Papike, J.J. (1998) Comparative planetary mineralogy: chemistry of melt-derived pyroxene, feldspar, and olivine. Planetary Materials. Am. Min. 36, 7-10.

80. Pedersen, A.K. (1981) Armalcolite-bearing Fe-Ti oxide assemblages in graphite-equilibrated salic volcanic rocks with native iron from Disko, central West Greenland. Contrib. Mineral. Petrol. 77, 307-324. https://doi.org/10.1007/BF00371560.

81. Pasek, M.A. (2008) Rethinking early Earth phosphorus geochemistry. Proc. Natl. Acad. Sci. U.S.A. 3, 853-858. https://doi.org/10.1073/pnas.0708205105.

82. Pasek, M.A. (2017) Schreibersite on the early Earth: scenarios for prebiotic phosphorylation. Geosci. Front. 8, 329-335. https://doi.org/10.1016/j.gsf.2016.06.008.

83. Pasek, M.A. (2020) Thermodynamics of Prebiotic Phosphorylation. Chem. Rev. 120, 11, 4690-470. https://doi.org/10.1021/acs.chemrev.9b00492.

84. Pasek, M.A. and Lauretta, D.S. (2005) Aqueous corrosion of phosphide minerals from iron meteorites: a highly reactive source of prebiotic phosphorus on the surface of the early Earth. Astrobiology 5, 515-535. https://doi.org/10.1089/ast.2005.5.515.

85. Pasek, M.A., Dworkin, J.P. and Lauretta, D.S. (2007) A radical pathway for organic phosphorylation during schreibersite corrosion with implications for the origin of life. Geochim. Cosmochim. Acta. 71, 1721-1736. https://doi.org/10.1016/j.gca.2006.12.018.

86. Pasek, M.A. and Block, K. (2009) Lightning-induced reduction of phosphorus oxidation state. Nat. Geosci. 2, 553-556. https://dx.doi.org/10.1038/ngeo580.

87. Pasek, M.A., Block, K. and Pasek, V. (2012) Fulgurite morphology: a classification scheme and clues to formation. Contrib. Mineral. Petrol. 164, 477-492. https://doi.org/10.1007/s00410-012-0753-5.

88. Pasek, M.A., Harnmeijer, J.P., Buick, R., Gull, M. and Atlas, Z. (2013) Evidence for reactive reduced phosphorus species in the early Archean Ocean. Proc. Natl. Acad. Sci. U.S.A. 25, 10089-10094. https://doi.org/10.1073/pnas.1303904110.

89. Pasek, M.A., Gull, M. and Herschy, B. (2017) Phosphorylation on the early earth. Chem. Geol. 475, 149-170. https://doi.org/10.1016/j.chemgeo.2017.11.008.

90. Pasek, M.A. and Pasek, V.D. (2018). The forensics of fulgurite formation. Miner. Petrol. 112, 185-198 https://doi.org/10.1007/s00710-017-0527-x.

91. Paxton, A.H., Gardner, R.L. and Baker, L. (1986) Lightning return stroke: a numerical calculation of the optical radiation. Lightning Electromagnetics, 29, 2736-41.

92. Petty, J.J. (1936) The origin and occurrence of fulgurites in the Atlantic coastal plain. Am. J. Sci. 31, 188–201.

93. Pérez-Invernón, F.J., Huntrieser, H., Jöckel, P. and Gordillo-Vázquez, F.J.A (2022) parameterization of long-continuing-current (LCC) lightning in the lightning submodel LNOX (version 3.0) of the Modular Earth Submodel System (MESSy, version 2.54). Geosci. Model Dev. 15, 1545-1565. https://doi.org/10.5194/gmd-15-1545-2022.

94. Pineda, N., Montanyà, J. and Van der Velde, O.A. (2014) Characteristics of lightning related to wildfire ignitions in Catalonia. Atmos. Res. 135-136, 380-387. https://doi.org/10.1016/j.atmosres.2012.07.011.

95. Purdom, W.P. (1966) Fulgurites from mount Thielsen, Oregon: The Ore Bin. 9, 153-159.

96. Rakov, V.A. (2016) Fundamentals of lightning. Cambridge University Press.

97. Rakov, V. and Uman, M. (2003) Downward negative lightning discharges to ground. In Lightning: Physics and Effects (pp. 108-213). Cambridge: Cambridge University Press. doi:10.1017/CBO9781107340886.005.

98. Rakov, V.A. (2008) Triggered lightning. In Lightning: principles, instruments and applications (eds H. D. Betz, U. Schumman & P. Laroche). The Netherlands: Springer, 23–56.

99. Ritson, D.J., Mojzsis, S.J. and Sutherland, J.D. (2020) Supply of phosphate to early Earth by photogeochemistry after meteoritic weathering. Nar. Geosci. 13, 344-348. https://doi.org/10.1038/s41561-020-0556-7.

100. Rodger, C.J., Brundell, J.B., Dowden, R.L. and Thomson, N.R. (2004) Location accuracy of long distance VLF lightning location network. Ann. Geophys. 22, 747-758, https://doi.org/10.5194/angeo-22-747-2004.

101. Rodger, C.J., Brundell, J.B. and Dowden, R.L. (2005) Location accuracy of VLF World Wide Lightning Location (WWLL) network: Postalgorithm upgrade. Ann. Geophys. 23, 277-290. https://doi.org/10.5194/angeo-23-277-2005.

102. Russell, M.J., Barge, L.M., Bhartia, R., Bocanegra, D., Bracher, P.J., Branscomb, E., Kidd, R., McGlynn, S., Meier, D.H., Nitschke, W. and Shibuya, T. (2014) The drive to life on wet and icy worlds. Astrobiology. 14, 308-343. https://doi.org/10.1089/ast.2013.1110.

103. Saba, M.M.F., Pinto Jr, O. and Ballarotti, M.G. (2006) Relation between lightning return stroke peak current and following continuing current. Geophys. Res. Lett. 33, L23807. https://doi.org/10.1029/2006GL027455.

104. Schwartz, A.W. and Chittenden, G.J.F. (1977) Synthesis of uracil and thymine under simulated prebiotic conditions. BioSystems. 9, 87-92. https://doi.org/10.1016/0303-2647(77)90016-8.

105. Silva, G.P.S., Nunes, M.C.S., Ulsen, C., Künzel, R., Yoshimura, E.M. and Trindade, N.M. (2021) Thermoluminescence of fluorapatite mineral. J. Lumin. 231, 117802. https://doi.org/10.1016/j.jlumin.2020.117802.

106. Smith, J. (1981) Halogen and phosphorus storage in the Earth. Nature. 289, 762-765. https://doi.org/10.1038/289762a0.

107. Springsklee, C., Scheu, B., Manga, M., Cigala, V., Cimarelli, C. and Dingwell, D.B. (2022) The Influence of Grain Size, Distribution on Laboratory-Generated Volcanic Lightning. J. Geophys. Res. Solid Earth. 127, 10. https://doi.org/10.1029/2022JB024390.

108. Sponholz, B., Baumhauer, R. and Felix-Henningsen, P. (1993) Fulgurites in the southern Central Sahara, Republic of Niger and their paleoenvironmental significance. The Holocene 3(2), 97–104. https://doi.org/10.1177/095968369300300201.

109. Stefano, C.J., Hackney, S.A. and Kampf, A.R. (2020) The occurrence of iron silicides in a fulgurite: Implications for fulgurite genesis. Can. Mineral. 58, 115-123. https://doi.org/10.3749/canmin.1900019.

110. Stern, S., Cimarelli, C., Gaudin, D., Scheu, B., and Dingwell, D.B. (2019) Electrification of experimental volcanic jets with varying water content and temperature. Geophys. Res. Lett. 46(20), 11136-11145. https://doi.org/10.1029/2019GL084678.

111. Şenel, M., Acarlar, M., Çakmakoğlu, A., Dağer, Z., Erkanol, D., Örçen, S., Taşkıran, M.A., Ünal Ulu, M.F. and Yıldırım, H. (1984) Özalp (Van)-İran sınırı arasındaki alanın jeolojisi. Maden Tetkik ve Arama Genel Müdürlüğü Rapor No: 7623, Ankara, (unpublished).

112. Teixera, L.M. (2019) Experimental fulgurites [MS.c. Thesis]: Luswig-Maximilians-Universität, 40.

113. Türkecan, A. (2017) İran sınırında bir volkan - Yiğit dağı. MTA Doğal Kaynaklar ve Ekonomi Bülteni, 23, 77-86.

114. Uman, M.A. (1969) Lightning. Monograph. McGraw-Hill, New York. Advanced physics.

115. Uman, M.A., Beasley, W.H., Tiller, J.A., Lin, Y.T., Krider, E.P., Weidmann, C.D., Krehbiel, P.R., Brook, M., Few Jr, A.A., Bohannon, J.I., Lennon, C.L., Poehler, H.A., Jafferis, W., Gulick, J.R. and Nicholson, J.R. (1978) An unusual lightning flash at Kennedy Space Centre. Science 201:9– 16. https://doi.org/10.1126/science.201.4350.9.

116. Uman, M.A. (2001) The lightning discharge. Courier Corporation.

117. Vyalikh, A., Simon, P., Rosseeva, E., Buder, J., Scheler, U. and Kniep, R. (2015) An NMR Study of Biomimetic Fluorapatite–Gelatine Mesocrystals. Sci. Rep. 5, 1-10. https://doi.org/ 10.1038/srep15797.

118. Yamagata, Y., Watanabe, H., Saitoh, M. and Namba, T. (1991) Volcanic production of polyphosphates and its relevance to prebiotic evolution. Nature, 35, 516-519. https://doi.org/10.1038/352516a0.

119. Yang, J.T.D., Lee, W.L. and Chun-Yen, T. (2005) A Web-based bookmark tool with ontological approach for knowledge sharing of special interest groups, 19th International Conference on Advanced Information Networking and Applications (AINA'05) Volume 1 (AINA papers), 2, 271-276. https:/doi.org/10.1109/AINA.2005.73.

120. Wadsworth, F.B., Vasseur, J., Liewellin, E.W., Genareau, K., Cimarelli, C. and Dingwell, D.B. (2017) Size limits for rounding of volcanic ash particles heated by lightning. J. Geophys. Res. Solid Earth 122, 1977-1989. https://doi.org/10.1002/2016JB013864.

121. Wagstaff, F.E. (1969) Crystallization and Melting Kinetics of Cristobalite. Journal of the American Ceramic Society 52(12), 650-654. https://doi.org/10.1111/j.1151-2916.1969.tb16069.x.

122. Walton, C.R., Shorttle, O., Jenner, F.E., Williams, H.M., Golden, J., Morrison, S.M., Downs, R.T., Zerkle, A., Hazen, R.M. and Pasek, M.A. (2021) Phosphorus mineral evolution and prebiotic chemistry: From minerals to microbes. Earth Sci. Rev. 221, 103806. https://doi.org/10.1016/j.earscirev.2021.103806.

123. Wasserman, A.A., Melosh, H.J. and Lauretta, D.S. (2002) Fulgurites: a look at transient high temperature processes in silicates. In Lunar and Planetary Science Conference, 1308.

124. White, A.K. and Metcalf, W.W. (2007) Microbial metabolism of reduced phosphorus compounds. Annu. Rev. Microbiol. 61, 379-400. https:/doi.org/10.1146/annurev.micro.61.080706.0933.

125. Wiesmann, H.J. and Zeller, H.R. (1986) A fractal model of dielectric breakdown and prebreakdown in solid dielectrics. J. Appl. Phys., 60 (5), 1770-1773, https://doi.org/10.1063/1.337219.

126. Wright, F. (1999) Florida's fantastic fulgurite find. Rocks and Minerals 74, 157-159.

127. Wörner, G. and Schmincke, H.U. (1984) Petrogenesis of the Zoned Laacher See Tephra. J. Petrol. 25, 836-851. https://doi.org/10.1093/petrology/25.4.836.

128. Zhu, Y., Stock, M., Lapierre, J. and DiGangi, E. (2022) Upgrades of the Earth networks total lightning network in 2021. Remote sensing. 14(9), 2209. https://doi.org/10.3390/rs14092209.

Acknowledgments

Don, I'm so glad that you replied to my first email, which brought me to Munich. You were a much better supervisor than I could have ever imagined for myself. I will always be grateful to you for giving me the freedom to speak and share my ideas. Your consistent encouragement has meant the world to me, and I couldn't have come this far without you by my side. My childhood dream has come true, thanks to you!

Thank you, Corrado, for your amazing support every single time. I feel incredibly fortunate that Don brought us together, giving me the opportunity to learn not only about science but also about life itself through your guidance. Your wisdom and advice have impacted me, and I will carry them with me throughout my life.

Thank you very much, Betty, for supporting me during my Ph.D. Discussing different topics and conducting research with you was a great opportunity.

Thank you Alessandra from the bottom of my heart for your insightful teaching and invaluable support. I am deeply grateful for the knowledge and wisdom you shared with me.

Joanna (my science sister), I can’t imagine my life in Munich without you. Having you as my office mate all these years has been fantastic! Caron, a million thanks to you for always being there. Our tennis matches and car travels bring me immense joy. To my Çıplak team members - Mathew, Pancho (Kazma), and Sid - thank you so much for every crazy moment we shared that made my Ph.D. journey perfectly crazy. Roberto, thanks for telling me every morning,. How are you?”. This added the missing Mediterranean soul to this journey and made me tremendously happy.

I want to thank all members of the LMU for excellent science discussions and tons of fun activities: Ana, Anthony, Arianna, Baha, Carolina, Cristina, Cristian, Daniel (grumpy), Daniel W., Edgar, Eleonora, Iphi, Jérémie, Jackie, Julia, Julia G., Kai-Uwe, Lukas, Luiz, Marize, Markus, Michi, Mila, Natasha, Omar, Ömer, Simon, Sönke, Steffi, Thomas, Ulli, Yan, Vale, and Werner.

Muzaffer hanım (abla) ve Ateş amca, annemin bana yaptığı en kıymetli jestlerden biri, beni size göndermesiydi. Hayatım tam da 2009 yılında hayal ettiğimiz gibi şekillendi, hala inanamıyorum! Tüm mutluluklarım, başarılarım ve zor günlerimde yanımda olduğunuz için size minnettarım.

Yağmur Sürmeli Ç. ve Arda Çalışıyor, bu doktorayı benim kadar kim biliyor desem aklıma ikiniz gelirsiniz. ☺ Yol boyu beni yalnız bırakmadığınız ve Covid-19 günlerini bile güzelleştirdiğiniz için size minnettarım. Gözde Toker, makalelerimi senin mükemmel evinde ve sohbetin eşliğinde yazma fırsatını bana verdiğin için çok mutluyum. Duygusal gelişimimin en tatlı "şahidisin", hep yanımda olduğun için binlerce teşekkürler. Ezgi Akbulut, doktoramın sonunda hayatıma "starlight^{muse}" olarak gönderildiğini düşünüyorum. Benimle her etkinliğe anında atlayıp, günlerime neşe kattığın için minnettarım.

Fatih Güler, o gün bilgisayarını yanında taşımamış olsaydın bu doktoraya başvuramazdım ve hayatım belki de bambaşka bir yöne akardı. Yani ilk ateşi sen yaktın. ☺ Münih'e gelmem konusunda beni desteklediğin için minnettarım.

Sevgili ailem, bitmek bilmeyen öğrenme merakıma olan şaşkın hoşgörünüze minnettarım. Sevgili abilerim (Mustafa ve Kerim), bana çocukken işe bisikletle gidebilme hayali veren, adını bile hatırlamayacağım, o filmi izlettirdiğiniz için teşekkür ederim. Yıllardır işe aynı filmdeki oyuncu gibi bisikletle gidiyorum ve bu harika bir şey! Ponçik yeğenlerim (Ali Emre, Elif Ada ve Selim) gülümsemeniz ve varlığınızla bana hayata umutlu bakmayı hatırlattığınız için sizi çok seviyorum. Sevgili Nur ve Sevil - asla yengelerim değil ☺- eve geldikçe sevdiğim şeyleri yaptığınız ve güzel kahve sohbetleri sunduğunuz için teşekkür ederim. Anne, burada olmanı ve sana "evet tıp doktoru olmuyorum ama yine de doktor oluyorum" diyebilmeyi çok isterdim. İtici gücüm olduğun için minnettarım. Baba, her zaman ne yapmaya çalıştığımı anlamasan da beni destekleme cesaretini gösterdiğin için çok şanlıyım ve sana binlerce kere teşekkür ederim.

Ayşe Zeynep Çalışkanoğlu